Universidad de Concepción
Dirección de Postgrado
Facultad de Ciencias Físicas y Matemáticas
Programa de Doctorado en Ciencias Aplicadas con Mención en Ingeniería Matemática

SOLUCIÓN NUMÉRICA DE MODELOS EPIDEMIOLÓGICOS ESPACIO-TEMPORALES

Tesis para optar al grado de Doctor en Ciencias Aplicadas con Mención en Ingeniería Matemática

ELVIS HERNALDO GAVILÁN GUTIÉRREZ
CONCEPCIÓN - CHILE 2018

Profesor Guía: Raimund Bürger
CI^2MA y Departamento de Ingeniería Matemática
Universidad de Concepción, Chile

Profesor Cotutor: Gerardo Chowell
School of Public Health
Georgia State University, Atlanta, GA, Estados Unidos

Numerical solution of spatio-temporal epidemic models

Elvis Gavilán Gutiérrez

Directores de Tesis : Raimund Bürger, Universidad de Concepción, Chile
Gerardo Chowell, Georgia State University, Estados Unidos

Director de Programa : Rodolfo Rodríguez, Universidad de Concepción, Chile

Comisión Evaluadora

Prof. Linda J. S. Allen, Texas Tech University, Estados Unidos

Prof. Paulo Verdasca Amorim, Universidade Federal do Rio de Janeiro, Brasil

Prof. Sebastiano Boscarino, University of Catania, Italia

Prof. Marcos Capistrán, CIMAT, México

Prof. James Mac Hyman, Tulane University, Estados Unidos

Comisión Examinadora

Firma: _____
Prof. Raimund Bürger, Universidad de Concepción, Chile

Firma: _____
Gerardo Chowell, Georgia State University, Estados Unidos

Firma: _____
Prof. Fernando Córdova-Lepe, Universidad Católica del Maule, Chile

Firma: _____
Prof. Mauricio Sepúlveda, Universidad de Concepción, Chile

Firma: _____
Prof. Luis Miguel Vilada, Universidad del Bío-Bío, Chile

Nota: _____

Concepción, Jueves 12 de Julio 2018

Abstract

The main objective of this thesis is to gain insight into the spatio-temporal dynamics of infectious diseases described by systems of convection-diffusion equations that on one hand, represent spatial extensions of well-knowm temporal compartmental epidemics, and on the other hand involve recently developed models of directed and undirected biological movement. Due to the involved nonlinear and nonlocal nature of the governing model, we aim to obtain insight by the implementation of advanced numerical methods. The choice of scenarios is motivated by the existing connection between dynamic systems of ordinary differential equations and spatio-temporal systems of partial differential equations. Roughly speaking, dynamic systems determine the variation of quantities with respect to the time variable. Considering that these quantities correspond to the number of individuals of a population which move in a certain environment, this motivates adding one or more spatial variables, from which a system of partial differential equations is obtained.

The dynamic systems to be presented correspond to models used mainly in the study of infectious diseases such as influenza AH1N1, malaria, hantavirus, Ebola, and sexually transmitted diseases. For the study of these diseases the starting point is to consider a certain population of individuals and classify them in two or more states acording to a particular disease. An important role is played by the basic reproductive R_0, which represents the average number of secondary cases that an infectious can cause during the infectious period. This number is determined by constant values that are obtained empirically for each particular disease model. If $R_0 < 1$, then the disease does not generate an outbreak, and if $R_0 > 1$, then an epidemic occurs. Other important concepts in epidemiology are those of an agent (person, animal or microorganism), a vector (any agent that transports and transmits an infectious pathogen in another living organism) and a host (any agent that hosts the infectious but does not transmit it). When in a dynamic system there is a vector that carries the disease to a host then we talk about an infectious disease transmitted by a vector.

In partial differential equations involving temporal and spatial derivatives, two important effects associated with spatial derivatives are the phenomenon of diffusion, which in this case is interpreted as how individuals tend to move away from each other and the phenomenon of convolution, which is related to the way in which some

individuals have the ability to locate others, and to move in their direction.

One zoonotic infectious disease present in Chile is the Hantavirus, which has two major manifestations in humans, a hemorrhagic fever with renal syndrome and the other as a cardiopulmonary syndrome. This disease that affects humans and can be fatal, it is transmited by contact with the long-tailed mouse *Oligoryzomys longicaudatus* or with the feces or urine of the animal.

In the first instance, we work with a system that deals with the spread of Hantavirus infection in rodents, which is described by a spatio-temporal compartmental model susceptible-exposed-infectious-recovered (SEIR) that distinguishes between male and female subpopulations. It is assumed in this case that both subpopulations differ in their movement with respect to the local variations of their respective own densities and of the opposite gender group; three alternative models for the movement of the masculine individuals are examined. In some cases, the movement is not only directed by the gradient of a density (as in the standard diffusive case), but also by a non-local convolution of density values. An efficient numerical method is then proposed for the reaction-diffusion convection model of the resulting partial differential equations system. This method involves essentially non-oscillatory weighted reconstruction techniques (WENO) in combination with explicit implicit methods of Runge-Kutta (IMEX-RK) for time stepping.

The second part of this work is based on another type of dynamic systems, known as predator-prey models, which are often studied in the context of ecology, as they are used to predict the number of prey and their predator. An interesting phenomenon in nature is the formation of patterns, which can be described through systems of partial differential equations associated with spatio-temporal extensions of predator-prey models that under certain conditions give rise to solutions that stabilize over time.

A spatio-temporal eco-epidemiological model is formulated by combining an available non-spatial model for predator-prey dynamics with infected prey with a spatio-temporal susceptible-infective (SI)-type epidemic model of pattern formation due to diffusion. It is assumed that predators exclusively eat infected prey, in agreement with the hypothesis that the infection weakens the prey and increases its susceptibility to predation. In addition, the movement of predators is described by a non-local convolution of the density of infected prey. In this part the objective is to observe the effect of convolution, the patterns formed by the prey change once the predator appears.

Resumen

El objetivo principal de esta tesis es conocer las dinámicas espacio-temporales de las enfermedades infecciosas descritas por los sistemas de ecuaciones convección-difusión que, por un lado, representan extensiones espaciales de epidemias compartimentales temporales bien conocidas y por otra parte involucran modelos recientemente desarrollados de movimiento biológico dirigido y no dirigido. Debido a la naturaleza no lineal y no local del modelo gobernante, apuntamos a obtener información mediante la implementación de métodos numéricos avanzados. La elección de los escenarios están motivados por la conexión existente entre los sistemas dinámicos de ecuaciones diferenciales ordinarias y los sistemas espacio-temporales de ecuaciones diferenciales parciales. En términos generales, los sistemas dinámicos determinan la variación de las cantidades con respecto a la variable de tiempo. Considerando que estas cantidades corresponden al número de individuos de una población que se mueven en un cierto entorno, esto motiva agregar una o más variables espaciales, a partir de las cuales se obtiene un sistema de ecuaciones diferenciales parciales.

Los sistemas dinámicos presentados corresponden a modelos utilizados principalmente en el estudio de enfermedades infecciosas como la influenza AH1N1, la malaria, el hantavirus, el Ébola y enfermedades de transmisión sexual. Para el estudio de estas enfermedades, el punto de partida es considerar una cierta población de individuos y clasificarlos en dos o más estados con respecto a una enfermedad en particular. Un rol importante está determinadi por el número básico de reproducción R_0, que corresponde al número promedio de casos secundarios que un infeccioso puede causar durante el periodo de enfermedad. Este número está determinado por valores constantes que se obtienen empíricamente para cada modelo de enfermedad en particular. Si $R_0 < 1$, entonces la enfermedad no genera un brote, y si $R_0 > 1$, se produce una epidemia. Otros conceptos importantes en epidemiología son los de un agente (persona, animal o microorganismo), un vector (cualquier agente que transporta y transmite un patógeno infeccioso en otro organismo vivo) y un huésped (cualquier agente que hospeda lo infeccioso pero no lo transmite). Cuando en un sistema dinámico hay un vector que transmite la enfermedad a un anfitrión, entonces se habla de enfermedad infecciosa transmitida por un vector.

En ecuaciones diferenciales parciales que consideran derivadas temporales y espa-

ciales, dos efectos importantes asociados con las derivadas espaciales son los fenómenos de difusión, que en este caso se interpreta como la tendencia de los individuos a alejarse unos de otros y el fenómeno de la convolución, que tiene relación con la manera en que algunos individuos tienen la capacidad de localizar a otros y moverse en su dirección.

Una enfermedad infecciosa zoonótica presente en Chile es el Hantavirus, que tiene dos manifestaciones principales en los humanos, una fiebre hemorrágica con síndrome renal y la otra como síndrome cardiopulmonar. Esta enfermedad que afecta a los humanos y puede ser fatal, se contrae por contacto con el ratón de cola larga *Oligoryzomys longicaudatus* o con las heces o la orina del animal.

En primera instancia se trabaja con un sistema que modela la propagación de la infección por Hantavirus en roedores el cual se describe mediante un modelo compartimental espacio-temporal susceptible-expuesto-infeccioso-recuperado (SEIR) que distingue entre subpoblaciones de machos y de hembras. Se supone que ambas subpoblaciones difieren en su movimiento con respecto a las variaciones locales de las densidades propias y del grupo de género opuesto. Se examinan tres modelos alternativos para el movimiento de los individuos masculinos. En algunos casos, el movimiento no solo está dirigido por el gradiente de una densidad (como en el caso difusivo estándar), sino también por una convolución no local de valores de densidad. Se propone entonces un método numérico eficiente para el modelo reacción-difusión convección del sistema de ecuaciones diferenciales parciales resultante. Este método involucra técnicas de reconstrucciones ponderadas esencialmente no oscilatorias (WENO) en combinación con métodos implícitos explícitos de Runge-Kutta (IMEX-RK) para el paso del tiempo.

En la segunda parte de este trabajo se trata de otro tipo especial de sistemas dinámicos, llamados modelos depredador-presa. Estos son a menudo estudiados en el contexto de la ecología pues ellos se utilizan para predecir la cantidad de presas y cazadores (depredadores) a lo largo del tiempo. Un fenómeno interesante en la naturaleza es la formación de patrones, el cual puede describirse a través de sistemas de ecuaciones diferenciales parciales asociados a modelos espacio-temporales y que bajo ciertas condiciones dan lugar a soluciones que se estabilizan a lo largo del tiempo.

Se formula un modelo ecoepidemiológico espacio-temporal combinando un modelo no espacial disponible para la dinámica depredador-presa con presas infectadas con un modelo espacio-temporal epidémico susceptible-infeccioso (SI) de formación de patrón debido a la difusión. Se supone que los depredadores atacan exclusivamente presas infectadas, de acuerdo con la hipótesis de que la infección debilita a la presa y aumenta su susceptibilidad a la depredación. Además, el movimiento de los depredadores se describe por una convolución no local de la densidad de presas infectadas. En esta parte el objetivo es observar el efecto de la convolución, los patrones formados por la presa cambian una vez que aparece el depredador.

Agradecimientos

Quiero agradecer aquí comenzando por mi director de tesis, el profesor Raimund Bürger, por su apoyo tanto en el sentido académico y personal. Además de destacar la manera en la cual trabaja, también son más que notables su muy buen sentido del humor y su paciencia.

A mi co-tutor, el profesor Gerardo Chowell, por su importante participación en el desarrollo de esta tesis y el cuidado casi paternal que tuvo en mi visita a la ASU.

A los profesores Pep Mulet y Luis Miguel Villada por todas las reuniones de trabajo, consejos, muestras de apoyo y palabras de ánimo, sin duda es muy motivante poder trabajar cerca de ellos.

Al Centro de Investigación en Ingenería Matemática (CI^2MA), por el espacio y excelentes instalaciones para trabajar. A su director, el profesor Gabriel Gatica, por su fundamental apoyo, tanto como profesor y como persona. Al personal administrativo del CI^2MA, principalmente a la Sra. Lorena Carrasco.

En el DIM, al profesor Freddy Paiva del DIM por los consejos, a Cecilia Leiva y a José Parra por su imprescindible ayuda toda vez que la necesité. En el Departamento de Matemática a Luis Castro y Erika Torres.

A mis compañeros del doctorado, especialmente a los de primer año: Gabriel, Carlos, Cinthya y a *Goga* a quien varias veces le llegué a sacar humos por la orejas con *preguntas*. También a Sergio, Joaquín, Felipe, Víctor, Ramiro y Patrick.

A mis padres Víctor y Margarita, a mi hermana favorita Úrsula, quienes siempre me han apoyado y querido, no tengo palabras para agradecerles por su cariño. También agradezco a mis tíos más cercanos: Tomás Contreras, Margarita Gavilán, Ricardo Gavilán y Gloria Pinto.

Agradezco también a mis amigos, profesor Gustavo Avello, Ulises Contreras, Alexis Gallardo, Gabriel Garrido, Erwin Ifland, Daniel Inzunza, Pedro Leiva, Álvaro Martínez, Camilo Mejías, Gladys Muñoz, profesor Héctor Palma, Diego Paredes, Juan Claudio Rivas, Yuliane Sánchez, Felipe Sánchez y Marcela Torrejón, quienes en este último tiempo estuvieron pendientes y mostraron preocupación por mí.

Gracias a CONICYT y su programa de becas de doctorado nacional que han financiado mis estudios, al Departamento de Ingeniería Matemática de la UdeC y al proyecto basal de la Universidad de Chile por el financiamiento en el etapa final.

Finalmente quiero agradecer a Paula, quien no podría apoyarme de mejor manera con su amor, cariño, humor y paciencia; este logro lo comparto contigo y porsupuesto con nuestro, ahora ya no tan pequeño hijo, Leonardo.

Contents

List of Tables

List of Figures

Chapter 1

Introduction

1.1 Scope of this thesis

Hantavirus (family Bunyaviridae) is a rodent-borne infectious disease of significant concern as it can generate high case fatality rates in the human population [68]. Transmission of hantavirus from infected rodents, the main known reservoir of the virus, to humans, typically occurs via inhalation of aerosols contaminated by virus shed in excreta, saliva, and urine [44]. Risk of infection with hantavirus in the human population is facilitated by crowding conditions and close proximity to rodent populations. Not surprisingly, the total population at risk for hantavirus infection has increased with urbanization rates. In the Americas, hantavirus represents a public health issue in South American countries including Chile [59]. The great majority of hantavirus cases have been reported in China, however [77, 78]. A better understanding of the transmission dynamics of hantavirus in rodent populations has the potential to directly guide interventions strategies aimed at minimizing the number of infections in the human population.

A first objective in this work, which develops in Chapter 2 is to advance a spatio-temporal compartmental model of hantavirus infection in rodents with a focus on its efficient numerical solution. The total population of rodents is subdivided into males and females (indices m and f), and for each of both subpopulations a variant of the well-known susceptible-exposed-infective-recovered (SEIR) compartmental model [40] is formulated. The compartments of male and female individuals are

$$\mathcal{C}_\mathrm{m} := \{S_\mathrm{m}, E_\mathrm{m}, I_\mathrm{m}, R_\mathrm{m}\} \quad \text{and} \quad \mathcal{C}_\mathrm{f} := \{S_\mathrm{f}, E_\mathrm{f}, I_\mathrm{f}, R_\mathrm{f}\}$$

respectively, and the final model for

$$\boldsymbol{u} = (u_1, \ldots, u_8)^\mathrm{T} = (S_\mathrm{m}, E_\mathrm{m}, I_\mathrm{m}, R_\mathrm{m}, S_\mathrm{f}, E_\mathrm{f}, I_\mathrm{f}, R_\mathrm{f})^\mathrm{T}$$

as a function of position $\boldsymbol{x} \in \Omega$ and time $t \in \mathcal{T} := [0, T]$ on a bounded domain $\Omega \subset \mathbb{R}^2$ is given

by a convection-diffusion reaction system of the type

$$\frac{\partial \boldsymbol{u}}{\partial t} + \nabla \cdot \boldsymbol{F}^{\mathrm{c}}(\boldsymbol{u}) = \boldsymbol{\mathcal{D}} \Delta \boldsymbol{u} + \boldsymbol{s}(\boldsymbol{u}), \tag{1.1}$$

supplied with initial and boundary conditions, where the convective fluxes $\boldsymbol{F}^{\mathrm{c}}(\boldsymbol{u})$, the diffusion matrix $\boldsymbol{\mathcal{D}}$ and the vector of reaction terms $\boldsymbol{s}(\boldsymbol{u})$ are specified in later parts of this Chapter. It is proposed to describe the movement of the male individuals in a particular way that depends non-locally on the density

$$N_{\mathrm{f}} = S_{\mathrm{f}} + E_{\mathrm{f}} + I_{\mathrm{f}} + R_{\mathrm{f}}$$

of female individuals, in combination with several alternative local or non-local dependences on the density

$$N_{\mathrm{m}} = S_{\mathrm{m}} + E_{\mathrm{m}} + I_{\mathrm{m}} + R_{\mathrm{m}}$$

of male individuals. These alternatives give rise to three models that will be discussed in parallel, and that are expressed by the respective choice of $\boldsymbol{F}^{\mathrm{c}}(\boldsymbol{u})$. In any case the movement of the male individuals is assumed to depend non-locally on N_{f}. All variants of (1.1) call for numerical methods that on one hand avoid the severe time step restriction incurred by explicit time discretizations of the diffusion term $\boldsymbol{\mathcal{D}} \Delta \boldsymbol{u}$, and on the other hand allow the efficient computation of numerical fluxes based on the non-local evaluation of data. The first goal can be achieved by an implicit-explicit (IMEX) discretization in combination with a technique based on Fast Fourier Transform (FFT) to handle the second. The simulator constructed in this way is applied to provide numerical results of several scenarios that allow comparing the model variants.

The above, which is presented in Chapter 2, has led to the following publication

- R. Bürger, G. Chowell, E. Gavilán, P. Mulet, and L.M. Villada, Numerical solution of a spatio-temporal gender-structured model for hantavirus infection in rodents, *Math. Biosci. Eng.*, **15** (2018), 95–123.

In general we consider that mathematical models are powerful tools to characterize the spatial-temporal changes in complex dynamical systems. More specifically, mathematical models are frequently used to gain novel insight into the dynamics and control of natural and social phenomena [66]. For example, mathematical models are often simple and crude approximations that aim to capture key mechanisms underlying the dynamics of infectious disease transmission in human, animal, and plant populations. Such first approximation models can be subsequently refined to study the effects of additional factors and processes including spatial heterogeneity in host density and their characteristics (e.g., fitness, susceptibility, infectivity) as well as specific host behaviors (e.g, movement patterns) in response to local host density or disease prevalence.

It is the purpose in the Chapter 3 a spatio-temporal predator-prey model taking into account infected prey with a particular focus on its efficient numerical solution. The resulting eco-epidemiological model combines several submodels that have been proposed in the recent

literature. The population of prey is described by a spatio-temporal SIR-type epidemiological model similar to the one studied by Sun [67] while the predator-prey interaction follows the treatment by Greenhalgh and Haque [32] (formulated in a non-spatial setting in that paper). The movement of predators is based on the nonlocal velocity model advanced for the predator movement in a spatio-temporal predator-prey model by Colombo and Rossi [22]. That velocity model is also used for the male compartments in the Chapter 2.

In most general terms, the governing model of Chapter 3 considers a prey population with a susceptible and infective compartment, denoted by S and I, and a variable Y denoting the population of the predator. In the spatio-temporal context, these variables are understood as local densities that are functions of position $\boldsymbol{x} \in \Omega$ and time $t \in \mathcal{T} := [0, T]$ on a bounded domain $\Omega \subset \mathbb{R}^2$. The final model for

$$\boldsymbol{u} := (u_1, u_2, u_3)^{\mathrm{T}} := (S, I, Y)^{\mathrm{T}}, \quad \boldsymbol{u} = \boldsymbol{u}(\boldsymbol{x}, t)$$

is given by a convection-diffusion reaction system of the type

$$\frac{\partial \boldsymbol{u}}{\partial t} + \nabla \cdot \boldsymbol{F}^{\mathrm{c}}(\boldsymbol{u}) = \boldsymbol{\mathcal{D}} \Delta \boldsymbol{u} + \boldsymbol{s}(\boldsymbol{u}), \tag{1.2}$$

supplied with initial and boundary conditions, where the convective fluxes $\boldsymbol{F}^{\mathrm{c}}(\boldsymbol{u})$, the diffusion matrix $\boldsymbol{\mathcal{D}}$, and the vector of reaction terms $\boldsymbol{s}(\boldsymbol{u})$ are specified later.

It is proposed to describe the movement of the predators in a particular way that depends non-locally on the density I of infected prey, while the movement of infected and susceptible prey, that is of members of the compartments I and S, is standard diffusion. The numerical method constructed in this way is applied to simulate several scenarios that allow comparing the effect of initial conditions and different parameter values. The numerical results exhibit a rich variety of behavior, including formation of patterns taking the shapes of spots, stripes, both from randomized perturbations of steady states and in a scenario that describes the invasion of a prey habitat by the predator. The structure of solutions obtained in the latter case are reminiscent of permanent wave fronts.

Chapter 3 has given rise to a second article, namely:

- R. Bürger, G. Chowell, E. Gavilán, P. Mulet, and L.M. Villada, Numerical solution of a spatio-temporal predator-prey model with infected prey, *Math. Biosci. Eng.*, in revision.

1.2 Related work

First of all, we mention that general references to the spatial spread of infectious diseases include [5, 24, 49, 52, 63, 73]. The basic assumption of our treatment, namely that all epidemiological compartments are distributed over the whole spatial domain, is opposed to the alternative metapopulation approach that describes spatial structure through the relations between a number of well-identified sub-populations or "patches" (cf., e.g., [3, 6, 7, 20, 43, 70, 71]).

In fact, the description of spatial structure by explicitly specifying the mobilities between "patches" is typical for characterizing the behavior of humans, who usually do not "disperse" in response to environmental stimuli (at least not in the relatively short time scales involved in epidemiological modelling) but undertake directed travels, while a description through a convection-diffusion-reaction mechanism is more suitable for non-human infectious agents such as spores, insects, and bacteria that would disperse. That diffusion is mostly associated with non-human beings is also supported by the fact that classical treatments of diffusion in ecology only include non-human populations (cf. [52, Ch. 13], [54]). This viewpoint is also assumed, for instance, in [24, Ch. 10]. Other references to the movement of animals and spread of diseases by reaction-diffusion equations include [49, 55, 62]. Furthermore, the distinction between metapopulation models and continuous in space models is also made in the alternative treatments in Sections 4.3 and 4.4 of Sattenspiel [63] and those by van den Driessche [71] and [74] in the same volume. In the latter, a decisive advantage of the spatially continuous approach, namely its amenability to mathematical analysis is emphasized. Furthermore, a reaction-diffusion system based on the well-known non-spatial SIR model [40] is proposed as a prototype spatio-temporal epidemic model is proposed, and the underlying assumptions of variants of reaction-diffusion models are broadly discussed, with particular reference to a seminal case study [36, 37, 53].

A less common ingredient in mathematical epidemiology is the convective term $\nabla \cdot \boldsymbol{F}^{\mathrm{c}}(\boldsymbol{u})$. Related advection terms, for which the essential functional dependence for one compartment is

$$\boldsymbol{F}^{\mathrm{c}} = \boldsymbol{F}^{\mathrm{c}}(\boldsymbol{x}, u) = \boldsymbol{b}(\boldsymbol{x})u$$

with a given velocity $\boldsymbol{b}(\boldsymbol{x})$, arise if the population under study is transported (as is the case with wind-borne infectious agents, plankton, etc.). A slightly different motivation of convective terms was advanced in [52, Ch. 14] in the context of a wolf territoriality model that describes directed movement of individuals towards a "den". Surprisingly, however, nonlinear convective models are less common in epidemiological applications (although they are widespread used to describe human behavior of, say, traffic and pedestrian flows [30, 35, 69]). Let us emphasize here that the main role of the convective term in our model is similar to that of [52, Ch. 14] in that it imposes a preferred direction of movement of (the male) individuals, where the global dependence of the direction is determined by convolution with population data within a certain horizon of current position. This idea of non-local dependence of biological fluxes goes back to a non-local predator-prey model introduced and analyzed by Colombo and Rossi [22], and for which a numerical scheme for that model is analyzed in [61]. The scheme proposed in that paper is based on the Lax-Friedrichs scheme for the (hyperbolic) equation (2.11a) for the ease of demonstrating convergence properties; in the first work we employ higher-order weighted essentially non-oscillatory (WENO) reconstructions (initially proposed in [34, 48]) to achieve high-order spatial accuracy.

Still within the framework of reaction-diffusion systems (but in simpler versions than considered here), a number of qualitative analyses of hantavirus models are available. For instance, Abramson and Kenkre [1] advance a two-equation reaction-diffusion model that is a spatial equation of the well-known susceptible-infectious-susceptible (SIS) model (the assumed population of mice is not structured in any other way), and demonstrate that one single lumped parameter, the

carrying capacity, essentially controls the dynamics of the system; moreover a spatial distribution of its value explains the formation and disappearance of "refugia", that is of habitat regions with favorable conditions that influence the spatio-temporal patterns of hantavirus [2, 42]. Furthermore, based on the Abramson and Kenkre model [1], Buceta et al. [18] study the impact of seasonality on hantavirus, with the remarkable result that the alternation of seasons, each of which associated with a constant set of epidemiological parameters, may induce the outbreak of Hantavirus infection even if neither season by itself satisfies the environmental requirements for propagation of the disease [18]. The same group also investigated the effects of intrinsic noise on hantavirus spread [27]. Finally, we mention that more recently the Abramson and Kenkre model was refined to give a stage-dependent model with delay [57], where a new compartment corresponds to virus-free young mice, and the new model consists of three ordinary differential equations with delay, or in its recent spatial version presented in [58], in a reaction-diffusion system with delay (where the diffusion operator is expressed in radial variables).

From a computational point of view, and coming back to our own model (1.1), we mention that IMEX Runge-Kutta (IMEX-RK) schemes play an important role. We therefore briefly provide some background on these methods. Roughly speaking, an IMEX-RK method for a convection-diffusion-reaction equation of the type (1.1) consists of a Runge-Kutta scheme with an implicit discretization of the diffusive term combined with an explicit one for the convective and reactive terms. To introduce the main idea, we consider the problem

$$\frac{\mathrm{d}\boldsymbol{v}}{\mathrm{d}t} = \Phi^*(\boldsymbol{v}) + \Phi(\boldsymbol{v}), \tag{1.3}$$

which is assumed to represent a method-of-lines semi-discretization of (1.1), where $\Phi^*(\boldsymbol{v})$ and $\Phi(\boldsymbol{v})$ are spatial discretizations of the convective and reactive terms and of the diffusive term, respectively. Assume, for simplicity, that the spatial mesh width is $h > 0$ in both the x- and y-direction. Then the stability restriction on the time step Δt that explicit schemes impose when applied to (1.3) is very severe (Δt must be proportional to the square h^2 of the grid spacing), due to the presence of $\Phi(\boldsymbol{v})$. The implicit treatment of both $\Phi^*(\boldsymbol{v})$ and $\Phi(\boldsymbol{v})$ would remove any stability restriction on Δt. However, the upwind nonlinear discretization of the convective terms contained in $\Phi^*(\boldsymbol{v})$ that is needed for stability, makes its implicit treatment extremely involved. This situation becomes even more complicated due to the WENO reconstructions. In fact, after the pioneering work of Crouzeix [23], numerical integrators that deal implicitly with $\Phi(\boldsymbol{v})$ and explicitly with $\Phi^*(\boldsymbol{v})$ can be used with a time step restriction dictated by the convective-reactive term alone. These schemes, apart from having been profusely used in convection-diffusion problems and convection problems with stiff reaction terms [8, 25], have been recently used to deal with stiff terms in hyperbolic systems with relaxation (see [11, 12, 13, 14, 56]). Finally, we mention that many authors have proposed IMEX-RK schemes for the solution of semi-discretized PDEs [8, 39, 56, 80].

The spatial spread of infectious diseases is described mathematically in a number of monographs that include [24, 49, 52, 63, 73]. The temporal evolution of diseases is also treated in [16, 29]. Our assumption that all epidemiological compartments are distributed over the whole spatial domain is opposed to the alternative metapopulation approach that describes spatial

structure through well-identified sub-populations or "patches" (cf., e.g., [3, 6, 7, 20, 70, 71]). The description of spatial structure by explicitly specifying the mobilities between "patches" is typical for characterizing the behavior of humans who undertake directed travels, while a description through a convection-diffusion-reaction mechanism is more suitable for non-human infectious agents such as spores, insects, and bacteria that would disperse [24, 52, 54]. A decisive advantage of the spatially continuous approach, namely its amenability to mathematical analysis is emphasized in [74].

The introduction of [32] and Hadeler and Freedman [33] provide extensive references to real-world examples of three-species eco-epidemiological systems of sound prey, infected prey, and predators. Specifically, in [33] a predator-prey model is described in which the prey is infected by a parasite and the prey in turn infects the predator with that parasite. The models studied in [32] and herein are based on the general assumption that the infection weakens the prey and increases its susceptibility to predation.

1.3 Organization of this thesis

The presentation of the work is described in this first introductory Chapter and the two contributions made, the first, "Numerical solution of a spatio-temporal gender-structured model for hantavirus infection in rodents", is presented in Chapter 2, and the second, "Numerical solution of a spatio-temporal predator-prey model with infected prey", is presented in Chapter 3. In general, Chapters 2 and 3 can be described as follows:

1. The mathematical model of Chapter 2 is introduced in Section 2.1, starting from the spatio-temporal balance equations of a gender-structured SEIR model (in Section 2.1.1). The three variants of convective fluxes $\boldsymbol{F}^{\mathrm{c}}(\boldsymbol{u})$ and the diffusion matrix $\boldsymbol{\mathcal{D}}$ arising in (1.1) are specified in Section 2.1.2, and it is shown in Section 2.1.3 that the model arising from ours for N_{m} and N_{f} by summing over all compartments in C_{m} and C_{f}, respectively, can be compared with the non-local predator-prey model studied in [22]. In Section 2.2 we introduce the numerical scheme. We will use the methods of lines to obtain a spatial semi-discretization of the initial-boundary value problem of (1.1) in the form of a system of ordinary differential equations (ODEs), to which a time-stepping procedure will be applied to obtain the final numerical scheme. To this end we introduce in Section 2.2.1 the Cartesian grid and discrete unknowns, and describe in Section 2.2.2 the discretization of non-local terms as in (2.6) that appear in the male convective fluxes. Then, in Section 2.2.3, we introduce the discretization of the the complete convective flux for the male species. This is essentially done by WENO reconstruction. The corresponding discretization for the female species is similar, and is omitted. Next, in Section 2.2.4 we describe the IMEX-RK time integrators used to solve the system of ODEs that represents the spatial discretization. Section 2.3 is devoted to the presentation of numerical results. Preliminaries are introduced in Section 2.3.1, including a definition of the constants arising in the model and of the initial scenarios. To make our results comparable with those of [4] (based on ordinary and stochastic differential equations), we adopt the parameters corresponding to the epizoology

of the rice rat and the Bayou virus utilized in that paper. On the other hand, Scenario 1 is based on the hypothesis that the initial population occupies a well-identified subdomain of Ω and therefore the numerical results also address the phenomenon of biological invasion (besides that of the progression of epidemic states), while Scenario 2 aims at studying the effect of a random perturbation of a constant initial state. The corresponding numerical examples are presented in Sections 2.3.2 and 2.3.3, respectively. Furthermore, we provide in Section 2.3.4 an example that shows that the numerical scheme exhibits experimental second-order convergence when the solution is smooth, and in Section 2.3.5 present a test case that addresses the effect of seasonal variability of some of the model parameters.

2. In Section 3.1 the governing mathematical model of Chpater 3 is introduced. To this end, we first formulate (in Section 3.1.1) a non-spatial predator-prey model, defined by three nonlinear ordinary differential equations (ODEs), in which an epidemic spreads in the prey. This model gives rise to five equilibrium points whose respective stability is discussed in Section 3.1.2. (These stability results will motivate the choice of parameters of the simulated spatio-temporal scenarios.) Then, in Section 3.1.3, we obtain the full spatio-temporal model by equipping the ODE model with diffusive terms for the prey species and a non-local convection term for predators. These ingredients are specified in detail in Section 3.1.4. Section 3.2 is devoted to the description of the numerical scheme proposed to solve the spatio-temporal model developed in Section 3.1.3. Specifically, the (standard) spatial discretization of local convection and diffusion terms is introduced in Section 2.2.1. The spatial discretization of the convolution defining the non-local predator velocities is described in Section 2.2.2. These velocities, in turn, are utilized in the definition of the final discretization of the convective flux by means of a fifth-order WENO discretization, as is detailed in Section 2.2.3. The time discretization of the complete model by an IMEX-RK scheme is outlined in Section 2.2.4. In Section 3.3, which is at the core of this second work, numerical solutions to the spatio-temporal model are presented. To motivate the choice of parameters, we focus on two equilibrium points of the three-equation ODE model of Section 3.1.1, as is briefly discussed in Section 3.3.1. In Section 3.3.2 we present a total number of 10 examples of numerical solutions of the spatio-temporal model that give rise to patterns. In Section 3.1.4 we present Example 11 that has been designed to demonstrate in a purely visual way the convergence of the numerical scheme to a definite solution upon refinement of the computational grid, while Example 12 illustrates the influence of the choice of the radius of the convolution kernel of the non-local prey velocity.

Finally in Chapter 4 we collect, conclusions, concluding observations and guidelines for future works.

1.4 Alcance de esta tesis

El Hantavirus (familia Bunyaviridae) es una enfermedad infecciosa transmitida por roedores de gran preocupación, ya que puede generar altas tasas de letalidad en la población humana [68].

La transmisión del hantavirus de los roedores infectados, el principal reservorio conocido del virus, a los humanos, generalmente ocurre por inhalación de aerosoles contaminados por virus en excrementos, saliva y orina [44]. El riesgo de infección con hantavirus en la población humana se ve facilitado por las condiciones de hacinamiento y la gran proximidad a las poblaciones de roedores. No es sorprendente que la población total en riesgo de infección por hantavirus haya aumentado con las tasas de urbanización. En América, el hantavirus representa un problema de salud pública en los países de América del Sur, incluido Chile [59]. Sin embargo, la gran mayoría de los casos de hantavirus han sido reportados en China, [77, 78]. Una mejor comprensión de la dinámica de transmisión de hantavirus en poblaciones de roedores tiene el potencial de dirigir directamente estrategias de intervenciones destinadas a minimizar el número de infecciones en la población humana.

Un primer objetivo en este trabajo, el cual se desarrolla en el Capítulo 2 es proponer al modelo compartimental espacio-temporal de infección por hantavirus en roedores con un enfoque en su solución numérica eficiente. La población total de roedores se subdivide en machos y hembras (índices m y f), y para cada una de las dos subpoblaciones una variante de la conocida modelo compartimental [40] susceptible-expuesto-infectado-recuperado (SEIR) está formulada. Los compartimientos de individuos machos y hembras son respectivamente

$$\mathcal{C}_{\mathrm{m}} := \{S_{\mathrm{m}}, E_{\mathrm{m}}, I_{\mathrm{m}}, R_{\mathrm{m}}\} \quad \text{y} \quad \mathcal{C}_{\mathrm{f}} := \{S_{\mathrm{f}}, E_{\mathrm{f}}, I_{\mathrm{f}}, R_{\mathrm{f}}\}$$

respectivamente, y el modelo final para

$$\boldsymbol{u} = (u_1, \ldots, u_8)^{\mathrm{T}} = (S_{\mathrm{m}}, E_{\mathrm{m}}, I_{\mathrm{m}}, R_{\mathrm{m}}, S_{\mathrm{f}}, E_{\mathrm{f}}, I_{\mathrm{f}}, R_{\mathrm{f}})^{\mathrm{T}}$$

como una función de la posición $\boldsymbol{x} \in \Omega$ en el tiempo $t \in \mathcal{T} := [0, T]$ sobre un dominio acotado $\Omega \subset \mathbb{R}^2$ está dado por un sistema de reacción-convección-difusión del tipo

$$\frac{\partial \boldsymbol{u}}{\partial t} + \nabla \cdot \boldsymbol{F}^{\mathrm{c}}(\boldsymbol{u}) = \boldsymbol{\mathcal{D}} \Delta \boldsymbol{u} + \boldsymbol{s}(\boldsymbol{u}),$$

provisto con condiciones iniciales y de contorno, donde los flujos convectivos $\boldsymbol{F}^{\mathrm{c}}(\boldsymbol{u})$, la matriz de difusión $\boldsymbol{\mathcal{D}}$ y el vector de términos de reacción $\boldsymbol{s}(\boldsymbol{u})$ se especifican en partes posteriormente. Se propone describir el movimiento de los individuos masculinos en una forma particular que depende no localmente de la densidad

$$N_{\mathrm{f}} = S_{\mathrm{f}} + E_{\mathrm{f}} + I_{\mathrm{f}} + R_{\mathrm{f}}$$

de hembras, en combinación con varias alternativas locales o no locales que dependen de la densidad

$$N_{\mathrm{m}} = S_{\mathrm{m}} + E_{\mathrm{m}} + I_{\mathrm{m}} + R_{\mathrm{m}}$$

de los machos. Estas alternativas dan lugar a tres modelos que serán discutidos en paralelo y que son expresados por la elección respectiva de $\boldsymbol{F}^{\mathrm{c}}(\boldsymbol{u})$. En cualquier caso, se supone que el movimiento de los individuos machos depende de manera no local de N_{f}. Todas las variantes de

(1.1) requieren de métodos numéricos que por un lado evitan la restricción de paso de tiempo severo incurridos por discretizaciones de tiempo explícitas del término de difusión $\boldsymbol{\mathcal{D}}\Delta\boldsymbol{u}$ y por otro lado permiten el cálculo eficientede flujos numéricos basados en la evaluación de datos no locales. El primer objetivo se puede lograr mediante una discretización implícita-explícita (IMEX) en combinación con una técnica basada en la Transformada rápida de Fourier (FFT) para manejar el segundo. El simulador construido de esta manera se aplica para proporcionar resultados numéricos de varios escenarios que permiten comparar las variantes del modelo.

Lo anterior, que se presenta en el Capítulo 2, ha dado lugar a la siguiente publicación:

- R. Bürger, G. Chowell, E. Gavilán, P. Mulet, and L.M. Villada, Numerical solution of a spatio-temporal gender-structured model for hantavirus infection in rodents, *Math. Biosci. Eng.*, **15** (2018), 95–123.

En general, consideramos que los modelos matemáticos son herramientas poderosas para caracterizar los cambios espacio-temporales en sistemas dinámicos complejos. Más específicamente, los modelos matemáticos se utilizan con frecuencia para obtener una nueva comprensión de la dinámica y el control de los fenómenos naturales y sociales [66]. Por ejemplo, los sistemas de modelos matemáticos son a menudo aproximaciones simples y crudas que pretenden capturar los mecanismos clave que subyacen a la dinámica de la transmisión de enfermedades infecciosas en poblaciones humanas, animales y vegetales. Dichos primeros modelos de aproximación pueden refinarse posteriormente para estudiar los efectos de factores y procesos adicionales, incluida la heterogeneidad espacial en la densidad del hospedador y sus características (por ejemplo la competencia, susceptibilidad, infectividad) así como comportamientos específicos del huésped (por ejemplo, patrones de movimiento) en respuesta a densidad del anfitrión local o prevalencia de la enfermedad.

Es el propósito del Capítulo 3 es proponer un modelo de predador-presa espacio-temporal teniendo en cuenta las presas infectadas con un enfoque particular en su solución numérica eficiente. El modelo ecoepidemiológico resultante combina varios submodelos que se han propuesto en la literatura reciente. La población de presas se describe mediante un modelo epidemiológico espacio-temporal tipo SIR similar al estudiado por Sun [67] mientras que la interacción depredador-presa sigue el tratamiento de Greenhalgh y Haque [32] (formulado en una configuración no espacial). El movimiento de depredadores se basa en el modelo de velocidad no local avanzado para el movimiento del predador en un modelo espacio-temporal predador-presa por Colombo y Rossi [22]. Ese modelo de velocidad también se usó para los compartimentos de machos en el Capítulo 2.

En términos más generales, el modelo gobernante considera una población presa con un compartimiento susceptible e infeccioso, denotado por S e I, y una variable Y que denota la población del predador. En el contexto espacio-temporal, estas variables se entienden como densidades locales que son funciones de posición $\boldsymbol{x} \in \Omega$ y tiempo $t \in \mathcal{T} := [0, T]$ en un dominio acotado $\Omega \subset \mathbb{R}^2$. El modelo final para

$$\boldsymbol{u} := (u_1, u_2, u_3)^{\mathrm{T}} := (S, I, Y)^{\mathrm{T}}, \quad \boldsymbol{u} = \boldsymbol{u}(\boldsymbol{x}, t)$$

está dado por un sistema de reacción-convección-difusión del tipo

$$\frac{\partial \boldsymbol{u}}{\partial t} + \nabla \cdot \boldsymbol{F}^{\mathrm{c}}(\boldsymbol{u}) = \boldsymbol{\mathcal{D}} \Delta \boldsymbol{u} + \boldsymbol{s}(\boldsymbol{u}),$$

provisto con condiciones iniciales y de contorno, donde los flujos convectivos $\boldsymbol{F}^{\mathrm{c}}(\boldsymbol{u})$, la matriz de difusión $\boldsymbol{\mathcal{D}}$ y el vector de términos de reacción $\boldsymbol{s}(\boldsymbol{u})$ se especifican más adelante.

Se propone describir el movimiento de los depredadores en un particular forma que depende no localmente de la densidad I de presas infectadas, mientras que el movimiento de presas infectadas y susceptibles, es decir los miembros de los compartimentos I y S, son de difusión estándar. El método numérico construido de esta manera se aplica para simular varios escenarios que permiten comparar el efecto de las condiciones iniciales y los diferentes valores de los parámetros. Los resultados numéricos exhiben una rica variedad de comportamiento, incluida la formación de patrones tomando la forma de manchas, rayas, ambas de perturbaciones aleatorias de estados estables y en un escenario que describe la invasión de un hábitat de presa por el depredador. La estructura de soluciones obtenido en este último caso son una reminiscencia de los frentes de onda permanentes.

El Capítulo 3, dio lugar a un segundo artículo, a saber:

- R. Bürger, G. Chowell, E. Gavilán, P. Mulet, and L.M. Villada, Numerical solution of a spatio-temporal predator-prey model with infected prey,*Math. Biosci. Eng.*, en revisión.

1.5 Trabajo relacionado

En primer lugar, mencionamos que las referencias generales a la propagación espacial de enfermedades infecciosas incluyen [5, 24, 49, 52, 63, 73]. La suposición básica de nuestro tratamiento, a saber, que todos los compartimentos epidemiológicos se distribuyen en todo el dominio espacial, se opone al enfoque alternativo de metapoblación que describe la estructura espacial a través de las relaciones entre una serie de subpoblaciones bien identificadas o "parches"(cf., por ejemplo [3, 6, 7, 20, 43, 70, 71]).

De hecho, la descripción de la estructura espacial al especificar explícitamente las movilidades entre "parches" es típico para caracterizar el comportamiento de los humanos, que generalmente no "se dispersan" en respuesta a estímulos ambientales (al menos no en las escalas de tiempo relativamente cortas involucradas en la modelización epidemiológica), sino que emprenden viajes dirigidos, mientras que una descripción a través de un mecanismo de convección-difusión-reacción es más adecuado para agentes infecciosos no humanos como esporas, insectos y bacterias que se dispersarían. Que la difusión se asocie principalmente con seres no humanos, es también algo respaldado por el hecho de que los tratamientos clásicos de difusión en ecología solo incluyen poblaciones no humanas (cf.[52, Ch. 13], [54]). Este punto de vista, también se asume, por ejemplo, en [24, Ch. 10]. Otras referencias al movimiento de animales y propagación de enfermedades por ecuaciones de reacción-difusión incluyen [49, 55, 62]. Además, la distinción entre los modelos de metapoblación y continuo en los modelos espaciales también se hace en los tratamientos alternativos en las Secciones 4.3 y 4.4 de Sattenspiel [63] y los Capítulos de van den Driessche [71] y

[74] en el mismo volumen. En esta última referencia, es enfatiza una ventaja decisiva del enfoque espacialmente continuo, a saber, su susceptibilidad al análisis matemático. Además, un sistema reacción-difusión basado en el modelo SIR no espacial bien conocido [40] se propone como prototipo de un modelo epidémico espacio-temporal y las suposiciones subyacentes de variantes de los modelos de reacción-difusión se discuten ampliamente, con particular referencia a un estudio de caso seminal [36, 37, 53].

Un ingrediente menos común en epidemiología matemática es el término convectivo $\nabla \cdot \boldsymbol{F}^{\mathrm{c}}(\boldsymbol{u})$. Términos de advección relacionados, para los cuales la dependencia funcional esencial para un compartimiento es

$$\boldsymbol{F}^{\mathrm{c}} = \boldsymbol{F}^{\mathrm{c}}(\boldsymbol{x}, u) = \boldsymbol{b}(\boldsymbol{x})u$$

con una velocidad dada $\boldsymbol{b}(\boldsymbol{x})$ surgen si la población estudiada se transporta (como es el caso de los agentes infecciosos transmitidos por el viento, plancton, etc.). Se propuso una motivación ligeramente diferente de los términos convectivos en [52, Ch. 14] en el contexto de un modelo de territorialidad de lobo que describe movimiento dirigido de individuos hacia una "madriguera". Sorprendentemente, sin embargo, modelos convectivos no lineales son menos comunes en aplicaciones epidemiológicas (aunque se utilizan ampliamente para describir el comportamiento humano de, digamos, tráfico y flujos peatonales [30, 35, 69]). Enfatizamos aquí que el rol principal del término convectivo en nuestro modelo es similar al de [52, Ch. 14] en que impone una preferencia en la dirección del movimiento de los individuos (machos), donde la dependencia de la dirección está determinada por convolución con datos de la población dentro de un cierto horizonte de la posición actual. Esta idea de la dependencia no local de los flujos biológicos se remonta a un modelo de predador-presa no local introducido y analizado por Colombo y Rossi [22], y para lo cual un esquema numérico para ese modelo se analiza en [61]. El esquema propuesto en ese trabajo se basa en el esquema de Lax-Friedrichs para la ecuación (hiperbólica) (2.11a) por la facilidad de demostrar propiedades de convergencia; en el primer trabajo empleamos reconstrucciones de orden ponderado esencialmente no oscilatorias (WENO) (propuestas inicialmente en [34, 48]) para lograr una precisión espacial de alto orden.

Todavía dentro del marco de los sistemas reacción-difusión de reacción (pero en versiones más simples, de lo considerado aquí), una serie de análisis cualitativos de los modelos de hantavirus están disponibles. Por ejemplo, Abramson y Kenkre [1] proponen un modelo de reacción-difusión de dos ecuaciones que es una ecuación espacial del conocido modelo susceptibles-susceptibles-infecciosos (SIS) (el supuesto población de ratones no está estructurado de ninguna otra manera), y demuestran que un solo parámetro agrupado, la capacidad de carga, esencialmente controla la dinámica del sistema; además, una distribución espacial de su valor explica la formación y la desaparición de "refugios", es decir de regiones de hábitat con condiciones favorables que influyen en los patrones espacio-temporales de hantavirus [2, 42]. Además, basado en el modelo de Abramson y Kenkre [1], Buceta et al. [18] estudian el impacto de la estacionalidad en el hantavirus, con el resultado notable de que la alternancia de las estaciones, cada una de las cuales se asocia con un conjunto constante de parámetros epidemiológicos, puede inducir el brote de infección por Hantavirus incluso si ninguna de las estaciones satisface por sí sola los requisitos ambientales para la propagación de la enfermedad [18]. El mismo grupo también investigó el

efecto del ruido intrínseco en la propagación del Hantavirus [27]. Finalmente, mencionamos que más recientemente el modelo de Abramson y Kenkre fue refinado para dar un modelo dependiente de la etapa con delay [57], donde un compartimento nuevo corresponde a ratones jóvenes libres de virus, y el nuevo modelo consta de tres ecuaciones diferenciales ordinarias con retraso, o en su reciente versión espacial presentada in [58], en un sistema de reacción-difusión con retraso (donde el operador de difusión se expresa en variables radiales).

Desde un punto de vista computacional, y volviendo a nuestro propio modelo (1.1), mencionamos que los esquemas IMEX Runge-Kutta (IMEX-RK) juegan un importante papel. Por lo tanto, proporcionamos brevemente algunos antecedentes en estos métodos. A grandes rasgos, un método IMEX-RK para una ecuación reacción-convección-difusión del tipo (1.1) consiste en un esquema de Runge-Kutta con una discretización implícita del término difusivo combinado con una explícita para los términos convectivo y reactivo. Para presentar la idea principal, consideramos el problema

$$\frac{\mathrm{d}\boldsymbol{v}}{\mathrm{d}t} = \Phi^*(\boldsymbol{v}) + \Phi(\boldsymbol{v}),$$

que se supone que representa una semi-discretización de método de líneas de (1.1), donde $\Phi^*(\boldsymbol{v})$ y $\Phi(\boldsymbol{v})$ son discretizaciones espaciales de la convectiva y términos reactivos y del término difusivo, respectivamente. Supongamos, por simplicidad, que el ancho de la malla espacial es $h > 0$ tanto en la dirección x como en y. Entonces la restricción de estabilidad en el paso de tiempo Δt que los esquemas explícitos imponen cuando se aplica a (1.3) es muy grande (Δt debe ser proporcional al cuadrado h^2 del espaciado de la cuadrícula), debido a la presencia de $\Phi(\boldsymbol{v})$. El tratamiento implícito de ambos $\Phi^*(\boldsymbol{v})$ y $\Phi(\boldsymbol{v})$ eliminaría cualquier restricción de estabilidad en Δt. Sin embargo, la discretización upwind no lineal de los términos convectivos contenidos en $\Phi^*(\boldsymbol{v})$ que se necesita para la estabilidad, hace que su tratamiento implícito esté extremadamente involucrado. Esta situación se vuelve aún más complicada debido a las reconstrucciones de WENO. De hecho, después del trabajo pionero de Crouzeix [23], integradores numéricos que trata implícitamente con $\Phi(\boldsymbol{v})$ y explícitamente con $\Phi^*(\boldsymbol{v})$ se puede usar con una restricción de paso de tiempo determinada solo por el término reactivo-convectivo. Estos esquemas, además de haber sido usados ampliamente en problemas de convección-difusión y problemas de convección con los términos de reacción rígida [8, 25], se han utilizado recientemente para tratar con términos rígidos en sistemas hiperbólicos con relajación (ver [11, 12, 13, 14, 56]). Finalmente, mencionamos que muchos autores han propuesto esquemas IMEX-RK para la solución de PDE semi-discretizadas [8, 39, 56, 80].

La extensión espacial de las enfermedades infecciosas se describe matemáticamente en una serie de monografías que incluyen [24, 49, 52, 63, 73]. La evolución temporal de las enfermedades también se trata en [16, 29]. Nuestra suposición de que todos los compartimentos epidemiológicos se distribuyen en todo el dominio espacial se opone al enfoque de metapoblación alternativa que describe la estructura espacial a través de subpoblaciones o "parches" bien identificados (cf., por ejemplo, [3, 6, 7, 20, 70, 71]). La descripción de la estructura espacial especificando explícitamente las movilidades entre "parches" es típica para caracterizar el comportamiento de los humanos que emprenden viajes dirigidos, mientras que la descripción a través de un mecanismo de convección-difusión-reacción es más adecuada para agentes infecciosos no humanos como esporas, insectos

y bacterias que se dispersarían [24, 52, 54]. En [74] se destaca una ventaja decisiva del enfoque espacialmente continuo, es decir, su susceptibilidad al análisis matemático. La introducción de [32] y Hadeler y Freedman [33] proporcionan amplias referencias a ejemplos del mundo real de sistemas ecoepidemiológicos de tres especies de presas sanas, presas infectadas y depredadores. Específicamente, en [33] se describe un modelo predador-presa en el que la presa está infectada por un parásito y la presa a su vez infecta al depredador con ese parásito. Los modelos estudiados en [32] y en dicho trabajo se basan en la suposición general de que la infección debilita a la presa y aumenta su susceptibilidad a la depredación.

1.6 Organización de esta tesis

La presentación del trabajo, se ha organizado aquí en este primer Capítulo introductorio y las dos contribuciones realizadas, la primera, "Numerical solution of a spatio-temporal gender-structured model for hantavirus infection in rodents", se presenta en el Capítulo 2 y la segunda, "Numerical solution of a spatio-temporal predator-prey model with infected prey", está presentada en el Capítulo 3. En líneas generales, los Capítulos 2 y 3 pueden describirse como sigue:

1. El modelo matemático del Capítulo 2 se presenta en la Sección 2.1, comenzando de las ecuaciones de equilibrio espacio-temporal de una estructura de género Modelo SEIR (en la Sección 2.1.1). Las tres variantes de flujos convectivos $\boldsymbol{F}^{\mathrm{c}}(\boldsymbol{u})$ y la matriz de difusión $\boldsymbol{\mathcal{D}}$ que surge en (1.1) se especifican en la Sección 2.1.2 y se muestra en la Sección 2.1.3 que el modelo material que surgió del nuestro para N_{m} y N_{f} sumando todos los compartimentos en C_{m} y C_{f}, respectivamente, se pueden comparar con el modelo predador-presa no local estudiado en [22]. En la Sección 2.2 presentamos el esquema numérico. Utilizaremos el método de líneas para obtener una semi-discretización espacial del problema de valor límite inicial de (1.1) en forma de un sistema de ecuaciones diferenciales ordinarias (ODE), a las cuales se le aplica el procedimiento de paso de tiempo para obtener el esquema numérico final. Con este fin, presentamos en la Sección 2.2.1 la malla cartesiana y las incógnitas discretas y se describe en la Sección 2.2.2 la discretización de los términos no locales como en (2.6) que aparecen en el flujo convectivo de los machos. Luego, en la Sección 2.2.3, presentamos la discretización del flujo convectivo completo para los machos. Esto se realiza esencialmente mediante la reconstrucción WENO. La discretización correspondiente para la especie hembra es similar y se omite. A continuación, en la Sección 2.2.4 describimos los integradores de tiempo IMEX-RK utilizados para resolver el sistema de ODE que representa la discretización espacial. La Sección 2.3 está dedicada a la presentación de resultados numéricos. Se introducen los preliminares en la Sección 2.3.1, que incluye una definición de las constantes que surgen en el modelo y de los escenarios iniciales. Para que nuestros resultados sean comparables con los de [4] (basados en ecuaciones diferenciales ordinarias y estocásticas), adoptamos los parámetros correspondientes a la epizoología de la rata de arroz y la Virus Bayou utilizado en ese trabajo. Por otro lado, el Escenario 1 se basa en la hipótesis que la población inicial ocupa un subdominio bien identificado de Ω y por lo tanto los resultados numéricos también abordan el fenómeno de la invasión biológica

(además de eso, la progresión de los estados epidémicos), mientras que el Escenario 2 tiene como objetivo estudiar el efecto de una perturbación aleatoria de un estado inicial constante. Los ejemplos numéricos correspondientes se presentan en las Secciones 2.3.2 y 2.3.3, respectivamente. Además, proporcionamos en la Sección 2.3.4 un ejemplo que muestra que el esquema numérico exhibe convergencia de segundo orden experimental cuando la solución es suave, y en la Sección 2.3.5 se presenta un caso de prueba que aborda el efecto de variabilidad estacional de algunos de los parámetros del modelo.

2. En la Sección 3.1 se introduce el modelo matemático gobernante del Capítulo 3. Para este fin, formulamos primero (en la Sección 3.1.1) el modelo predador-presa no espacial, definido por tres ecuaciones diferenciales ordinarias no lineales (ODE), en el que se propaga una epidemia en la presa. Este modelo da lugar a cinco puntos de equilibrio cuya estabilidad respectiva se discute en la Sección 3.1.2. (Estos resultados de estabilidad motivarán la elección de los parámetros de los escenarios espaciotemporales simulados). Luego, en la Sección 3.1.3, obtenemos el modelo espacio-temporal completo al equipar el modelo ODE con términos difusivos para la presa y una convección no local término para el depredador. Estos ingredientes se especifican en detalle en la Sección 3.1.4. La Sección 3.2 está dedicada a la descripción del esquema numérico propuesto para resolver el modelo espacio-temporal desarrollado en la Sección 3.1.3. Específicamente, la discretización espacial (estándar) de la convección local y los términos de difusión se introduce en la Sección 2.2.1. La discretización espacial de la convolución que define las velocidades de los depredadores no locales se describe en en la Sección 2.2.2. Estas velocidades, a su vez, se utilizan en la definición de la discretización final del flujo convectivo mediante una discretización WENO de quinto orden, como se detalla en la Sección 2.2.3. La discretización del tiempo del modelo completo mediante un esquema IMEX-RK que se describe en la Sección 2.2.4. En la Sección 3.3, que está en el centro de este segundo trabajo, son presentadas las soluciones numéricas al modelo espacio-temporal. Para motivar la elección de los parámetros, nos centramos en dos puntos de equilibrio del modelo ODE de tres ecuaciones de la Sección 3.1.1, como se discute brevemente en Sección 3.3.1. En la Sección 3.3.2 presentamos un número total de 10 ejemplos de soluciones numéricas del modelo espacio-temporal que dan lugar a patrones. En la Sección 3.3.3 presentamos el Ejemplo 11 que ha sido diseñado para demostrar de una manera puramente visual la convergencia del esquema numérico a una solución definitiva al refinar la malla computacional, mientras que el Ejemplo 12 ilustra la influencia de la elección del radio del kernel de convolución de la velocidad de presa no local.

Finalmente en el Capítulo 4 reunimos conclusiones, observaciones finales y directrices para trabajos futuros.

Chapter 2

Numerical solution of a spatio-temporal gender-structured model for hantavirus infection in rodents

2.1 Mathematical model

2.1.1 Gender-structured spatio-temporal SEIR model

The model for the eight unknowns in $\mathcal{C} := \mathcal{C}_{\mathrm{m}} \cup \mathcal{C}_{\mathrm{f}}$, as functions of $\boldsymbol{x}$ and t, is given as follows:

$$\frac{\partial S_{\mathrm{m}}}{\partial t} + \nabla \cdot F_{S_{\mathrm{m}}}(S_{\mathrm{m}}, N_{\mathrm{f}}, N_{\mathrm{m}}) = \frac{B(N_{\mathrm{m}}, N_{\mathrm{f}})}{2} - S_{\mathrm{m}} d(N) - S_{\mathrm{m}}(\beta_{\mathrm{f}} I_{\mathrm{f}} + \beta_{\mathrm{m}} I_{\mathrm{m}}), \tag{2.1a}$$

$$\frac{\partial E_{\mathrm{m}}}{\partial t} + \nabla \cdot F_{E_{\mathrm{m}}}(E_{\mathrm{m}}, N_{\mathrm{f}}, N_{\mathrm{m}}) = -E_{\mathrm{m}} d(N) + S_{\mathrm{m}}(\beta_{\mathrm{f}} I_{\mathrm{f}} + \beta_{\mathrm{m}} I_{\mathrm{m}}) - \delta E_{\mathrm{m}}, \tag{2.1b}$$

$$\frac{\partial I_{\mathrm{m}}}{\partial t} + \nabla \cdot F_{I_{\mathrm{m}}}(I_{\mathrm{m}}, N_{\mathrm{f}}, N_{\mathrm{m}}) = \delta E_{\mathrm{m}} - I_{\mathrm{m}} d(N) - \gamma_{\mathrm{m}} I_{\mathrm{m}}, \tag{2.1c}$$

$$\frac{\partial R_{\mathrm{m}}}{\partial t} + \nabla \cdot F_{R_{\mathrm{m}}}(R_{\mathrm{m}}, N_{\mathrm{f}}, N_{\mathrm{m}}) = \gamma_{\mathrm{m}} I_{\mathrm{m}} - R_{\mathrm{m}} d(N), \tag{2.1d}$$

$$\frac{\partial S_{\mathrm{f}}}{\partial t} - \nabla \cdot \left(\mu_{S_{\mathrm{f}}} \nabla S_{\mathrm{f}}\right) = \frac{B(N_{\mathrm{m}}, N_{\mathrm{f}})}{2} - S_{\mathrm{f}} d(N) - S_{\mathrm{f}}(\beta_{\mathrm{f}} I_{\mathrm{f}} + \beta_{\mathrm{m,f}} I_{\mathrm{m}}), \tag{2.1e}$$

$$\frac{\partial E_{\mathrm{f}}}{\partial t} - \nabla \cdot \left(\mu_{E_{\mathrm{f}}} \nabla E_{\mathrm{f}}\right) = -E_{\mathrm{f}} d(N) + S_{\mathrm{f}}(\beta_{\mathrm{f}} I_{\mathrm{f}} + \beta_{\mathrm{m,f}} I_{\mathrm{m}}) - \delta E_{\mathrm{f}}, \tag{2.1f}$$

$$\frac{\partial I_{\mathrm{f}}}{\partial t} - \nabla \cdot \left(\mu_{I_{\mathrm{f}}} \nabla I_{\mathrm{f}}\right) = \delta E_{\mathrm{f}} - I_{\mathrm{f}} d(N) - \gamma_{\mathrm{f}} I_{\mathrm{f}}, \tag{2.1g}$$

$$\frac{\partial R_{\mathrm{f}}}{\partial t} - \nabla \cdot \left(\mu_{R_{\mathrm{f}}} \nabla R_{\mathrm{f}}\right) = \gamma_{\mathrm{f}} I_{\mathrm{f}} - R_{\mathrm{f}} d(N), \tag{2.1h}$$

where $\nabla\cdot$ denotes the (spatial) divergence operator. The right-hand sides of (2.1) are identical to that of the non-spatial model proposed in [4], i.e., this model, to which we refer as Model 0 for ease of reference, is recovered if all divergence terms on the left-hand sides are set to zero and variables are considered to depend on t only, and the unknowns represent suitably scaled densities. In particular $d(N)$ is the density-dependent death rate, β_{f} is the contact rate of an infective female with either a susceptible female or a susceptible male, $\beta_{\mathrm{m,f}}$ is the contact rate of an infective male with a susceptible female, β_{m} is the contact rate of an infective male with a susceptible male, δ is the inverse of the average length of the incubation period (assumed to be the same for males and females), and γ_{m} and γ_{f} are the inverse of average length of the infectious periods for males and females, respectively. Following [4], we assume a harmonic birth function,

$$B(N_{\mathrm{m}}, N_{\mathrm{f}}) = \frac{2bN_{\mathrm{m}}N_{\mathrm{f}}}{N_{\mathrm{m}} + N_{\mathrm{f}}},$$

where b is the average litter size, and regarding the contact rates and infectious periods, we assume

$$\beta_{\mathrm{m}} \geq \beta_{\mathrm{m,f}} \geq \beta_{\mathrm{f}} \quad \text{and} \quad \gamma_{\mathrm{f}} > \gamma_{\mathrm{m}}.$$

The incubation period is the same for males and females (namely $1/\delta$), as is the density-dependent death rate

$$d(N) = a + cN,$$

where $0 < a < b/2$ and $c > 0$.

2.1.2 Convective fluxes and diffusion matrix

The fluxes appearing in the left-hand sides of the full spatio-temporal model (2.1) have two components for the male compartments, and one for the female compartments. Several alternative choices of F_X for the males in compartment $X \in \mathcal{C}_{\mathrm{m}}$ will be considered in parallel and compared. Model 1 is given by (2.1) along with

$$F_X(X, N_{\mathrm{f}}, N_{\mathrm{m}}) = X\big(\kappa_X \boldsymbol{V}(N_{\mathrm{f}}) - \mu_X \boldsymbol{V}(N_{\mathrm{m}})\big), \tag{2.2}$$

where $\kappa_X \geq 0$ and $\mu_X \geq 0$ are constants and $\boldsymbol{V}$ is a non-local velocity function that will be specified below. Model 2 is given by (2.1) in combination with

$$F_X(X, N_{\mathrm{f}}, N_{\mathrm{m}}) = X\varphi(N_{\mathrm{m}} + N_{\mathrm{f}})\big(\kappa_X \boldsymbol{V}(N_{\mathrm{f}}) - \mu_X \boldsymbol{V}(N_{\mathrm{m}})\big), \tag{2.3}$$

where the function φ is given by

$$\varphi(u) = \begin{cases} 1 - u/K & \text{for } 0 \leq u \leq K, \\ 0 & \text{for } u < 0 \text{ or } u > K, \end{cases} \tag{2.4}$$

where K is a maximum value (carrying capacity) of the total density. Finally, we consider Model 3 that is given by

$$F_X(X, N_\mathrm{f}, N_\mathrm{m}) = X\kappa_X \boldsymbol{V}(N_\mathrm{f}) - \mu_X \nabla X, \tag{2.5}$$

where ∇X is the spatial gradient of X.

The non-local unscaled velocity $\boldsymbol{V}$ is defined as

$$\boldsymbol{V}(w) = \frac{\nabla(w * \eta)}{\sqrt{1 + \|\nabla(w * \eta)\|^2}}, \tag{2.6}$$

where η denotes a radial convolution kernel with radius ε, i.e., η is a piecewise smooth function such that

$$\eta(\boldsymbol{x}) = \eta(\|\boldsymbol{x}\|_2),\ \eta(\boldsymbol{x}) \geq 0\,, \eta(\boldsymbol{x}) = 0 \quad \text{for} \quad \|\boldsymbol{x}\| > \varepsilon, \quad \text{and} \int_{\mathbb{R}^2} \eta(\boldsymbol{x})\,\mathrm{d}\boldsymbol{x} = 1$$

i.e., for any function w defined on $\Omega \times \mathcal{T}$ and $\boldsymbol{x} \in \Omega$ such that

$$B_\varepsilon(\boldsymbol{x}) := \{\boldsymbol{y} \in \mathbb{R}^2 : \|\boldsymbol{y} - \boldsymbol{x}\| < \varepsilon\} \subset \Omega,$$

we have

$$(w(\cdot, t) * \eta)(\boldsymbol{x}) = \int_{B_\varepsilon(\boldsymbol{x})} w(\boldsymbol{y}, t)\eta(\boldsymbol{x} - \boldsymbol{y})\,\mathrm{d}\boldsymbol{y} = \int_{\mathbb{R}^2} w(\boldsymbol{y}, t)\eta(\boldsymbol{x} - \boldsymbol{y})\,\mathrm{d}\boldsymbol{y}.$$

(This definition will be modified slightly for points $\boldsymbol{x}$ with $\mathrm{dist}(\boldsymbol{x}, \partial\Omega) < \varepsilon$.) It is worth recalling that

$$\nabla(w * \eta) = w * \nabla\eta, \tag{2.7}$$

so that $\boldsymbol{V}(w)$ indeed depends (non-locally) on w and not on its gradient.

The non-local velocity function (2.6) was introduced recently in a two-species predator-prey model by Colombo and Rossi [22], for which convergence of a numerical scheme was proved by Rossi and Schleper [61]. The evaluation of this velocity function at $w = N_\mathrm{f}$ in the equations for male individuals describes that males are attracted by females since the corresponding biological fluxes $\kappa_C \boldsymbol{V}(N_\mathrm{f})$, $C \in \mathcal{C}_\mathrm{m}$, are directed toward increasing densities of females. The movement of male individuals to females is balanced by a term that describes that males avoid groups of their own gender. This is achieved in Models 1 and 2 by another evaluation of the nonlocal function but this time at $w = N_\mathrm{m}$, and with a coefficient, namely $-\mu_X$, of opposite sign (see (2.2) and (2.3)), while in Model 3 the movement of males away from regions of large densities of their group is described by diffusive movement through the term $-\mu_X \nabla X$ (see (2.5)). The biological movement of females is standard diffusion.

Summarizing, we obtain that the convective fluxes $\boldsymbol{F}^\mathrm{c}(\boldsymbol{u})$ and the diffusion matrix $\boldsymbol{\mathcal{D}}$ arising in (1.1) are given by the respective expressions

$$\begin{aligned}
\boldsymbol{F}^\mathrm{c}(\boldsymbol{u}) &= \big(F_{S_\mathrm{m}}(S_\mathrm{m}, N_\mathrm{f}, N_\mathrm{m}), F_{E_\mathrm{m}}(E_\mathrm{m}, N_\mathrm{f}, N_\mathrm{m}), F_{I_\mathrm{m}}(I_\mathrm{m}, N_\mathrm{f}, N_\mathrm{m}), F_{R_\mathrm{m}}(R_\mathrm{m}, N_\mathrm{f}, N_\mathrm{m}), 0, 0, 0, 0\big)^\mathrm{T}, \\
\boldsymbol{\mathcal{D}} &= \mathrm{diag}(0, 0, 0, 0, \mu_{S_\mathrm{f}}, \mu_{E_\mathrm{f}}, \mu_{I_\mathrm{f}}, \mu_{R_\mathrm{f}}),
\end{aligned}$$

when the definition of the fluxes is (2.2) (Model 1) or (2.3) , (2.4) (Model 2), and

$$\begin{aligned} \boldsymbol{F}^{\mathrm{c}}(\boldsymbol{u}) &= \big(S_{\mathrm{m}}\kappa_{S_{\mathrm{m}}}\boldsymbol{V}(N_{\mathrm{f}}), E_{\mathrm{m}}\kappa_{E_{\mathrm{m}}}\boldsymbol{V}(N_{\mathrm{f}}), I_{\mathrm{m}}\kappa_{I_{\mathrm{m}}}\boldsymbol{V}(N_{\mathrm{f}}), R_{\mathrm{m}}\kappa_{R_{\mathrm{m}}}\boldsymbol{V}(N_{\mathrm{f}}), 0, 0, 0, 0\big)^{\mathrm{T}}, \\ \boldsymbol{\mathcal{D}} &= \mathrm{diag}(\mu_{S_{\mathrm{m}}}, \mu_{E_{\mathrm{m}}}, \mu_{I_{\mathrm{m}}}, \mu_{R_{\mathrm{m}}}, \mu_{S_{\mathrm{f}}}, \mu_{E_{\mathrm{f}}}, \mu_{I_{\mathrm{f}}}, \mu_{R_{\mathrm{f}}}), \end{aligned} \tag{2.8}$$

for the definition of the fluxes (2.5) (Model 3). In all cases, the vector of reaction terms $\boldsymbol{s}(\boldsymbol{u}) = (s_1(\boldsymbol{u}), \dots, s_8(\boldsymbol{u}))^{\mathrm{T}}$ is given by the right-hand sides of (2.1), i.e.,

$$s_1(\boldsymbol{u}) = \frac{B(N_{\mathrm{m}}, N_{\mathrm{f}})}{2} - S_{\mathrm{m}}d(N) - S_{\mathrm{m}}(\beta_{\mathrm{f}}I_{\mathrm{f}} + \beta_{\mathrm{m}}I_{\mathrm{m}}), \dots, s_8(\boldsymbol{u}) = \gamma_{\mathrm{f}}I_{\mathrm{f}} - R_{\mathrm{f}}d(N).$$

The system (2.1) is considered on $\Omega \times \mathcal{T}$ together with the initial condition

$$\boldsymbol{u}(\boldsymbol{x}, 0) = \boldsymbol{u}_0(\boldsymbol{x}), \quad \boldsymbol{x} \in \Omega, \tag{2.9}$$

where $\boldsymbol{u}_0$ is a given function, and zero-flux boundary conditions

$$\big(\boldsymbol{F}^{\mathrm{c}}(\boldsymbol{u}) - \boldsymbol{\mathcal{D}}\nabla\boldsymbol{u}\big) \cdot \boldsymbol{n} = \boldsymbol{0}, \quad \boldsymbol{x} \in \partial\Omega, \quad t \in (0, T], \tag{2.10}$$

where $\boldsymbol{n}$ is the unit exterior normal vector to the boundary $\partial\Omega$ of Ω.

2.1.3 Comparison with the model by Colombo and Rossi [22]

Assume that the convective fluxes $\boldsymbol{F}^{\mathrm{c}}(\boldsymbol{u})$ and the diffusion matrix $\boldsymbol{D}$ are given by (2.8) according to Model 3, and that $\kappa_C = \kappa_{\mathrm{m}}$ and $\mu_C = \mu_{\mathrm{m}}$ for all $C \in \mathcal{C}_{\mathrm{m}}$ and $\mu_C = \mu_{\mathrm{f}}$ for all $C \in \mathcal{C}_{\mathrm{f}}$. Then, summing (2.1a)–(2.1d) and (2.1e)–(2.1h), respectively, we get the two equations

$$\frac{\partial N_{\mathrm{m}}}{\partial t} + \nabla \cdot \big(\kappa_{\mathrm{m}}N_{\mathrm{m}}\boldsymbol{V}(N_{\mathrm{f}}) - \mu_{\mathrm{m}}\nabla N_{\mathrm{m}}\big) = \frac{B(N_{\mathrm{m}}, N_{\mathrm{f}})}{2} - N_{\mathrm{m}}d(N_{\mathrm{m}} + N_{\mathrm{f}}), \tag{2.11a}$$

$$\frac{\partial N_{\mathrm{f}}}{\partial t} - \mu_{\mathrm{f}}\Delta N_{\mathrm{f}} = \frac{B(N_{\mathrm{m}}, N_{\mathrm{f}})}{2} - N_{\mathrm{f}}d(N_{\mathrm{m}} + N_{\mathrm{f}}). \tag{2.11b}$$

This model is similar to the non-local predator-prey model recently analyzed by Colombo and Rossi [22]. In fact, their model is precisely recovered if we identify N_{m} as the density of "predators", N_{f} as that of "prey", set $\kappa_{\mathrm{m}} = 1$ and $\mu_{\mathrm{m}} = 0$, and replace the right-hand sides of (2.11a) and (2.11b) by the respective expressions $(\alpha N_{\mathrm{f}} - \beta)N_{\mathrm{m}}$ and $(\gamma - \delta N_{\mathrm{m}})N_{\mathrm{f}}$, with positive constants $\alpha, \beta, \gamma, \delta$, of the well-known Lotka-Volterra predator-prey kinetics [15].

2.2 Numerical scheme

2.2.1 Discretization of local convection and diffusion terms

We take $\Omega = [0, L] \times [0, L]$ and use a Cartesian grid with nodes (x_i, y_j), $i, j = 1, \dots, M$, with $x_i = y_i = (i - 1/2)h$, $h = L/M$.

We discretize $\nabla \cdot \boldsymbol{F}^{\mathrm{c}}(\boldsymbol{u})$ on this grid by weighted essentially non-oscillatory (WENO) finite differences and $\Delta \boldsymbol{u}$ by the standard second-order scheme with a five-point stencil to get a spatial semi-discretization of (1.1) for an $8 \times M \times M$-matrix $\boldsymbol{v}(t)$ of unknown approximations

$$\boldsymbol{v}_{\ell,i,j}(t) \approx u_\ell(x_i, y_j, t), \quad i,j = 1,\dots,M, \quad \ell = 1,\dots,8$$

given by

$$\boldsymbol{v}' = -\nabla_h \cdot \widetilde{\boldsymbol{F}}^{\mathrm{c}}(\boldsymbol{v}) + \boldsymbol{\mathcal{B}}\boldsymbol{v} + \boldsymbol{S}(\boldsymbol{v}), \tag{2.12}$$

to which suitable implicit-explicit Runge-Kutta (IMEX-RK) schemes will be applied for obtaining the final fully-discrete scheme (see Section **??**). In this equation $\nabla_h \cdot \widetilde{\boldsymbol{F}}^{\mathrm{c}}(\boldsymbol{v})$ is the discretization of $\nabla \cdot \boldsymbol{F}^{\mathrm{c}}(\boldsymbol{u})$, to be defined in Section **??**, and

$$(\boldsymbol{\mathcal{B}}\boldsymbol{v})_{\ell,i,j} = \mu_\ell(\boldsymbol{\Delta}_h \boldsymbol{v}_\ell)_{i,j}, \quad i,j = 1,\dots,M, \quad \ell = 1,\dots,8 \tag{2.13}$$

is the discretization of the diffusion terms. Notice that we take $\mu_\ell = 0$ for $\ell \in \{1,2,3,4\}$ and models (2.2) or (2.3), for these models do not have diffusion for male species. Here we have used the notation $\boldsymbol{v}_\ell$ for the $M \times M$ submatrix given by $(\boldsymbol{v}_\ell)_{i,j} = \boldsymbol{v}_{\ell,i,j}$ and $\boldsymbol{\Delta}_h$ for the standard two-dimensional Laplacian operator with Neumann boundary conditions. Furthermore, $\boldsymbol{S}(\boldsymbol{v})$ is the $8 \times M \times M$-matrix with components

$$\boldsymbol{S}(\boldsymbol{v})_{\ell,i,j} = s_\ell(\boldsymbol{v}_{\ell,i,j}), \quad i,j = 1,\dots,M, \quad \ell = 1,\dots,8,$$

with corresponding submatrices $\boldsymbol{S}_\ell(\boldsymbol{v})$, given by

$$\boldsymbol{S}_\ell(\boldsymbol{v})_{i,j} = s_\ell(\boldsymbol{v}_{\ell,i,j}). \tag{2.14}$$

We explain the discretization of the convective term appearing in (2.12) in the next two subsections.

2.2.2 Discretization of the convolutions

We will use the following identity for the implementation that arises from (2.6) if we take into account (2.7):

$$\boldsymbol{V}(w) = \frac{w * \boldsymbol{\nu}}{\sqrt{1 + \|w * \nu\|^2}}, \quad \boldsymbol{\nu} = \left(\frac{\partial \eta}{\partial x}, \frac{\partial \eta}{\partial y}\right). \tag{2.15}$$

The convolutions $w * \chi$, $\chi = \partial\eta/\partial x$ or $\chi = \partial\eta/\partial y$, namely

$$(w * \chi)(\boldsymbol{x}) = \int_{B_\varepsilon(0)} w(\boldsymbol{x} - \boldsymbol{y})\chi(\boldsymbol{y})\,\mathrm{d}\boldsymbol{y},$$

are calculated approximately on the discrete grid via a composite Newton-Cotes quadrature formula, such as the composite Simpson rule.

Since $B_\varepsilon(0) \subseteq [-rh, rh]^2$, $r = \lceil \varepsilon/h \rceil < M$, and considering that, according to boundary conditions, w is extended to the exterior of Ω by reflection, e.g. by setting $w(-x, y) = w(x, y)$, $(x, y) \in \Omega$, we obtain

$$\begin{aligned}(w * \chi)(x_i, y_j) &= \int_{-rh}^{rh} \int_{-rh}^{rh} w(x_i - x, y_j - y)\chi(x, y)\,\mathrm{d}x\,\mathrm{d}y \\ &\approx h^2 \sum_{p=-r}^{r} \sum_{q=-r}^{r} \alpha_p \alpha_q w(x_i - x_p, y_j - y_q)\chi(x_p, y_q),\end{aligned}$$

where α_p and α_q are the coefficients in the quadrature rule (e.g., for the composite Simpson rule, $\boldsymbol{\alpha} = (1, 4, 2, 4, \ldots, 2, 4, 1)$). This can be written as

$$(w * \chi)(x_i, y_j) \approx \sum_{p=-r}^{r} \sum_{q=-r}^{r} \beta_{p,q} w(x_{i-p}, y_{j-q}), \quad \beta_{p,q} = h^2 \alpha_p \alpha_q \chi(x_p, y_q). \tag{2.16}$$

The accuracy order of this approximation is given by that of the quadrature rule, e.g., it is fourth-order accurate for the composite Simpson rule. Consequently, the approximation (2.16) for $\boldsymbol{W} = (w_{i,j}) \in \mathbb{R}^{M \times M}$, $w_{i,j} \approx w(x_i, y_j)$, is given by

$$(w * \chi)(x_i, y_j) \approx (\boldsymbol{W} *_h \beta)_{i,j} := \sum_{p=-r}^{r} \sum_{q=-r}^{r} \beta_{p,q} w_{[i-p]_M, [j-q]_M}, \tag{2.17}$$

where we define

$$[i]_M := \begin{cases} -i + 1 & \text{for } -r + 1 \le i \le 0, \\ i & \text{for } 1 \le i \le M, \\ 2M + 1 - i & \text{for } M + 1 \le i \le M + r. \end{cases}$$

The discrete approximation of $\boldsymbol{V}(w)$ in (2.15) obtained from the approximation $\boldsymbol{W} \approx w$ is given by

$$\boldsymbol{V}_h(\boldsymbol{W}) = \frac{\boldsymbol{W} *_h \boldsymbol{\nu}}{\sqrt{1 + \|\boldsymbol{W} *_h \nu\|^2}}, \quad \boldsymbol{\nu} = \left(\frac{\partial \eta}{\partial x}, \frac{\partial \eta}{\partial y} \right).$$

Since $r \approx \varepsilon/h = \varepsilon M/L$, the computational cost of this discrete convolution is $M^2(2r + 1)^2 \approx 4\varepsilon^2 M^4/L^2$, which can be very high for large M. This cost can be substantially reduced to $\mathcal{O}(M^2 \log M)$ by performing a convolution with periodic data by Fast Fourier Transforms (FFTs) (see [65, 38]). To achieve this goal, we define from $\boldsymbol{W} = (w_{i,j}) \in \mathbb{R}^{M \times M}$ a matrix $\widetilde{\boldsymbol{W}} = (\tilde{w}_{i,j}) \in \mathbb{R}^{2M \times 2M}$ such that

$$\tilde{w}_{i,j} = w_{[i]_M, [j]_M}, \quad i, j = 1, \ldots, 2M$$

and use the notation $[i]'_{2M} = i + 2kM$, with k being the integer such that $1 \le [i]'_{2M} \le 2M$. With this notation it is readily checked that

$$w_{[i]_M,[j]_M} = \tilde{w}_{[i]'_{2M},[j]'_{2M}}, \quad i,j = -r+1,\dots,M+r.$$

Therefore (2.17) for $i,j = 1,\dots,M$ can be rewritten as

$$(\boldsymbol{W} *_h \beta)_{i,j} = \sum_{p=-r}^{r}\sum_{q=-r}^{r} \beta_{p,q}\tilde{w}_{[i-p]'_{2M},[j-q]'_{2M}}. \tag{2.18}$$

The convolution on the right-hand side of (2.18) can be performed by FFTs applied to the $(2M)\times(2M)$ matrix $\widetilde{\boldsymbol{W}}$. To save further computational costs, the FFT of the kernel $\beta_{p,q}$ is performed only once, son each convolution entails two two-dimensional FFT of $(2M)\times(2M)$ matrices and a product of $4M^2$ numbers, with an overall computational cost of $\mathcal{O}(M^2\log M)$.

2.2.3 Discretization of the convective term

The convective flux for the ℓ (female) species, $\ell \in \{5,6,7,8\}$, is zero and the convective flux for the ℓ (male) species, $\ell \in \{1,2,3,4\}$, in e.g., model (2.2) is given by

$$\boldsymbol{F}^c_\ell(\boldsymbol{u}) = \boldsymbol{u}_\ell\big(\kappa_\ell \boldsymbol{V}\,(u_5+u_6+u_7+u_8) - \mu_\ell \boldsymbol{V}\,(u_1+u_2+u_3+u_4)\big).$$

To discretize its divergence $\nabla\cdot\boldsymbol{F}^c_\ell(\boldsymbol{u})$, for the approximation $\boldsymbol{v}$, we first approximate the convolution terms as expounded in Section **??** to obtain

$$\widetilde{\boldsymbol{F}}^c_\ell(\boldsymbol{v})_{i,j} = \boldsymbol{v}_{\ell,i,j}\big(\kappa_\ell \boldsymbol{V}_h\,(v_5+v_6+v_7+v_8)_{i,j} - \mu_\ell \boldsymbol{V}_h\,(v_1+v_2+v_3+v_4)_{i,j}\big) \in \mathbb{R}^2.$$

Similar arguments are carried out for the other models (2.3) and (2.5).

We introduce the following notation

$$\big(f^x_{i,j}, f^y_{i,j}\big) := \widetilde{\boldsymbol{F}}^c_\ell(\boldsymbol{v})_{i,j},$$

where we have dropped the ℓ index for obtaining clearer expressions.

Our purpose is to use a fifth-order WENO finite difference discretization [64, 48, 34] of $\nabla\cdot\boldsymbol{F}^c_\ell(\boldsymbol{u})$ for which

$$\nabla\cdot\boldsymbol{F}^c_\ell(\boldsymbol{u})(x_i,y_j) \approx \nabla_h\cdot\tilde{\boldsymbol{F}}^c(\boldsymbol{v})_{\ell,i,j} := \frac{\hat{f}^x_{i+1/2,j} - \hat{f}^x_{i-1/2,j}}{h} + \frac{\hat{f}^y_{i,j+1/2} - \hat{f}^y_{i,j-1/2}}{h}, \tag{2.19}$$

for suitable numerical fluxes $\hat{f}^x_{i+1/2,j}, \hat{f}^y_{i,j+1/2}$ obtained by WENO reconstructions of split fluxes. For the numerical flux in the x-direction, the Lax-Friedrichs-type flux splitting $f^{x,\pm}$ is given by:

$$f^{x,\pm}_{i,j} = \frac{1}{2}\big(f^x_{i,j} \pm \alpha^x v_{\ell,i,j}\big), \quad \alpha^x = \max_{i,j}|\boldsymbol{V}^x_h(\boldsymbol{v})_{i,j}|.$$

Likewise, the numerical flux $\hat{f}^y_{i,j+1/2}$ is obtained by WENO reconstructions of split fluxes given by

$$f^{y,\pm}_{i,j} = \frac{1}{2}\big(f^y_{i,j} \pm \alpha^y v_{\ell,i,j}\big), \quad \alpha^y = \max_{i,j} |\boldsymbol{V}^y_h(\boldsymbol{v})_{i,j}|.$$

If $\mathcal{R}^\pm$ denotes fifth-order WENO upwind biased reconstructions, then

$$\begin{aligned}\hat{f}^x_{i+1/2,j} &= \mathcal{R}^+\big(f^{x,+}_{i-2:i+2,j}\big) + \mathcal{R}^-\big(f^{x,-}_{i-1:i+3,j}\big),\\ \hat{f}^y_{i,j+1/2} &= \mathcal{R}^+\big(f^{y,+}_{i,j-2:j+2}\big) + \mathcal{R}^-\big(f^{y,-}_{i,j-1:j+3}\big),\end{aligned}$$

where we have used matlab-type notation for submatrices.

2.2.4 Implicit-Explicit Runge-Kutta schemes

We will use IMEX-RK integrators for ODEs, for which only the diffusion term will be treated implicitly, so we rewrite (2.12) as (1.3), where

$$\Phi^*(\boldsymbol{v}) := -\nabla_h \cdot \widetilde{\boldsymbol{F}}^{\mathrm{c}}(\boldsymbol{v}) + \boldsymbol{S}(\boldsymbol{v}), \qquad \Phi(\boldsymbol{v}) := \boldsymbol{\mathcal{B}}\boldsymbol{v}. \tag{2.20}$$

For the diffusive part $\Phi(\boldsymbol{v})$ we utilize an implicit s-stage diagonally implicit (DIRK) scheme with coefficients $\boldsymbol{A} \in \mathbb{R}^{s\times s}$, $\boldsymbol{b}, \boldsymbol{c} \in \mathbb{R}^s$, in the common Butcher notation, where $\boldsymbol{A} = (a_{ij})$ with $a_{ij} = 0$ for $j > i$. For the term $\Phi^*(\boldsymbol{v})$ containing the convective and reactive parts we employ an s-stage explicit scheme with coefficients $\hat{\boldsymbol{A}} \in \mathbb{R}^{s\times s}$, $\hat{\boldsymbol{b}}$, $\hat{\boldsymbol{c}} \in \mathbb{R}^s$ and $\hat{\boldsymbol{A}} = (\hat{a}_{ij})$ with $\hat{a}_{ij} = 0$ for $j \geq i$. We will denote the corresponding Butcher arrays by

$$\boldsymbol{D} := \begin{array}{c|c} \boldsymbol{c} & \boldsymbol{A} \\ \hline & \boldsymbol{b}^{\mathrm{T}} \end{array}, \qquad \hat{\boldsymbol{D}} := \begin{array}{c|c} \hat{\boldsymbol{c}} & \hat{\boldsymbol{A}} \\ \hline & \hat{\boldsymbol{b}}^{\mathrm{T}} \end{array}.$$

In our simulations, we limit ourselves to the second-order IMEX-RK scheme H-DIRK2(2,2,2) that corresponds to

$$\boldsymbol{D} = \begin{array}{c|cc} 1/2 & 1/2 & 0 \\ 1/2 & 0 & 1/2 \\ \hline & 1/2 & 1/2 \end{array}, \qquad \hat{\boldsymbol{D}} = \begin{array}{c|cc} 0 & 0 & 0 \\ 1 & 1 & 0 \\ \hline & 1/2 & 1/2 \end{array}.$$

Alternative choices are provided and discussed in [10, 11, 56]. If applied to the equation (1.3), the IMEX-RK scheme gives rise to the following algorithm (see [56]).

Algorithm 2.2.1.

Input: *approximate solution vector* $\boldsymbol{v}^n$ *of* (1.3) *for* $t = t^n$

for $p = 1, \ldots, s$

if $p = 1$ *then*

$$\hat{\boldsymbol{v}}^{(1)} \leftarrow \boldsymbol{v}^n, \quad \bar{\boldsymbol{v}}^{(1)} \leftarrow \boldsymbol{v}^n$$

else *compute* $\hat{\boldsymbol{v}}^{(p)}$ *and* $\bar{\boldsymbol{v}}^{(p)}$ *from the known values* $\boldsymbol{K}_1, \ldots, \boldsymbol{K}_{p-1}$*:*

$$\hat{\boldsymbol{v}}^{(p)} \leftarrow \boldsymbol{v}^n + \Delta t \sum_{j=1}^{p-1} \hat{a}_{pj} \boldsymbol{K}_j, \quad \bar{\boldsymbol{v}}^{(p)} \leftarrow \boldsymbol{v}^n + \Delta t \sum_{j=1}^{p-1} a_{pj} \boldsymbol{K}_j$$

endif

solve for $\boldsymbol{K}_p$ *the linear system*

$$\boldsymbol{K}_p = \Phi^*\big(\hat{\boldsymbol{v}}^{(p)}\big) + \Phi\big(\bar{\boldsymbol{v}}^{(p)} + \Delta t a_{pp} \boldsymbol{K}_p\big) \tag{2.21}$$

endfor

$$\boldsymbol{v}^{n+1} \leftarrow \boldsymbol{v}^n + \Delta t \sum_{j=1}^{s} b_j \boldsymbol{K}_j$$

Output: *approximate solution vector* $\boldsymbol{v}^{n+1}$ *of* (1.3) *for* $t = t^{n+1} = t^n + \Delta t$.

To solve the linear equation (2.21) that arises in Algorithm 2.2.1 for $\boldsymbol{K}_p$, in view of (2.20), we rewrite it as

$$\big(\boldsymbol{I} - \Delta t a_{pp} \boldsymbol{\mathcal{B}}\big) \boldsymbol{K}_p = \boldsymbol{b}^{(p)}, \quad \boldsymbol{b}^{(p)} := \Phi^*\big(\hat{\boldsymbol{v}}^{(p)}\big) + \boldsymbol{\mathcal{B}} \bar{\boldsymbol{v}}^{(p)}, \tag{2.22}$$

where $\boldsymbol{I}$ denotes the identity operator for $8 \times M \times M$ matrices. From the definition of the matrix $\boldsymbol{\mathcal{B}}$ in (2.13) and from the definition of Φ^* in (2.20), if we equate the ℓ submatrices along the first dimension of both sides of (2.22) we get

$$\big(\boldsymbol{I}_{M\times M} - \Delta t a_{pp} \mu_\ell \boldsymbol{\Delta}_h\big)(\boldsymbol{K}_p)_\ell = -\nabla_h \cdot \tilde{\boldsymbol{F}}^{\mathrm{c}}_\ell(\hat{\boldsymbol{v}}^{(p)}) + \boldsymbol{S}_\ell(\hat{\boldsymbol{v}}^{(p)}) + \mu_\ell \boldsymbol{\Delta}_h \bar{\boldsymbol{v}}^{(p)}_\ell, \quad \ell = 1, \ldots, 8, \tag{2.23}$$

where $\boldsymbol{I}_{M\times M}$ is the identity operator on $M \times M$ matrices and, e.g., $(\boldsymbol{K}_p)_\ell$ is the ℓ submatrix of $\boldsymbol{K}_p$ along the first dimension, i.e., $((\boldsymbol{K}_p)_\ell)_{i,j} = (\boldsymbol{K}_p)_{\ell,i,j}$. Some remarks are due here to detail the final implementation: for $\ell = 1, \ldots, 8$, the right hand side of (2.23) is computed from (2.14), (2.13) and (2.19), taking into account that

$$\nabla_h \cdot \tilde{\boldsymbol{F}}^{\mathrm{c}}_\ell(\hat{\boldsymbol{v}}^{(p)}) = 0 \quad \text{for } \ell \in \{5, 6, 7, 8\}$$

(i.e., there is no convection in the models for females); if $\mu_\ell = 0$ (for $\ell \in \{1, 2, 3, 4\}$ and models (2.2) and (2.3) there is no diffusion term for males), then

$$(\boldsymbol{K}_p)_\ell = -\big(\nabla_h \cdot \tilde{\boldsymbol{F}}^{\mathrm{c}}(\hat{\boldsymbol{v}}^{(p)})\big)_\ell + \boldsymbol{S}_\ell(\boldsymbol{v}),$$

otherwise the solution of (2.23) is performed by Fast Cosine Transforms (due to boundary conditions), which entails a nearly optimal computational cost of $\mathcal{O}(M^2 \log M)$.

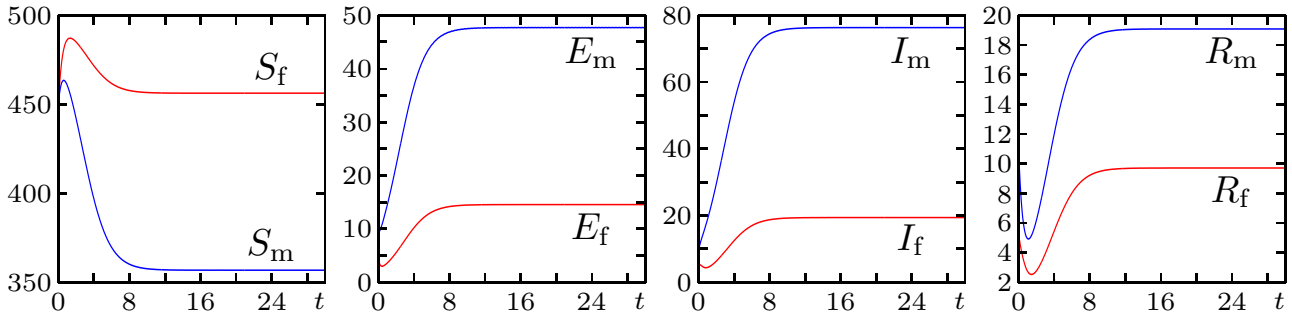

Figure 2.1: Numerical solution of the ODE version of (2.1), Model 0, for the initial data (2.24) (figure produced by author).

2.3 Numerical examples

2.3.1 Preliminaries

According to [4], we assume that two months (60 days) is the basic time unit, $\delta = 4$ ($1/\delta = 15\,\mathrm{days}$), $b = 4$ (average litter size), $\beta_\mathrm{m} = 5\beta_\mathrm{f}$, and $\beta_\mathrm{m,f} = \beta_\mathrm{f}$. Moreover, the infectious period for males is assumed to be twice that of females ($1/\gamma_\mathrm{m} = 2/\gamma_\mathrm{f}$), and the carrying capacity is $K = 1000$ animals. Furthermore, we set $\beta_\mathrm{m} = 0.01$, $\gamma_\mathrm{m} = 0.5$, $a = 0.01$ and $c = 1.99 \times 10^{-3}$. For these values, the next-generation-matrix method [72] employed in [4] yields a basic reproductive ratio $\mathcal{R}_0 = 1.38$.

We wish to present numerical solutions of the versions of the spatio-temporal model, Models 1 to 3, that can be compared with the example simulated in [4] (that is, by Model 0), and that corresponds to

$$(S_\mathrm{m}, E_\mathrm{m}, I_\mathrm{m}, R_\mathrm{m}, S_\mathrm{f}, E_\mathrm{f}, I_\mathrm{f}, R_\mathrm{f})(0) = (450, 10, 10, 10, 450, 5, 5, 5) =: \boldsymbol{U}_0^\mathrm{T}. \tag{2.24}$$

(Figure 2.1 shows the solution of Model 0 for this case.) To this end, we assume that the spatial domain is $\Omega = [0,1]^2$ (i.e., $L = 1$ in a scale not specified) and that $K = 1000$ is the maximum density feasible on a unit square. For the simulation, we consider Scenario 1, which corresponds to identifying a subdomain $\Omega_0 \subseteq \Omega$ with

$$\Omega_0 = \{(x, y) \in \Omega : |x - 0.5| + |y - 0.5| \leq 0.2\}$$

in which the initial population is uniformly distributed and setting

$$\boldsymbol{u}(\boldsymbol{x}, 0) = \chi_{\Omega_0}(\boldsymbol{x})\boldsymbol{U}_0, \quad \text{where} \quad \chi_{\Omega_0}(\boldsymbol{x}) = \begin{cases} 1 & \text{if } \boldsymbol{x} \in \Omega_0, \\ 0 & \text{otherwise,} \end{cases}$$

and alternatively Scenario 2, in which we stipulate a "random" distribution by setting

$$\boldsymbol{u}(\boldsymbol{x}, 0) = \frac{1}{|\Omega|}\big(1 + r(\boldsymbol{x})\big)\boldsymbol{U}_0, \quad \text{where} \quad \int_\Omega r(\boldsymbol{x})\,\mathrm{d}\boldsymbol{x} = 0 \tag{2.25}$$

and r is a given oscillatory function assuming values in $(-1, 1)$. (The idea is not to impose any initial "pattern" in Scenario 2.)

A total number of six cases is considered by combining Scenarios 1 and 2 with Models 1, 2 and 3. We always choose $\mu_X = 0.05$ for all species X, $\kappa_X = 0.1$ and $h = 1/200$. Furthermore, we wish to compare the numerical results with the predictions made by the non-spatial ODE model, Model 0 (Figure 2.1). To this end we determine for each compartment $X \in \mathcal{C}$ and time instants $t^n = n\Delta t$ the following quantity:

$$\mathcal{I}(X) = \mathcal{I}(X, t^n) := h^2 \sum_{i,j=1}^{\mathrm{N}} X_{i,j}^n \approx \int_\Omega X(\boldsymbol{x}, t^n)\, \mathrm{d}\boldsymbol{x}, \tag{2.26}$$

which represents the approximate total number in Ω of individuals of compartment X at time t^n. We recall that in the PDE model (2.1), the unknowns $X \in \mathcal{C}$ are *densities*, and so an integration over Ω is necessary to make results can be comparable with those of a model that predicts the *total number* of individuals in each compartment (as does Model 0). Similar "integrals" of the numerical solution are utilized by Colombo and Rossi [22, Fig. 3.2] to study the global behaviour of their predator-prey model.

2.3.2 Cases 1 to 3: simulations with a structured initial datum

In Figures 2.2 to 2.4 we show the numerical solution for N_m, N_f, I_m and I_f, in each case at three different times, for Cases 1 to 3 that arise for Scenario 1 with Model 1, Model 2 with $K = 1000$, and Model 3. First of all, we observe that according to the results for N_m and I_m, within Models 1 and 2 the male individuals keep confined to a growing but sharply limited region, with zero values outside that region. Model 3, with its linear diffusive term $-\mu_X \nabla X$ for $X \in \mathcal{C}_\mathrm{m}$ (instead of the expressions $-\mu_X X \boldsymbol{V}(N_\mathrm{m})$ or $-\mu_X X \varphi(N_\mathrm{m}+N_\mathrm{f})\boldsymbol{V}(N_\mathrm{m})$ in Models 1 or 2), produces a solution that fills the entire domain. Numerical results obtained for larger times than those shown in Figure 2.4 indicate that the solutions of all variables become constant on the entire computational domain, and the integral quantities assume a stationary state similar (but not identical) to that of Model 0 (see Figure 2.1). Furthermore, comparing the results between Models 1 and Models 2 (Figures 2.2 and 2.3), we observe that Model 1 gives rise to a distinct spatial structure, including regions that are nearly void of males combined with "peaks" of the solution where $N_\mathrm{m} \approx 1500$. Clearly, this feature is expected since Model 1 has no mechanism that would limit the value of the total density of males N_m. (We recall that although the total numbers of male or female individuals, $\mathcal{I}(N_\mathrm{m})$ and $\mathcal{I}(N_\mathrm{f})$, are bounded by the terms with the death rates in all models, it may well happen that the densities N_m or N_f become locally unbounded.)

The results obtained for Case 1 are in marked contrast to those for Case 2, especially those for N_m, produced by Model 2 shown in Figure 3.3, where we observe that N_m does not exceed a value of about 500, and stays close to that value within a region of approximately the same shape as for Model 1. A similar observation is true for the compartment I_m: Model 1 (Figure 2.2) predicts a structure with "peaks" that roughly mirrors that of N_m, while Model 2 (Figure 2.3)

predicts a more uniform distribution (with I_{m} assuming values between 70 and 90) in the interior of the domain. Furthermore, we recall that for all models the flux for the female compartments is always given by $-\mu_X \nabla X$ for $X \in \mathcal{C}_{\mathrm{f}}$, so differences in solution behavior of the female individuals are exclusively due to those in describing the male behavior. In general, this diffusive behavior tends to produce less sharp, smooth spatial structures.

Finally, Figure 2.5 indicates that Models 1, 2 and 3 lead to quite different numerical results in terms of the integrated quantities (2.26). We commented above that the results of Model 3 are similar to those of Model 0. On the other hand, while Models 1 and 2 produce integral results whose order of magnitude for each compartment is similar to that of Model 3, it can be noted that no stationary state is attained at $t = 30$; as the discussion of Cases 4 to 6, and in particular comparing Figures 2.5 and 2.9 show, this is a consequence of the respective model structure in combination with the choice of initial data. In any case, it is calling to attention that while Models 2 and 3 predict a smooth variation of the integrated quantity in time, the curves generated by Model 1 are somewhat oscillatory. This behavior is consistent with our observation that Model 1 does not only generate a spatial solution structure with strong variations, "peaks" and sharp gradients, but also produces rapid transitions within time. This unsteady and unstable behavior is due to the strong competence of advective and repulsive mechanisms inherent in the definition (2.2).

2.3.3 Cases 4 to 6: simulations with a randomly fluctuating initial datum

Figures 2.6 to 2.9 provide numerical solutions for Scenario 2. The "random" initial datum (2.25) has been chosen to test whether small perturbations would give rise to large-scale regular structures akin to the well-known mechanism of pattern formation (cf., e.g., [49, 52]), or rather, the small fluctuations in the initial datum would simply be smoothed out. Figure 2.6, corresponding to Model 1, illustrates that male individuals aggregate in a kind of filamentous structure, including some marked peaks with N_{m} reaching values close to 3000. On the other hand, we observe the formation of areas of roughly the same shape and size that are nearly void of male individuals. This behavior is similar to that observed by Colombo and Rossi for the predator density in their predator-prey model (cf., e.g., [22, Figs. 3.3–3.5]). In our cases, the densities of the female populations N_{f} and I_{f} do not vary much over the computational domain, and do so smoothly. For the same scenario with Model 2 and $K = 1000$, Figure 2.7 indicates that while for small times we observe the formation of spatial structures similar those of Figure 2.6, eventually all variables become nearly constant on the whole domain. Figure 2.8 for Model 3 illustrates that marked circular spatial structures persist over long times. Similar results (not shown here) were obtained in other numerical experiments for times up to $t = 87$. We also comment that Figure 3.5 illustrates that Model 2 leads to a nearly stationary behavior of the integral quantities within shorter time than for Scenario 1, and results for Models 2 and 3 are quite similar. The curves observed in Figure 2.9 for Model 1 are, again, oscillatory, which lends further support to the conjecture that this model (at least with the parameters chosen) exhibits spatial-temporal oscillatory behavior.

For Cases 4 to 6, we calculate the evolution of Moran's index [51, 28, 60], denoted here I, for each species at each time step, and which is here computed by

$$\mathsf{I} = \mathsf{I}(X) := \sum_{i,j=1}^{M} \frac{1}{4} Y_{i,j}(Y_{i-1,j} + Y_{i+1,j} + Y_{i,j-1} + Y_{i,j+1}) \Big/ \sum_{i,j=1}^{M} Y_{i,j}^2, \tag{2.27}$$

where X is the numerical data obtained for some species at a certain time step and

$$Y_{i,j} = X_{i,j} - \frac{1}{M^2} \sum_{p,q=1}^{M} X_{p,q}. \tag{2.28}$$

Overall, the results shown in Figure 3.15 indicate that a strong spatial autocorrelation ($\mathsf{I} \approx 1$) is developed through the simulation from initial random data ($\mathsf{I} \approx 0$). It is, however, interesting to note for that for Cases 4 and 5 the values of I for the female compartments remain consistently below those of the male compartments, while for Case 6 the limit value $\mathsf{I} = 1$ is closely approximated by all species. This confirms the trend evident already from the results of Figure 2.8 compared with those of Figures 2.6 and 2.7, namely that the presence of diffusive movement in the male species significantly contributes to generating smoothly varying solution patterns, that is, to creating a high degree of spatial autocorrelation.

2.3.4 Case 7: order test with smooth solution

The purpose of this test is to show that the numerical scheme exhibits experimental second order convergence when the solution is smooth. For this purpose, we choose a smooth initial configuration given by

$$X_{\mathrm{m}}(x, y, t = 0) = c_X \exp\left(-\frac{1}{2}\big((x-3)^6 + (y-3)^6\big)\right),$$
$$X_{\mathrm{f}}(x, y, t = 0) = c_X \exp\left(-\frac{1}{2}\big((x-7)^6 + (y-7)^6\big)\right)$$

for $X \in \{S, E, I, R\}$, constants $c_S = 1000$, $c_E = 1$, $c_I = 10$ and $c_R = 1$, and a sufficiently small final time $T = 0.1$ to ensure that no singularities are formed during the simulation. We choose $\mu_X = 10^{-4}$ for $X \in \mathcal{C}_{\mathrm{m}}$ and $\mu_X = 10^{-3}$ and $\kappa_X = 10^{-2}$ for $X \in \mathcal{C}_{\mathrm{f}}$.

We compute approximate L^1 errors for approximate solutions obtained with $M \times M$ meshes, $M = 2^s$, $s = 3, \ldots, 8$, using a reference solution with a resolution of $M_{\mathrm{ref}} \times M_{\mathrm{ref}}$ cells, for $M_{\mathrm{ref}} = 2048$, as follows. We denote by $(v^M_{\ell,j,k})_{j,k=1}^{M}$ and $(v^{\mathrm{ref}}_{\ell,j,k})_{j,k=1}^{M_{\mathrm{ref}}}$ the numerical solution for the ℓ-th component ($\ell = 1, \ldots, 8$, see Section **??**) at time T calculated with M and M_{ref}, respectively. We project the reference solution to the coarser grids by bicubic interpolation, since the numerical scheme is designed to compute second-order approximations to the exact solutions at the nodes (x_i, y_j), with $x_i = y_i = (i - 1/2)L/M$, for the coarse mesh, and $(\bar{x}_i, \bar{y}_j)$,

M	8	16	32	64	128	256
$e_M^{tot} \times 10^3$	368.90	383.19	379.01	153.73	34.70	9.14
θ_M	-0.05	0.02	1.30	2.15	1.92	—

Table 2.1: Case 7 (Model 1, order test with smooth solution): approximate total L^1 errors e_M^{tot} and observed convergence rates θ_M.

with $\bar{x}_i = \bar{y}_i = (i - 1/2)L/M_{\text{ref}}$ for the fine mesh and these points do not coincide. Specifically, this projection $\tilde{v}^M_{\ell,j,k}$ for $j, k = 1, \ldots, M$ is computed by

$$\tilde{v}^M_{\ell,j,k} = \sum_{j_1,k_1=-2}^{1} \xi_{j_1}\xi_{k_1} v^{\text{ref}}_{\ell,\bar{j}-j_1,\bar{k}-k_1}, \quad \bar{j} = \left(j - \frac{1}{2}\right)\frac{M_{\text{ref}}}{M}, \quad \bar{k} = \left(k - \frac{1}{2}\right)\frac{M_{\text{ref}}}{M},$$

where $\xi_{-2} = \xi_1 = -1/16$ and $\xi_0 = \xi_{-1} = 9/16$. Notice that $M_{\text{ref}}/M = 2^{11-s} \geq 8$ in this test and the previous formula is therefore computable.

The total approximate L^1 error of the numerical solution $(v^M_{\ell,j,k})_{j=1}^M$ at time T is then given by

$$e_M^{\text{tot}} := \frac{1}{M^2}\sum_{\ell=1}^{8}\sum_{j,k=1}^{M} |\tilde{v}^M_{\ell,j,k} - v^M_{\ell,j,k}|. \tag{2.29}$$

Based on the approximate errors defined by (2.29), we may calculate a numerical order of convergence from pairs of total approximate L^1 errors e_M^{tot} and e_{2M}^{tot} by

$$\theta_M := \log_2\left(e_M^{\text{tot}}/e_{2M}^{\text{tot}}\right).$$

These data are displayed in Table 2.1. It can be deduced that the errors start diminishing for $M = 64$ and do so roughly at a second-order rate.

2.3.5 Case 8: seasonal alternation for Models 0 and 3

Sometimes, due to climatic variations, for example due to large periods of rain or of drought, there are variation in some parameters, for example those that determinate death and birth rates. To study the effect of seasonal variability, in this example we identify two different set of parameter that can represent two different seasons, $\{a_i, b_i, c_i\}$ for $i = 1, 2$. We wish to know the transmission dynamics of hantavirus due to an alternation in time of the parameters between these two seasons. We implement square-periodic season alternation where the duration of the each season is $T/2$, where T units is a year. Any given quantity $u(t)$ alternating in this way can be expressed as $u(t) = u_+ + u_-\mu(t)$, where $u_\pm = \frac{1}{2}(u_1 \pm u_2)$ and $\mu(t)$ is a periodic square wave $\mu(t) = 1$ if $t \in (0, T/2)$ and $\mu(t) = -1$ if $t \in (T/2, T)$.

We consider $a_1 = 0.01$, $b_1 = 4$, $c_1 = 1.99 \times 10^{-3}$ and $a_2 = 0.05$, $b_2 = 3$, $c_2 = 0.0015$ in order that the carrying capacity be $K_1 = K_2 = 1000$ for both choices, so $R_{0,1} = 1.38$ and $R_{0,2} = 2.26$

are obtained. The remaining parameters and initial condition are the same as in Cases 4 to 6 (Scenario 2).

In Figure 2.11 we display the numerical solution for Model 3. Roughly speaking we observe that the seasonal alternation in the parameters produces a solution similar to that of Model 3 also with a randomly fluctuating initial datum. In Figure 2.12 we display the solutions for (the ODE) Model 0 and for Model 3. We observe that the seasonal alternation in the parameters generates a oscillatory and bounded solution for each case, and Model 3 displays a smaller amplitude.

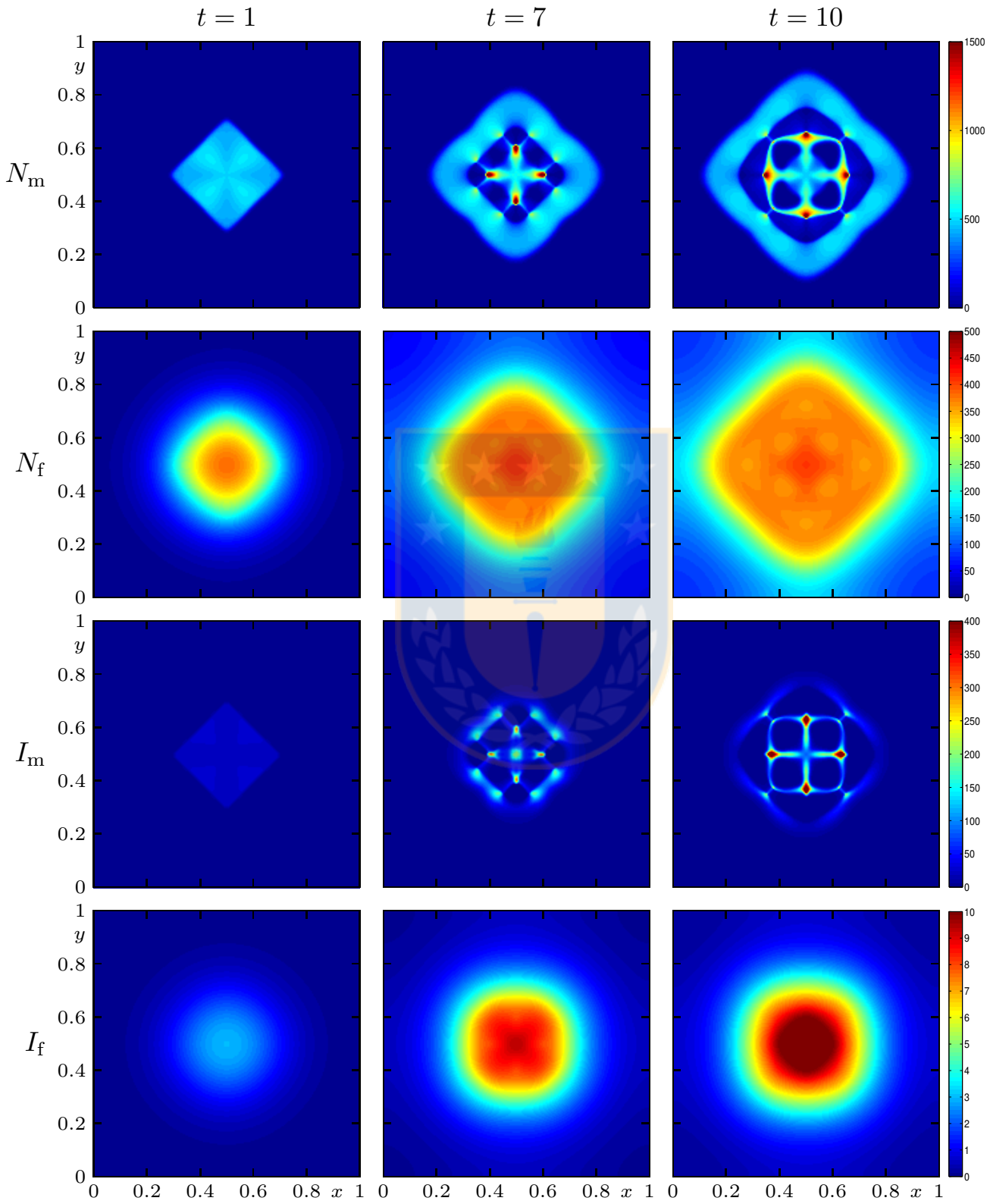

Figure 2.2: Case 1 (Model 1, Scenario 1): numerical solution for N_{m}, N_{f}, I_{m} and I_{f} at the indicated times (figure produced by author).

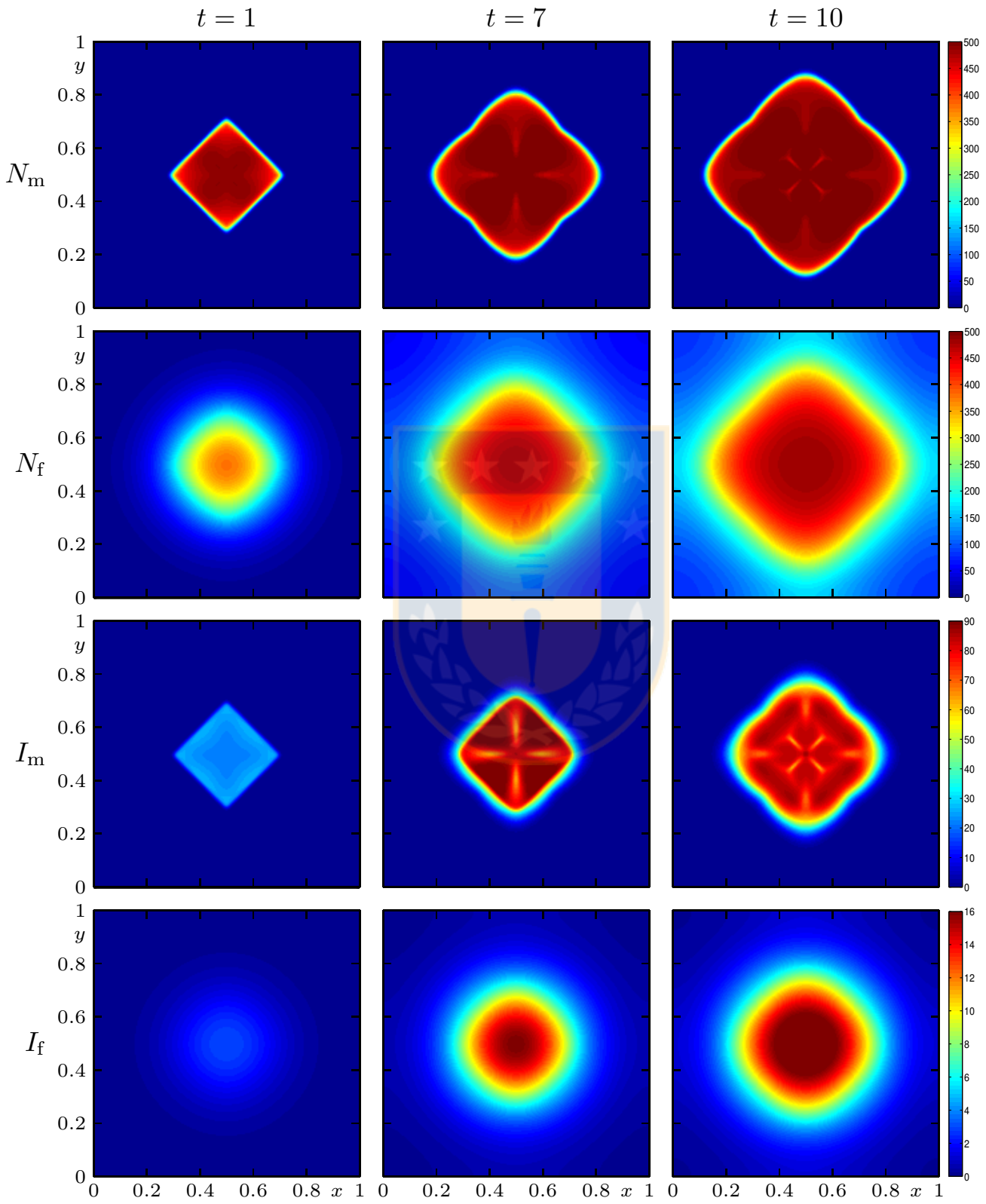

Figure 2.3: Case 2 (Model 2 with $K = 1000$, Scenario 1): numerical solution for N_{m}, N_{f}, I_{m} and I_{f} at the indicated times (figure produced by author).

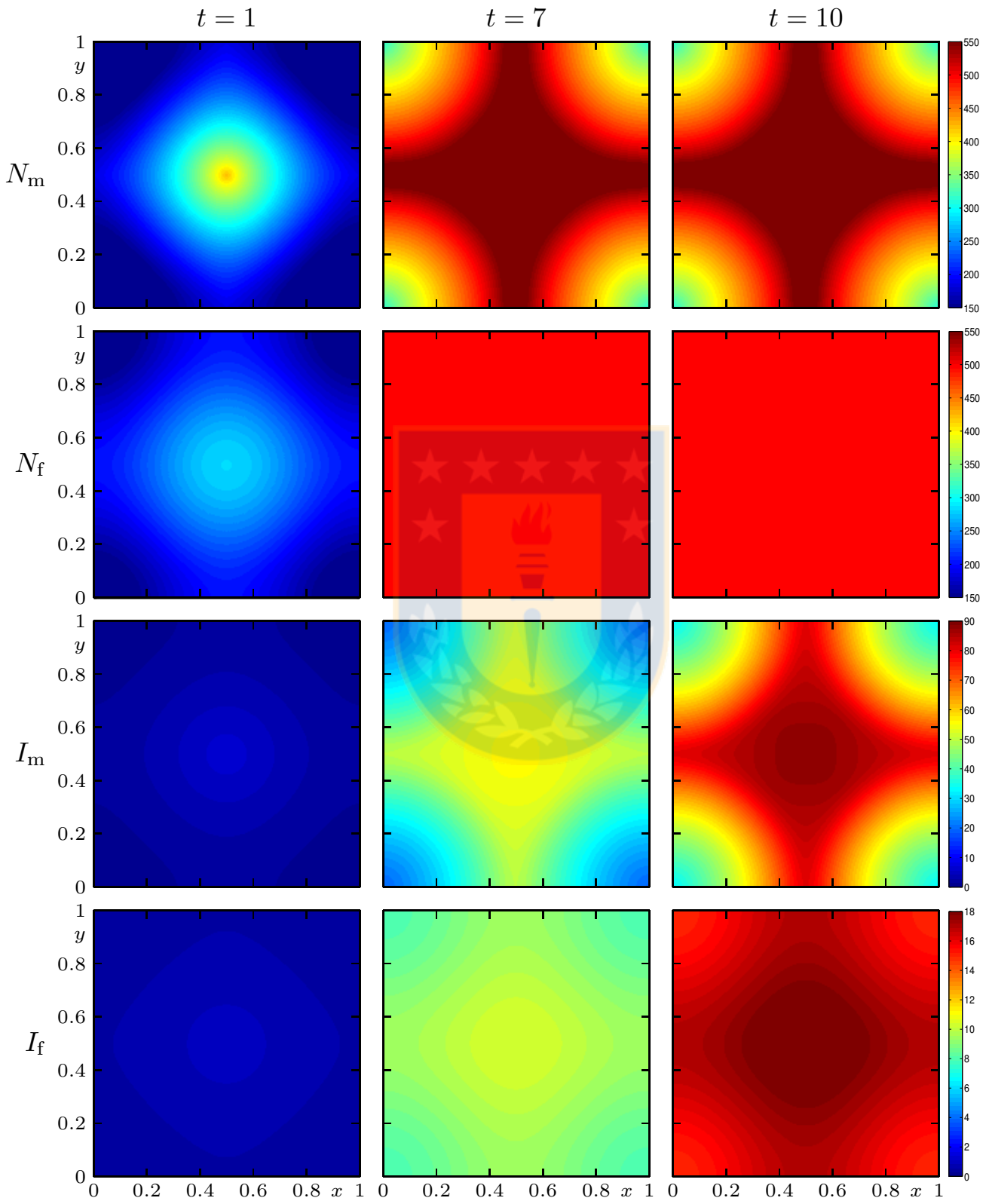

Figure 2.4: Case 3 (Model 3, Scenario 1): numerical solution for N_{m}, N_{f}, I_{m} and I_{f} at the indicated times (figure produced by author).

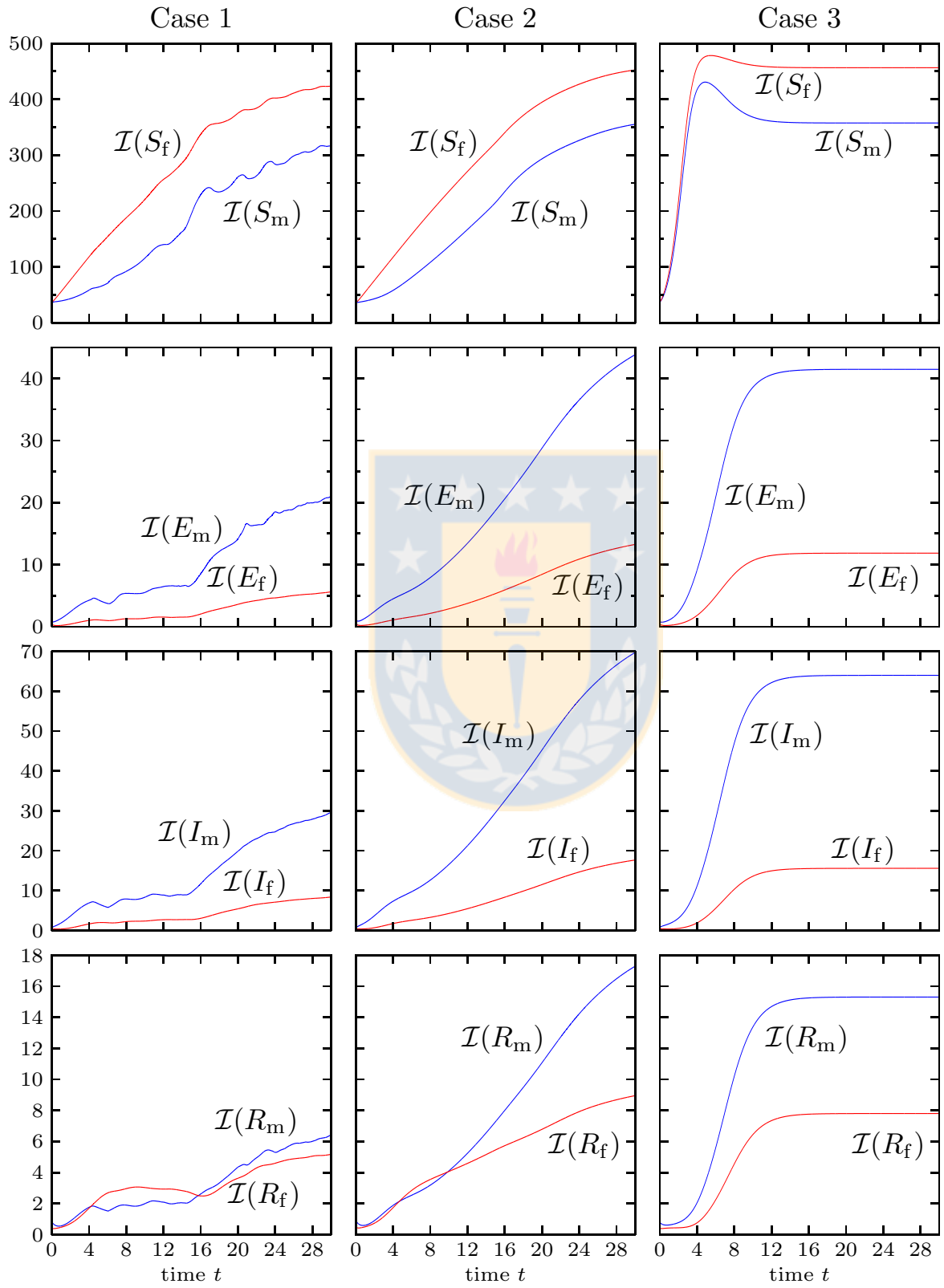

Figure 2.5: Cases 1–3: integral quantities $\mathcal{I}(X)$ defined by (2.26) for each compartment obtained by evaluating numerical solutions (figure produced by author).

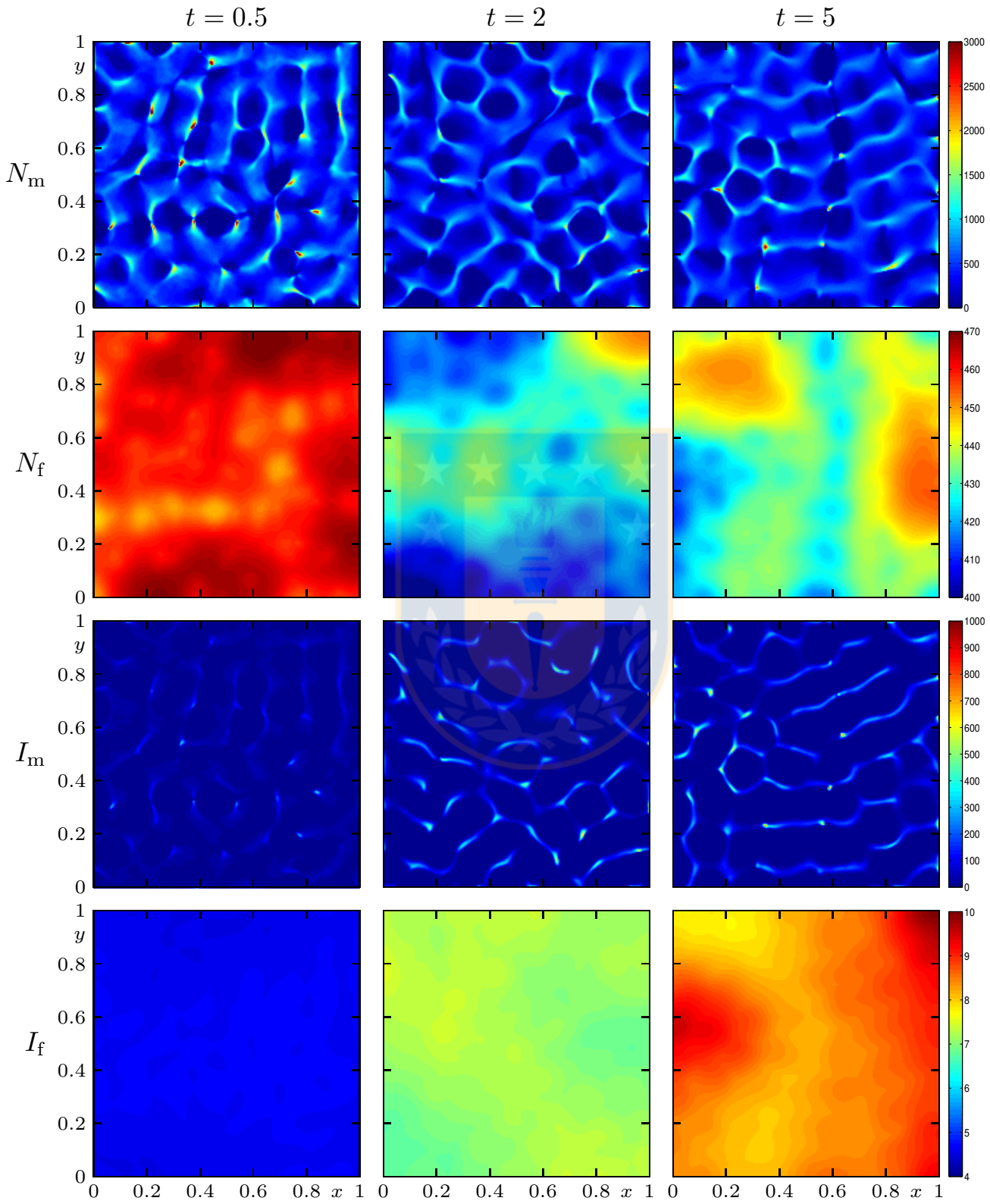

Figure 2.6: Case 4 (Model 1, Scenario 2): numerical solution for N_{m}, N_{f}, I_{m} and I_{f} at the indicated times (figure produced by author).

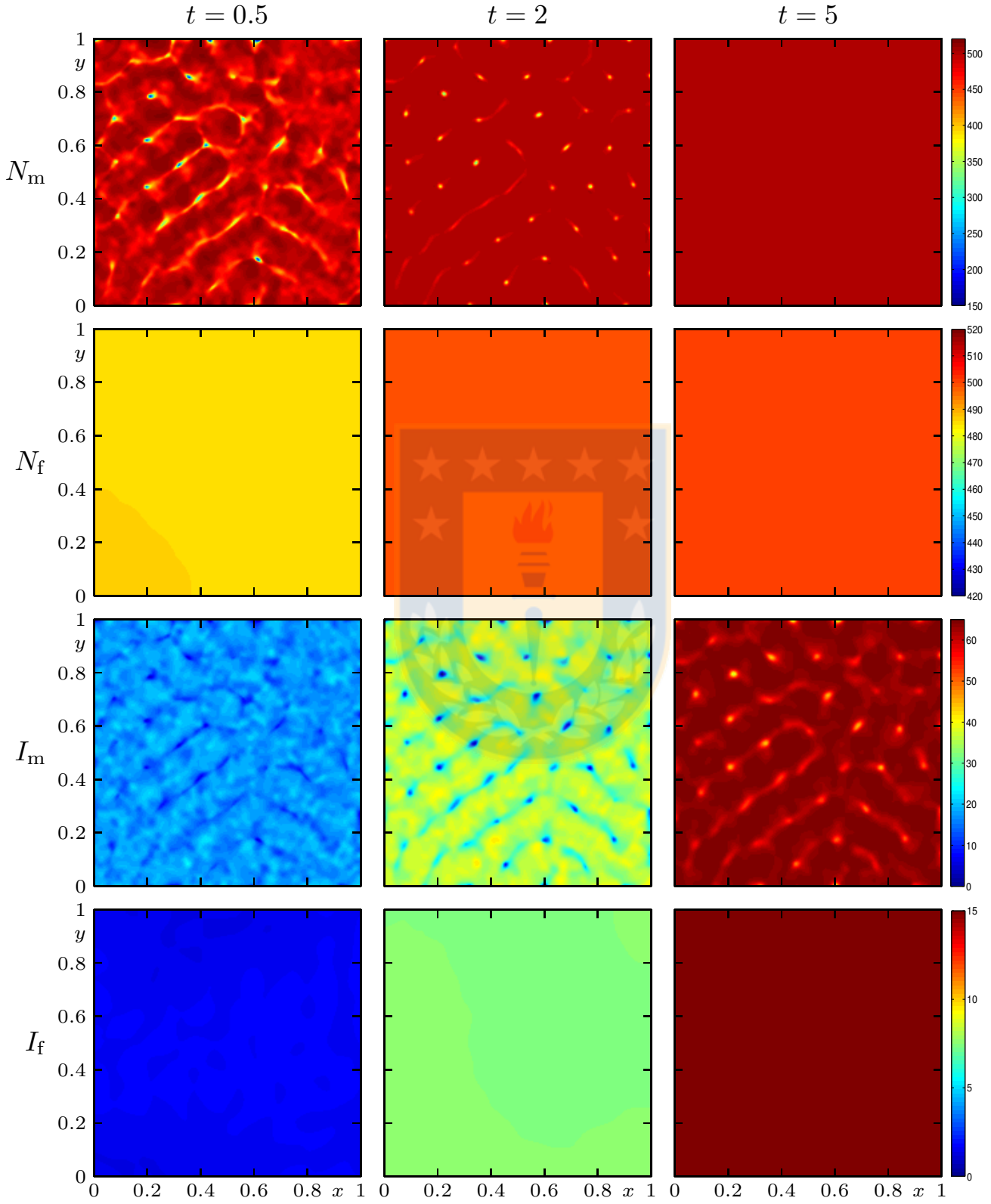

Figure 2.7: Case 5 (Model 2 with $K = 1000$, Scenario 2): numerical solution for N_{m}, N_{f}, I_{m} and I_{f} at the indicated times (figure produced by author).

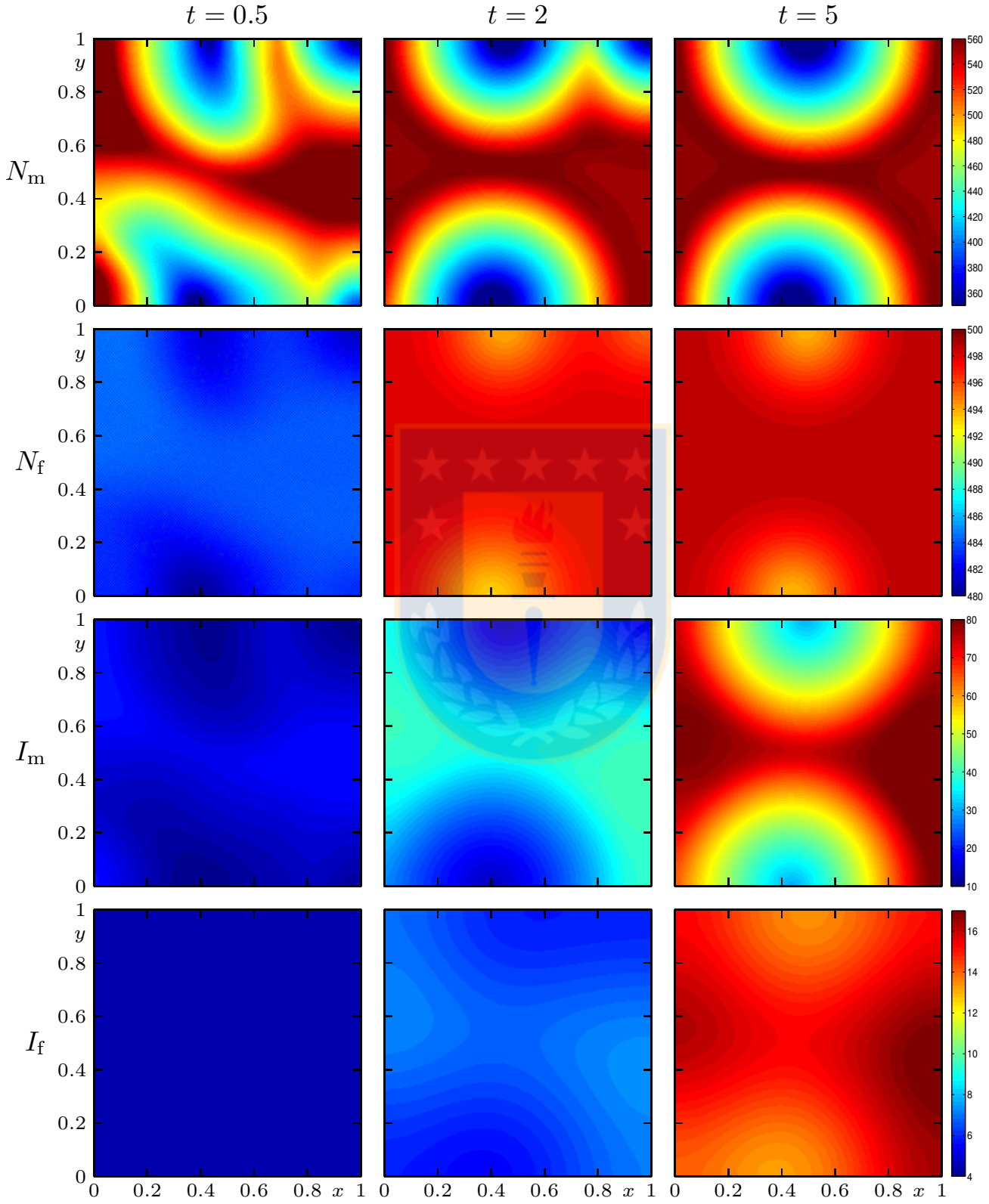

Figure 2.8: Case 6 (Model 3, Scenario 2): numerical solution for N_{m}, N_{f}, I_{m} and I_{f} at the indicated times (figure produced by author).

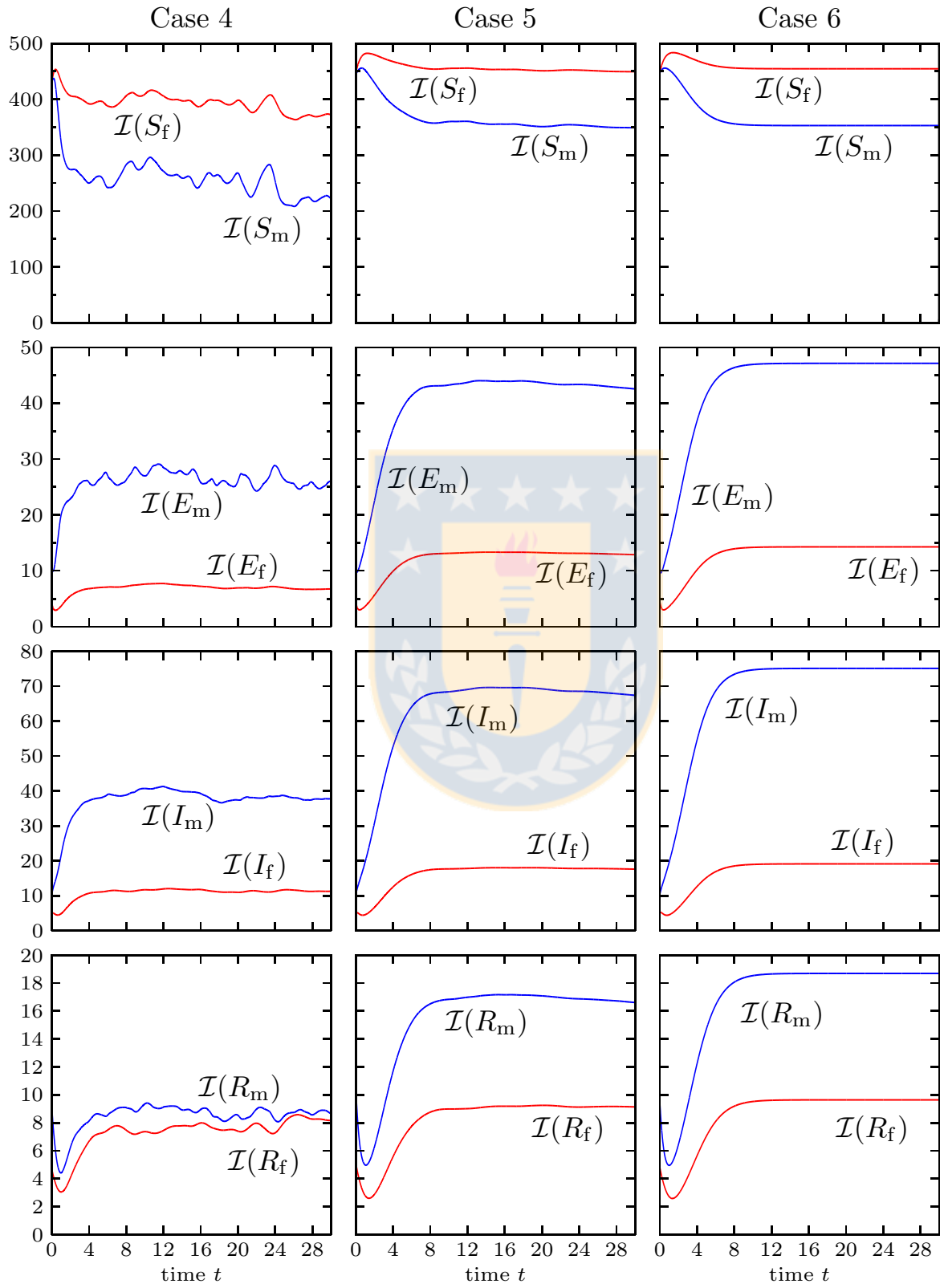

Figure 2.9: Cases 4–6: integral quantities $\mathcal{I}(X)$ defined by (2.26) for each compartment obtained by evaluating numerical solutions (figure produced by author).

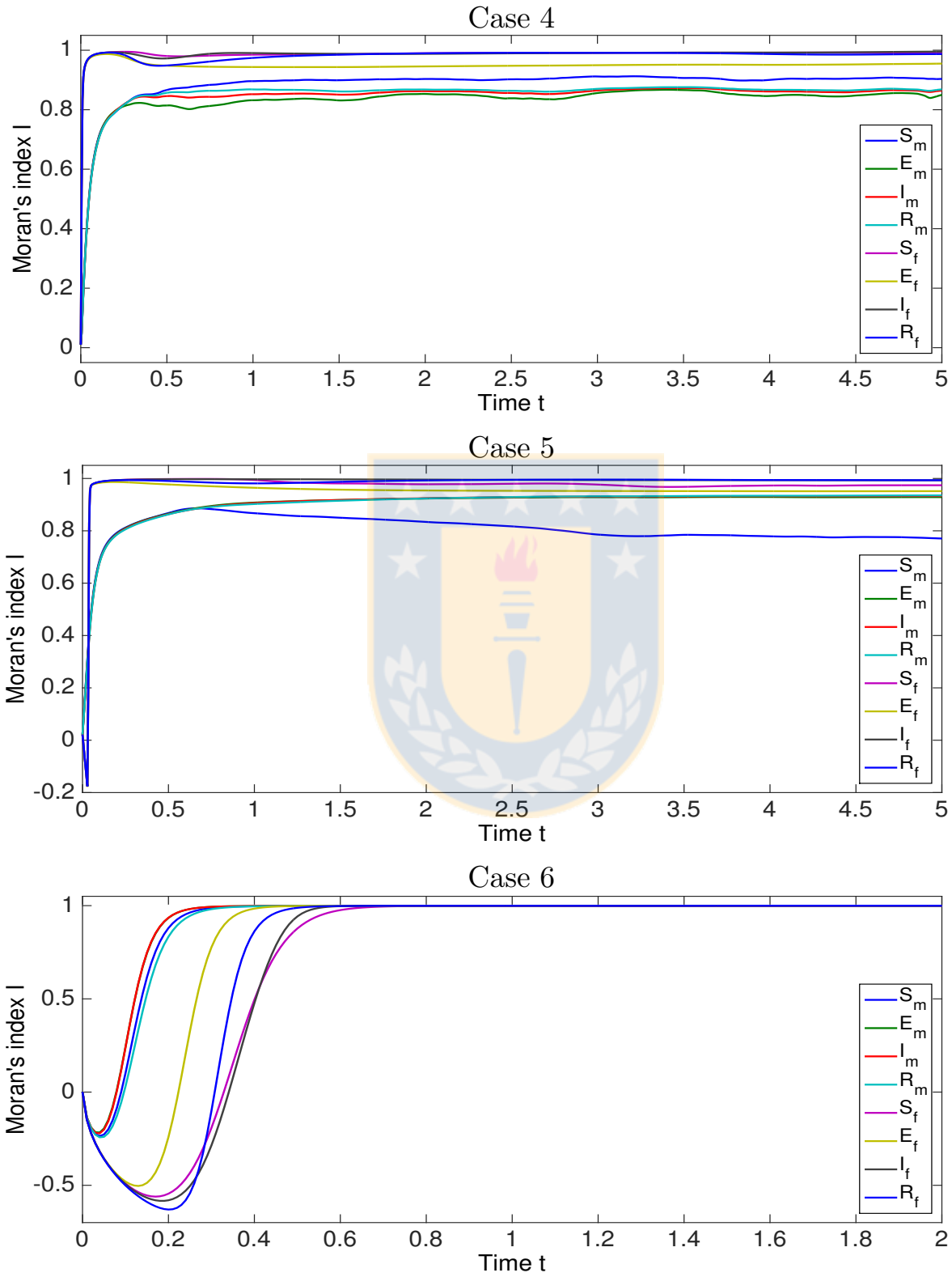

Figure 2.10: Cases 4–6: Moran's index I defined by (2.27), (2.28) for each compartment obtained by evaluating numerical solutions (figure produced by author).

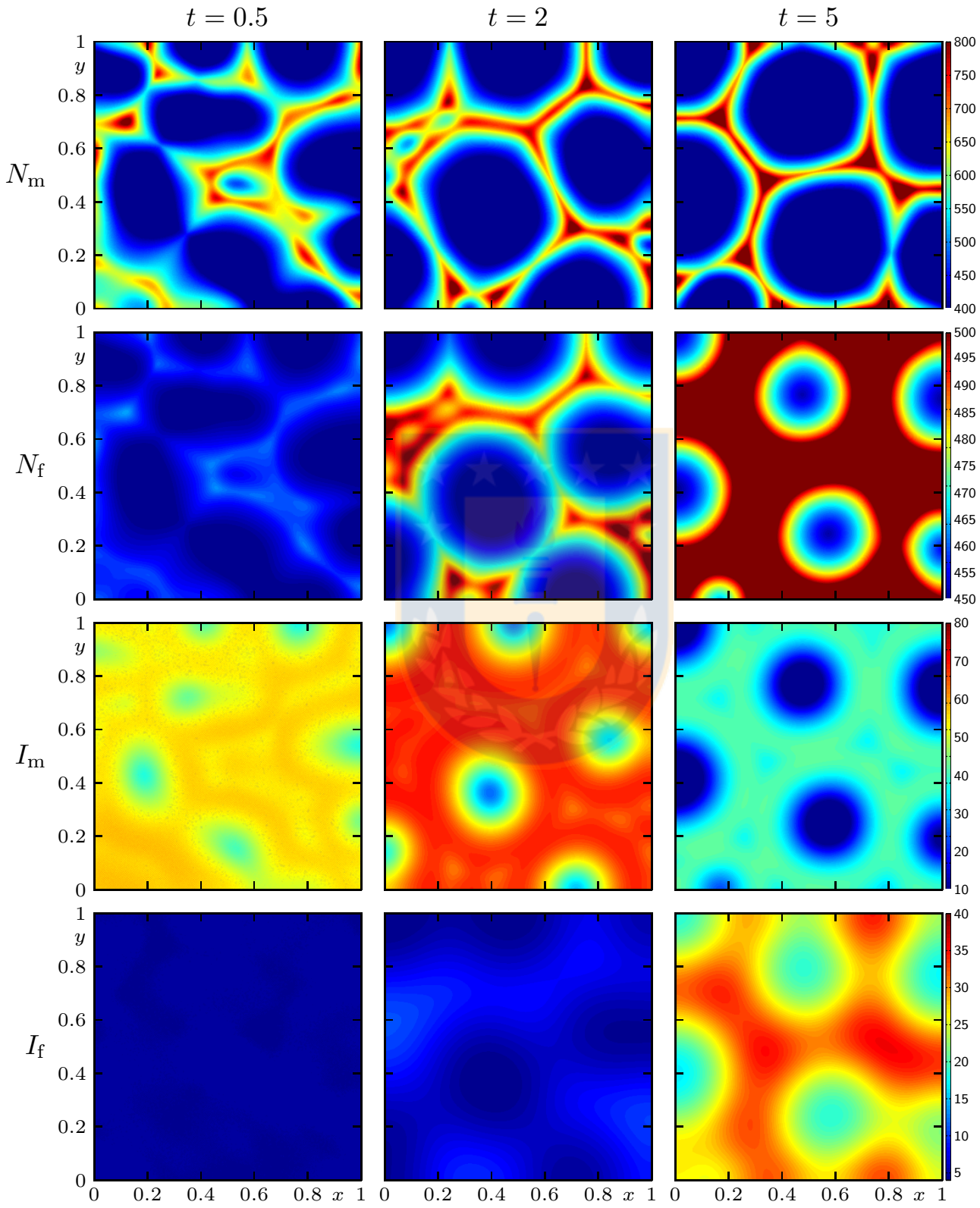

Figure 2.11: Case 8 (Model 3, Scenario 2, periodic variation of parameters): numerical solution for N_{m}, N_{f}, I_{m} and I_{f} at the indicated times (figure produced by author).

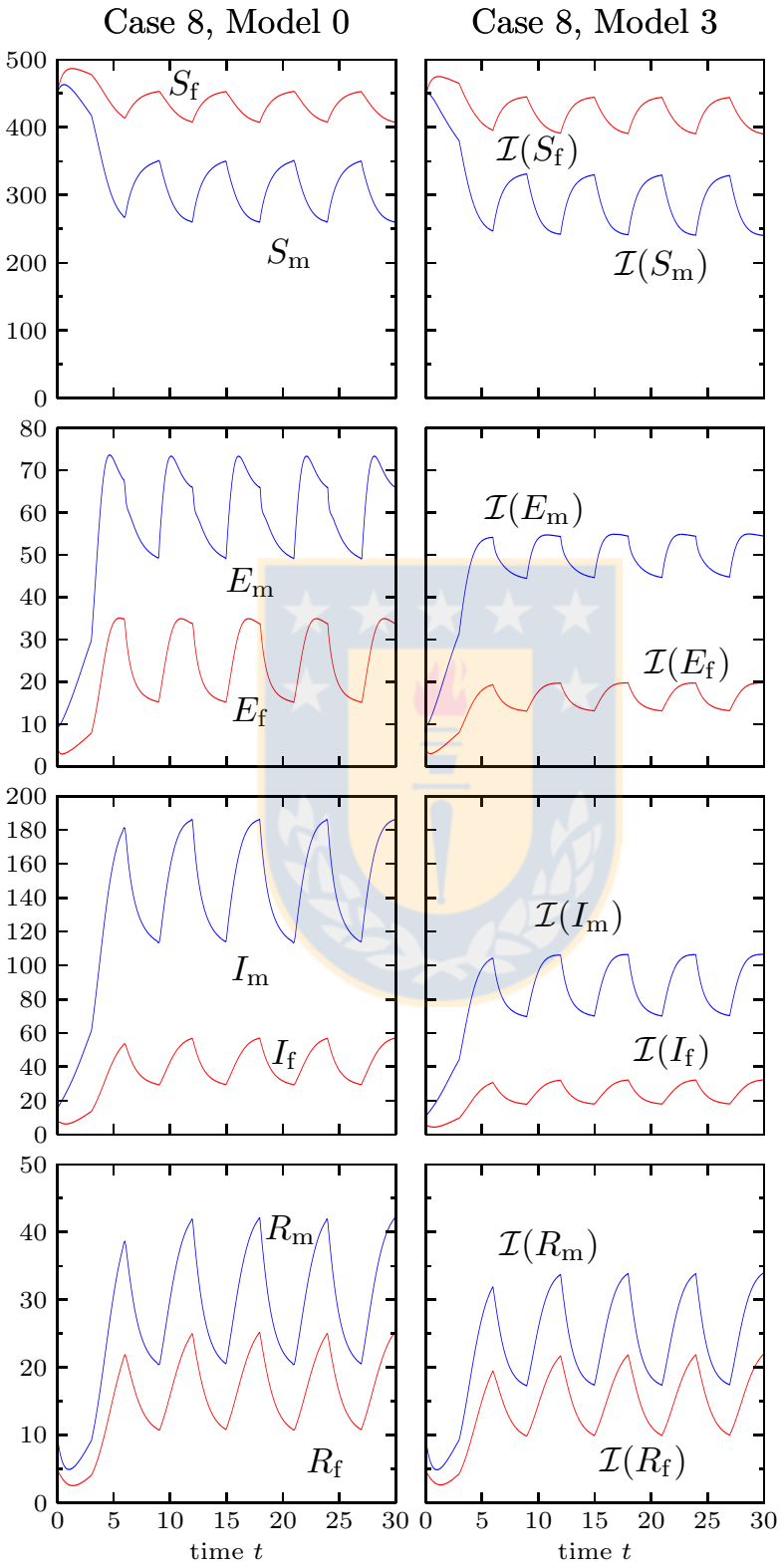

Figure 2.12: Case 8: (Model 3, Scenario 2, periodic variation of parameters): solutions of Model 0 (left column) and integral quantities $\mathcal{I}(X)$ of Model 3 (right column) defined by (2.26) for each compartment obtained by evaluating numerical solutions (figure produced by author).

Chapter 3

Numerical solution of a spatio-temporal predator-prey model with infected prey

3.1 Mathematical model

3.1.1 Dynamical system for a predator-prey model

Combining the SIR epidemic model of [67] with a second species corresponding to a predator (as in the model of [32]), and assuming that the predator only eats infected prey, we obtain the following model:

$$\frac{\mathrm{d}S}{\mathrm{d}t} = A - dS - \beta SI^2, \tag{3.1a}$$

$$\frac{\mathrm{d}I}{\mathrm{d}t} = \beta SI^2 - (d+\mu)I - \frac{cYI}{mY+I}, \tag{3.1b}$$

$$\frac{\mathrm{d}Y}{\mathrm{d}t} = \delta Y\left(1 - \frac{hY}{I}\right), \tag{3.1c}$$

where t is time, $S(t)$ is the population of susceptible prey, $I(t)$ is the population of infected prey, A is the recruitment rate of the prey population, d is the natural death rate of the prey population, β is the force of infection or the rate of transmission, μ is the disease-related death from the infected, $Y(t)$ is the population of predators, c is the search rate of the predators towards infected prey, δ is the per capita growth rate of the predators, h is a constant related to the density dependent mortality of the predator population, and $m > 0$ is a constant.

The incidence rate in (3.1a) and (3.1b) is chosen here as the nonlinear βSI^2 expression in agreement with Sun [67], who in turn appeals to the justification by Liu et al. [47, 46]. The last term in the right-hand side of (3.1b) is a ratio-dependent predation term; see, e.g., [41] for further justification of such expressions. Furthermore, note that (3.1c) coincides with the

predator equation [32, Eq. (1)], and that hY/I in that equation is the Leslie-Gower term [45] which measures the loss in the predator population due to the relative scarcity of the (infected) prey [31].

It is well known that the use of a ratio-dependent terms requires carefully handling situations of zero denominators. The right-hand sides of the ODE version (3.1) are potentially ill-defined if $I(0) = 0$. This issue is treated in [32] as follows: if $I(0) = 0$ and $Y(0) \geq 0$, then (3.1c) is interpreted as implying that $Y(t) = 0$ for $t > 0$ and if $I(0) = Y(0) = 0$, then (3.1b) is interpreted as implying that $I(t) = 0$ for all t. With respect to the PDE version (3.5), we have not encountered any difficulty of division by zero in our numerical experiments since in all cases we choose the initial datum $I(\boldsymbol{x}, 0) > 0$ for $\boldsymbol{x} \in \Omega$.

Theorem 3.1.1. *The system* (3.1) *has the following equilibrium points:*

i) The equilibrium $E_1 = (A/d, 0, 0)$ *corresponding to the extinction of the epidemic.*

ii) The following equilibria in absence of the predator:

$$E_2 = \left(\frac{A\beta + \sqrt{R}}{2d\beta}, \frac{2d(d+\mu)}{A\beta + \sqrt{R}}, 0 \right), \quad E_3 = \left(\frac{A\beta - \sqrt{R}}{2d\beta}, \frac{2d(d+\mu)}{A\beta - \sqrt{R}}, 0 \right),$$

where we define

$$R := A^2\beta^2 - 4d^3\beta - 8d^2\beta\mu - 4d\beta\mu^2.$$

These equilibria are feasible if $R > 0$*, which occurs if* $\beta > 4d(d+\mu)^2/A^2$.

iii) The following equilibria with presence of the predator:

$$E_4 = \left(\frac{A}{d + \beta I_4^2}, I_4, \frac{I_4}{h} \right), \quad E_5 = \left(\frac{A}{d + \beta I_5^2}, I_5, \frac{I_5}{h} \right), \tag{3.2}$$

where $I_4 < I_5$ *are the solutions of the quadratic equation*

$$\alpha\beta I^2 - \beta A I + d\alpha = 0, \quad \text{where } \alpha = d + \mu + \frac{c}{m+h}.$$

They are feasible if $\beta > 4d\alpha^2/A^2$*; then*

$$I_4 = \frac{A}{2\alpha} - \left(\frac{A^2}{4\alpha^2} - \frac{d}{\beta} \right)^{1/2}, \quad I_5 = \frac{A}{2\alpha} + \left(\frac{A^2}{4\alpha^2} - \frac{d}{\beta} \right)^{1/2}.$$

3.1.2 Behavior of the dynamical system

The point E_1 corresponds to the extinction of the epidemic. On the other hand, it is obtained in [67] that E_2 is unstable and E_3 is stable. To handle the dynamics of the system around E_4

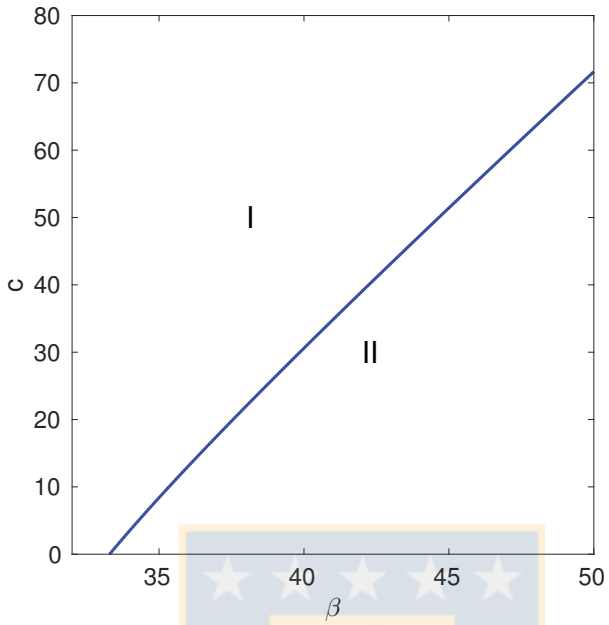

Figure 3.1: Hopf bifurcation diagram of the stability of equilibria E_4 and E_5 (3.2) of the dynamical system (3.1) in the (β, c)-plane, based on the Routh-Hurwitz conditions (3.3) and with (3.4). In region I, the conditions (3.3) for $e = e_i(\beta, c)$, $i = 1, 2, 3$, are not satisfied, and in region II they are satisfied (figure produced by author).

and E_5, we first recall that at E_5, the stability matrix is given by

$$\boldsymbol{J}^*(E_5) = \begin{bmatrix} -\beta I_5^2 - d & -\dfrac{2c}{m+h} - 2d - 2\mu & 0 \\ \beta I_5^2 & \dfrac{2c}{m+h} + d + \mu - \dfrac{cm}{(m+h)^2} & -\dfrac{ch^2}{(m+h)^2} \\ 0 & \delta/h & -\delta \end{bmatrix},$$

and that $\boldsymbol{J}^*(E_4)$ is given by the same expression with I_4 in place of I_5. The characteristic equation associated with possible equilibria E_4 and E_5 is

$$\det(\boldsymbol{J}^* - \lambda \boldsymbol{I}) = 0 \Leftrightarrow \lambda^3 + e_1\lambda^2 + e_2\lambda + e_3 = 0,$$

where $e_1 = -\operatorname{tr}(\boldsymbol{J}^*)$, $e_2 = \sum_{i=1}^{3} M_i$, where M_i is the determinant of the matrix obtained by eliminating row i and column i from $\boldsymbol{J}^*$, and $e_3 = -\det \boldsymbol{J}^*$. Here, the Routh-Hurwitz conditions (cf., e.g., [26, Sect. 6.4]) mean that there are only roots with strictly negative real parts, and hence the corresponding state is stable, when

$$e_1 > 0, \quad e_3 > 0, \quad \text{and} \quad e_1 e_2 > e_3. \tag{3.3}$$

This criterion is applied to $\boldsymbol{J}^*(E_5)$. In order to determine a set of parameters, where scenarios will be studied to determine the effect of considering different values of the infectious force of the epidemic expressed by the parameter β and of the search rate c of the predators towards infected prey, we fix the parameters

$$A = 1, \quad \mu = 1.8, \quad d = 1, \quad m = 30, \quad h = 0.1, \quad \delta = 0.4, \tag{3.4}$$

where the values of A, μ, and d are those proposed in [67] while the choices of m, h, and δ are assumed but are comparable with those utilized in [32]. To determine suitable choices of β and c, we assume that $e_1 = e_1(\beta, c)$, $e_2 = e_2(\beta, c)$ and $e_3 = e_3(\beta, c)$ and analyze satisfaction of the Routh-Hurwitz condition (3.3). This gives rise to two distinct regions in the (β, c)-plane, see Figure 3.1. A Hopf bifurcation occurs across the curve that separates these regions.

3.1.3 Spatio-temporal predator-prey model

The ODE model (3.1) exhibits a rich solution behaviour, which motivates us to analyze a spatial variant that in turn generalizes the spatio-temporal hyperbolic-parabolic predator-prey model studied by Colombo and Rossi [22]. Following [19, 22], we then replace (3.1c) by a non-local spatio-temporal PDE that contains a term describing the spatial movement of predators towards infected prey, and equip (3.1a) and (3.1b) with diffusion terms. The resulting spatio-temporal model is given by

$$\frac{\partial S}{\partial t} - D_S \Delta S = A - dS - \beta S I^2, \tag{3.5a}$$

$$\frac{\partial I}{\partial t} - D_I \Delta I = \beta S I^2 - (d + \mu) I - \frac{cYI}{mY + I}, \tag{3.5b}$$

$$\frac{\partial Y}{\partial t} + \nabla \cdot \boldsymbol{F}_Y(S, I, Y) = \delta Y \left(1 - \frac{hY}{I}\right), \tag{3.5c}$$

where $\nabla\cdot$ denotes the (spatial) divergence operator. Here x and y are the space variables, $\Delta = \partial^2/\partial x^2 + \partial^2/\partial y^2$ is the two-dimensional Laplace operator, and D_S and D_I are the diffusion coefficients, i.e. we assume standard linear diffusion for the prey compartments S and I.

The right-hand sides of (3.5) are identical to that of the non-spatial ODE model (3.1), i.e., this model is recovered if all divergence terms on the left-hand sides are set to zero and variables are considered to depend on t only, and the unknowns represent suitably scaled densities.

3.1.4 Convective fluxes and diffusion matrix

The flux $\boldsymbol{F}_Y$ appearing in the left-hand side of (3.5c) is assumed to have the form $\boldsymbol{F}_Y(I, Y) = \kappa_Y Y \boldsymbol{V}(I)$, where $\kappa_Y \geq 0$ is constant and

$$\boldsymbol{V}(w) = \frac{\nabla(w * \eta)}{\sqrt{1 + \|\nabla(w * \eta)\|^2}} \tag{3.6}$$

is the non-local unscaled velocity function [22]. Here η denotes a radial convolution kernel with radius ε, i.e., η is a piecewise smooth function such that

$$\eta(\boldsymbol{x}) = \eta(\|\boldsymbol{x}\|_2), \quad \eta(\boldsymbol{x}) \geq 0, \quad \eta(\boldsymbol{x}) = 0 \text{ for } \|\boldsymbol{x}\| > \varepsilon, \quad \text{and} \int_{\mathbb{R}^2} \eta(\boldsymbol{x}) \, \mathrm{d}\boldsymbol{x} = 1, \tag{3.7}$$

i.e., for any function w defined on $\Omega \times \mathcal{T}$ and $\boldsymbol{x} \in \Omega$ such that $B_\varepsilon(\boldsymbol{x}) := \{\boldsymbol{y} \in \mathbb{R}^2 : \|\boldsymbol{y} - \boldsymbol{x}\| < \varepsilon\} \subset \Omega$, we have

$$(w(\cdot, t) * \eta)(\boldsymbol{x}) = \int_{B_\varepsilon(\boldsymbol{x})} w(\boldsymbol{y}, t)\eta(\boldsymbol{x} - \boldsymbol{y}) \, \mathrm{d}\boldsymbol{y} = \int_{\mathbb{R}^2} w(\boldsymbol{y}, t)\eta(\boldsymbol{x} - \boldsymbol{y}) \, \mathrm{d}\boldsymbol{y}$$

(with slight modifications for points $\boldsymbol{x}$ with $\operatorname{dist}(\boldsymbol{x}, \partial\Omega) < \varepsilon$.) Since $\nabla(w * \eta) = w * \nabla\eta$, the velocity $\boldsymbol{V}(w)$ indeed depends (non-locally) on w and not on its gradient.

Summarizing, we obtain $\boldsymbol{F}^{\mathrm{c}}(\boldsymbol{u}) = \big(0, 0, F_Y(I, Y)\big)^{\mathrm{T}}$ and $\boldsymbol{\mathcal{D}} = \operatorname{diag}(D_S, D_I, 0)$. The vector $\boldsymbol{s}(\boldsymbol{u}) = (s_1(\boldsymbol{u}), s_2(\boldsymbol{u}), s_3(\boldsymbol{u}))^{\mathrm{T}}$ is given by the right-hand sides of (3.5). The system (3.5) is considered on $\Omega \times \mathcal{T}$ along with the initial condition

$$\boldsymbol{u}(\boldsymbol{x}, 0) = \boldsymbol{u}_0(\boldsymbol{x}), \quad \boldsymbol{x} \in \Omega, \tag{3.8}$$

where $\boldsymbol{u}_0$ is a given function, and zero-flux boundary conditions

$$\big(\boldsymbol{F}^{\mathrm{c}}(\boldsymbol{u}) - \boldsymbol{\mathcal{D}}\nabla\boldsymbol{u}\big) \cdot \boldsymbol{n} = \boldsymbol{0}, \quad \boldsymbol{x} \in \partial\Omega, \quad t \in (0, T], \tag{3.9}$$

where $\boldsymbol{n}$ is the unit exterior normal vector to the boundary $\partial\Omega$ of Ω.

3.2 Numerical method

The numerical scheme described in Section 2 of Chapter 2 is adapted here to solve the problem given by the equations (3.5), where the spatial semi-discretization is given by

$$\boldsymbol{v}' = -\nabla_h \cdot \tilde{\boldsymbol{F}}^{\mathrm{c}}(\boldsymbol{v}) + \boldsymbol{\mathcal{B}}\boldsymbol{v} + \boldsymbol{S}(\boldsymbol{v}). \tag{3.10}$$

The convective flux for the prey compartments (S and I, corresponding to $\ell \in \{1, 2\}$) is zero and for the predator (species Y, $\ell = 3$) is given by $\boldsymbol{F}_3^{\mathrm{c}}(\boldsymbol{u}) = u_3(\kappa_3 \boldsymbol{V}(u_2))$. To discretize its divergence $\nabla \cdot \boldsymbol{F}_3^{\mathrm{c}}(\boldsymbol{u})$ for the approximation $\boldsymbol{v}$, we first approximate the convolution terms as explained in Section **??** to obtain

$$\tilde{\boldsymbol{F}}_3^{\mathrm{c}}(\boldsymbol{v})_{i,j} = \boldsymbol{v}_{\ell,i,j}\big(\kappa_3 \boldsymbol{V}_h \left(v_2\right)_{i,j}\big) \in \mathbb{R}^2.$$

The difussion term is treated as follows

$$(\boldsymbol{\mathcal{B}}\boldsymbol{v})_{\ell,i,j} = \boldsymbol{\mathcal{D}}_{\ell\ell}(\boldsymbol{\Delta}_h \boldsymbol{v}_\ell)_{i,j}, \quad i, j = 1, \ldots, M, \quad \ell = 1, \ldots, 3 \tag{3.11}$$

and the reactive term $\boldsymbol{S}(\boldsymbol{v})$ is the $3 \times M \times M$-matrix with components

$$\boldsymbol{S}(\boldsymbol{v})_{\ell,i,j} = s_\ell(v_{\ell,i,j}), \quad i, j = 1, \ldots, M, \quad \ell = 1, \ldots, 3,$$

with corresponding submatrices $\boldsymbol{S}_\ell(\boldsymbol{v})$, given by $\boldsymbol{S}_\ell(\boldsymbol{v})_{i,j} = s_\ell(v_{\ell,i,j})$.

Finally we will use IMEX-RK integrators for (3.10), we rewrite (3.10) as (1.3) and we apply the Algorithm 2.2.1.

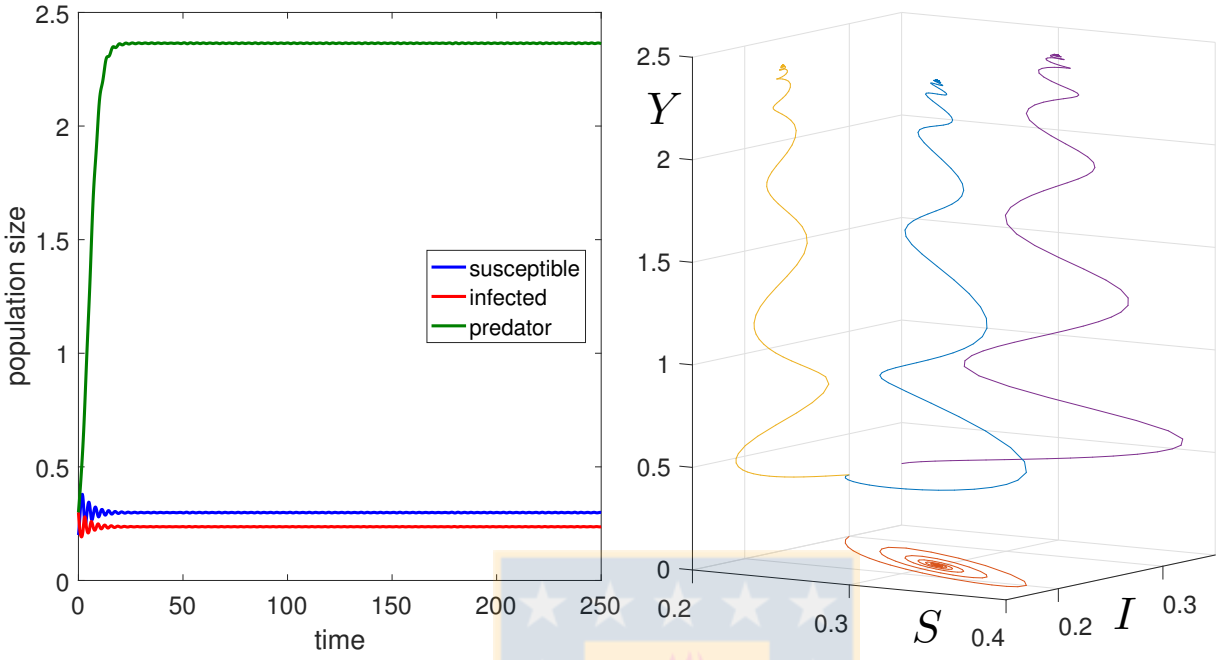

Figure 3.2: Numerical solution of the ODE model (3.1) with parameters (3.4) and (3.12), starting from $S(0) = 0.2$, $I(0) = 0.3$, and $Y(0) = 0.3$. The blue curve in the right plot is the solution curve in (S, I, Y)-space. The other curves represent projections into the (S, I)-, (Y, S)- and (Y, I)-planes (figure produced by author).

3.3 Numerical results

We wish to compare the ODE model (3.1) with the spatio-temporal model (3.5) in different scenarios.

3.3.1 Solution to the ODE model

For this model we consider parameter values (3.4) along with

$$\beta = 42, \quad c = 5. \tag{3.12}$$

This choice is in accordance with the region of stability shown in Figure 3.1 (these parameters will be varied within the numerical solution of spatio-temporal models). For the parameters (3.4) and (3.12), we obtain the following equilibria of Theorem 3.1.1 (besides $E_1 = (1, 0, 0)$) where the predator is absent:

$$E_2 = (0.7516611, 0.0886924, 0), \quad E_3 = (0.2483389, 0.2684504, 0), \tag{3.13}$$

as well as the two points

$$E_4 = (0.7013155, 0.1006989, 1.0069894), \quad E_5 = (0.2986844, 0.2364426, 2.3644263).$$

Since all eigenvalues of

$$\boldsymbol{J}^*(E_5) = \begin{bmatrix} -3.3480149 & -5.9322259 & 0 \\ 2.3480149 & 2.9666648 & -0.000055 \\ 0 & 4 & -0.4 \end{bmatrix}$$

have negative real part, the equilibrium E_5 is stable. On the other hand, $\boldsymbol{J}^*(E_4)$ has an eigenvalue with positive real part and therefore the point E_4 is unstable. As a consequence, whenever predators and prey are present the solution orbits of (3.1) approach the stable equilibrium E_5, as is illustrated in Figure 3.2.

3.3.2 Solution to the spatio-temporal model

In Examples 1 to 10 we select the spatial domain $\Omega = [0, L] \times [0, L]$ with $L = 100$. For the spatial discretization we use $M = 400$, such that $\Delta x = L/M = 0.25$. For the time discretization we employ Algorithm 2.2.1. The parameters $\varepsilon = 4$ and $\kappa_Y = 1$ are chosen in the nonlocal term, and the diffusion constants are chosen as $D_S = 6$ and $D_I = 1$, corresponding to the assumption that infected individuals of the prey population exhibit a lower degree of mobility than their susceptible counterparts. The initial condition for S and I is always a spatially distributed random perturbation of the respective values 0.3 and 0.2. Three cases will be considered for the initial condition of the predators, namely (a) absence of predators, (b) a "triangular" initial condition for predators to describe how predators invade a region initially occupied by prey only, and (c) a random initial condition for predators. These three scenarios are illustrated in Figure 3.3. The simulations are carried out until the nonlocal system (3.5) attains a stable non-homogeneous steady state.

Furthermore, we wish to compare the numerical results with the predictions made by the non-spatial ODE model. To this end we determine for each compartment $X \in \{S, I, Y\}$ and time instants $t^n = n\Delta t$ the following quantity:

$$\mathcal{I}(X) = \mathcal{I}(X, t^n) := h^2 \sum_{i,j=1}^{\mathrm{N}} X_{i,j}^n \approx \int_\Omega X(\boldsymbol{x}, t^n)\, \mathrm{d}\boldsymbol{x}, \tag{3.14}$$

which represents the approximate total number in Ω of individuals of compartment X at time t^n. We recall that in the PDE model, the unknowns $X \in \mathcal{C}$ are *densities*, and so an integration over Ω is necessary to make results comparable with those of a model that predicts the *total number* of individuals in each compartment (as does the dynamical system (3.1)).

Example 1

Here, we consider absence of the predators, i.e., only the equations (3.5a), (3.5b) are considered, with the parameters given by (3.4) and (3.12). The values of β and μ in combination with $D_S = 6$ and $D_I = 1$ have been chosen such that they lie in the Turing region, see [67, Example 6], which means that the formation of a permanent spatial pattern by the standard Turing mechanism in

reaction-diffusion systems (see, e..g., [52]) is expected. In our simulation the initial conditions for S and I are those of Figure 3.3 (a). In Figure 3.4 we display the numerical solution at three different times. We observe the formation of a pattern of spots similar to that observed in [67]. This distribution will remain constant over time. Moreover, Figure 3.5 shows the integral quantities $\mathcal{I}(S)$, $\mathcal{I}(I)$, and wherever appropriate $\mathcal{I}(Y)$, for Examples 1 to 6. For Example 1, and consistently with the nearly stationary spatial pattern, we observe (in Figures 3.5 (a) and (b)) that $\mathcal{I}(S)$ and $\mathcal{I}(I)$ become practically stationary after very short time, and assume values close to $L^2 \times 0.2483389 \approx 2483$ and $L^2 \times 0.2684504 \approx 2684$ that would be obtained if the solution were equal to the stable equilibrium E_3 (see (3.13)) on the whole domain. In this sense, in this example the global behaviour of the model is consistent with (3.1).

Example 2

Here we introduce predators through the "triangular" initial condition of Figure 3.3 (b). All other parameters are the same as in Example 1. In Figure 3.6 we display the dynamics of model (3.5). The convective term in (3.5c) defined in terms of the non-local velocity function (3.6) allows the movement of the predators to places where infective prey are present. At simulated time $t = 30$ we observe that the distribution of prey varies in comparison with Example 1 in places where predators are present. At $t = 90$ we observe that in places where the predators are absent, preys are distributed in forming spots as in Example 1, however, where predators are present, these patterns take the form of stripes. At $t = 200$, predators are present in the whole domain, and this has motivated that the distribution of the prey in the domain varies drastically from its natural distribution without predator (Example 1). This distribution will remain constant over time. The corresponding plots of $\mathcal{I}(S)$ and $\mathcal{I}(I)$ (Figure 3.5 (c)) and $\mathcal{I}(Y)$ indicate a growth of the predator population over a very long period of time. Shortly before $t = 200$ these quantities become constant. It is worth noting that while $\mathcal{I}(S)$ and $\mathcal{I}(I)$ tend to values that are close to L^2 times the first and second component of E_5, namely 2986.8 and 2364.4, respectively, the limit value of $\mathcal{I}(Y)$ exceeds L^2 times the Y-component of E_5, that is 23644.3, by more than a factor of two.

Example 3

Here we consider a random initial condition for predators with the same parameters of Example 1. The initial condition is shown in Figure 3.3 (c). In Figure 3.7 we display the dynamics of the model with this initial condition. At simulated time $t = 30$ we observe that stripes and some spots patterns emerge mixed in the distribution of each species. After the stripe patterns form, they grow steadily with time until they reach certain arm length, and the spatial patterns become distinct at $t = 200$. It is observed that these stripe patterns are not similar to those obtained in Example 1, instead these patterns in form of stripes or filaments are very similar to those observed in Example 2. Furthermore, Figures 3.5 (e) and (f) indicate that $\mathcal{I}(S)$, $\mathcal{I}(Y)$ and $\mathcal{I}(Y)$ quickly attain steady states, with final values similar to those of Example 2.

Example 4

Here, we consider absence of predators like in Example 1 and we use here and in Examples 5 and 6 the parameter values

$$\beta = 46, \quad c = 4. \tag{3.15}$$

In this case the parameters β and μ together with the diffusion constants are not in the Turing space. The steady states according to Theorem 3.1.1 are now, besides $E_1 = (1, 0, 0)$,

$$E_2 = (0.7820731, 0.0778310, 0), \quad E_3 = (0.2179270, 0.2793118, 0), \tag{3.16}$$

$$E_4 = (0.7510048, 0.0848976, 0.8489759), \quad E_5 = (0.2489953, 0.2560630, 2.5606299). \tag{3.17}$$

Considering the initial conditions of Figure 3.3 (a), we obtain in this case that no patterns are formed and the system quickly arrives at a constant equilibrium (uniform distribution for S and I in whole domain), which is maintained over time, as can be observed in Figure 3.8. This figure, as well as Figures 3.5 (g) and (h), indicate that the global equilibrium is E_3 given by (3.16).

Example 5

In this case we consider the same scenario as in Example 2, namely the triangular initial condition of Figure 3.3 (b), but utilize the parameters (3.15) instead of (3.12). In this case, as in Example 2, predators are heading towards the infected prey, and as is shown in Figure 3.9, the whole domain becomes successively filled with a pattern formed of stripes. Note that in regions occupied by the prey before the arrival of predators the solution is constant (see Example 4), and in particular does not exhibit any formed pattern (in contrast to Example 2). In a sense this scenario illustrates how the model (3.5), under the appropiate choice of parameters, predicts the formation of spatial patterns among the prey upon arrival of the predators. Furthermore, we observe that a "front" of predators is moving into the domain initially occupied by prey only, which seems to move at a lower velocity than in Example 2. It is worth noting that the final distribution of prey corresponds to total S and I populations close to L^2 times the corresponding entries of E_5 given by (3.17), while as in previous cases the final population of predators is much higher than L^2 times the Y-component of E_5.

Example 6

This case is the analogue of Example 2, namely we impose the initial conditiom of Figure 3.3 (c). In Figure 3.10 we display the dynamics of the model with this initial condition. We observe that at simulated time $t = 50$, some stripes and spots emerge as patterns in the distribution of each species. Comparing the successive solutions for $t = 50$, $t = 100$ and $t = 200$, we observe that once the stripes form, they grow steadily in time incorporating "spots", until they reach certain arm length, and the spatial patterns become slightly distinct at $t = 200$ since at this time there are strips and spots. It is observed that these patterns differ from those obtained in

Example 5, where only stripe-like patterns are formed. The observations corresponding to the evolution of $\mathcal{I}(S)$, $\mathcal{I}(I)$ and $\mathcal{I}(Y)$ are analogous to those of Example 3.

Example 7

Here and in Examples 8 and 9 we use the values

$$\beta = 46, \quad c = 10. \tag{3.18}$$

The equilibrium points are $E_1 = (1, 0, 0)$, E_2 and E_3 given by (3.16), and

$$E_4 = (0.6916269, 0.984517, 0.9845173), \quad E_5 = (0.3083731, 0.2208100, 2.2081005).$$

The integral quantities for this case and Examples 8 to 10 are plotted in Figure 3.12.

As in Example 4, the parameters β and μ together with the diffusion constants are not in the Turing space. Considering the initial condition of Figure 3.3 (a), it is obtained that in this case no patterns are formed and the system rapidly tends to constant equilibrium which is maintained in time, see Figure 3.11. For this case we observe a behavior similar to that of Example 7.

Example 8

This case is based on the same initial "triangular" scenario (Figure 3.3 (b)) as Examples 2 and 5. The numerical solution (Figure 3.13) shows that the predators are heading towards the infected prey, and for $t = 50$ and $t = 150$ we observe that the distribution of the prey varies in comparison with the uniform distribution of Example 7 in those places were the predators are present. The final spatial configuration is marked by spots and stripes for the prey as well as for the predators, and remains in time. However, the stucture of patterns that are formed differs from the results of Example 5. It is interesting to note that the stripes visible at $t = 600$ are still roughly aligned with the original "front" of predators separating the triangular region from the rest of the domain. The conclusions concerning the evolution of $\mathcal{I}(S)$, $\mathcal{I}(I)$ and $\mathcal{I}(Y)$ (see Figure 3.12 (c) and (d)) are similar to those for Example 5.

Example 9

We now consider an analogue of Examples 3 and 6 corresponding to the initial configuration of Figure 3.3 (c). In Figure 3.14 we display the dynamics of the model with this initial condition. At $t = 50$ we observe that some stripes and spots patterns emerge mixed in the distribution of each species. The pattern distribution is maintained over time after its formation. It is observed that these patterns differ from those obtained in Examples 5, 6, and 8. As in Examples 3 and 6, the quantities $\mathcal{I}(S)$, $\mathcal{I}(I)$ and $\mathcal{I}(Y)$ very quickly attain constant values (see Figures 3.12 (e) and (f)).

Example 10

In this example, a constant value is considered for $\beta = 48$ and in combination with the three different values $c = 4$, $c = 6$ and $c = 10$. For these three pairs that are in the region of stability shown in the Figure 3.1 a variation is obtained in the formation of patterns for the different values of c. The initial datum is given by Figure 3.1(c). In Figure 3.15 the corresponding numerical results are shown. It turns out that with increasing c the species tend to form more filament-like rather than spot-like spatial structures. Moreover, there is a marked difference in behavior of $\mathcal{I}(S)$, $\mathcal{I}(I)$ and $\mathcal{I}(Y)$, as can be inferred from Figures 3.12 (g) to (l). Note that the steady-state value of $\mathcal{I}(I)$ decreases with increasing c, as does the steady-state value of $\mathcal{I}(Y)$.

3.3.3 Convergence test and effect of the choice of ε

In Example 11, we investigate the sensitivity of (3.5) to the variation of discretization parameter $\Delta x = L/M$. We take $L = 25$ and the model parameters (3.4), (3.15) as in Examples 4 to 6. The initial datum is a random distribution (similar to Figure 3.1 (c)) defined for a 50×50 discretization, which is also utilized for finer discretizations with $M = 100$, 200, and 400, so the initial condition is exactly the same in all cases. We compute the solution at time $t = 15$ until we obtain a steady state. The results are displayed in Figure 3.16. It is observed that the resolution in the solution is improved as Δx is reduced, and that the steady-state solution is apparently the same (modulo, of course, sharpness of resolution) for all values of M. These results do not provide a rigorous convergence proof but indicate that the numerical simulator is reliable.

Finally, in Example 12 we utilize the same scenario as in Example 11, and now fix the spatial discretization $M = 400$ but vary the parameter ε, that is the radius of the convolution kernel of the nonlocal velocity function (see (3.7)). The corresponding results are given in Figures 3.17 and 3.18. We observe that the results for the prey compartments S and I are practically the same for all values of ε condered, while the prey distribution depends appreciably on ε. As ε decreases, the regions in which predators concentrate become smaller and the densities become higher. Moreover, Figures 3.18 (b), (d), (f), and (h) indicate a decrease of the steady state value of $\mathcal{I}$ as ε is decreased.

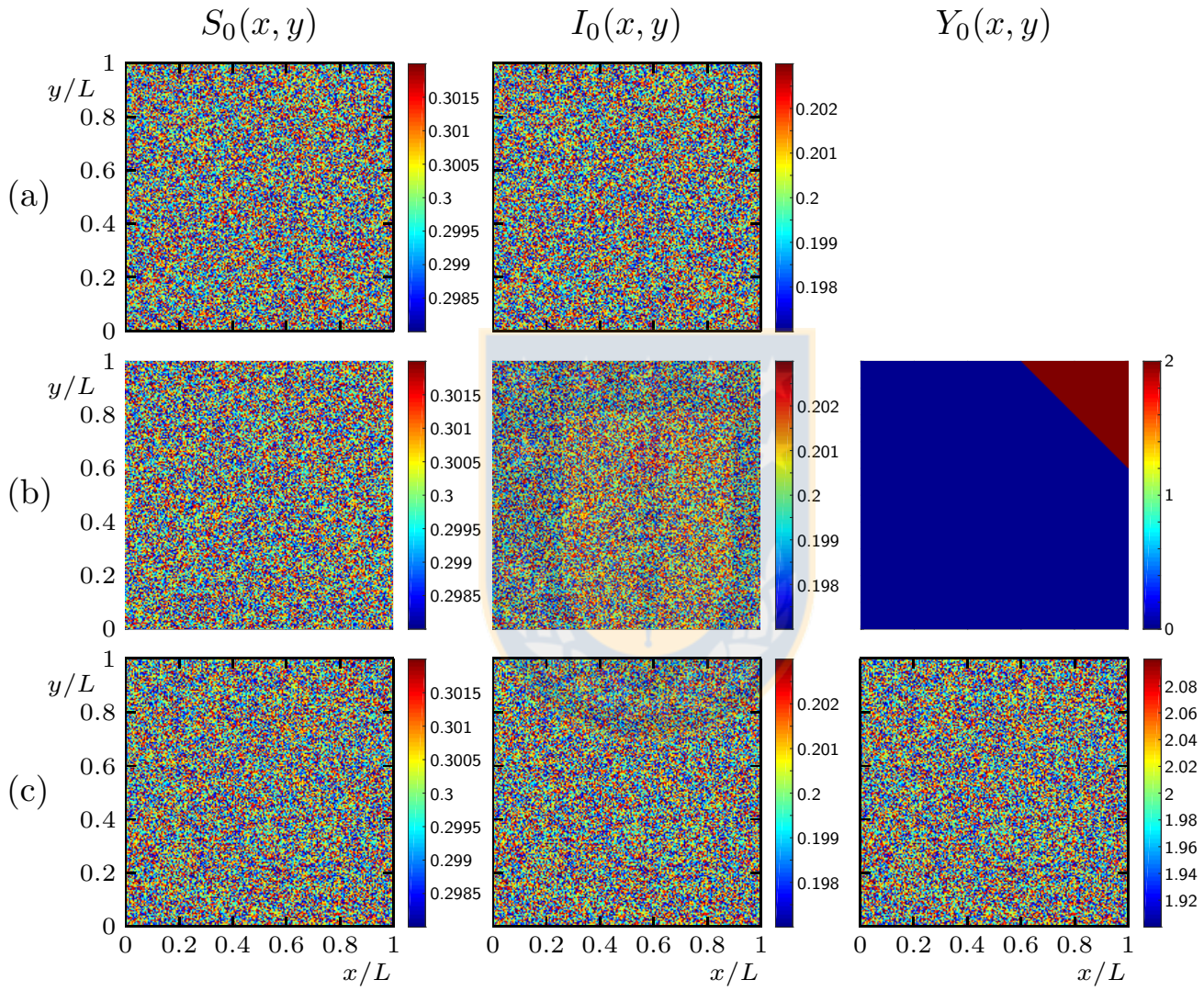

Figure 3.3: Examples 1 to 10: initial data $S_0(x,y)$, $I_0(x,y)$, and $Y_0(x,y)$ (a) for Examples 1, 4, and 7, (b) for Examples 2, 5, and 8, (c) for Examples 3, 6, 9, and 10 (figure produced by author).

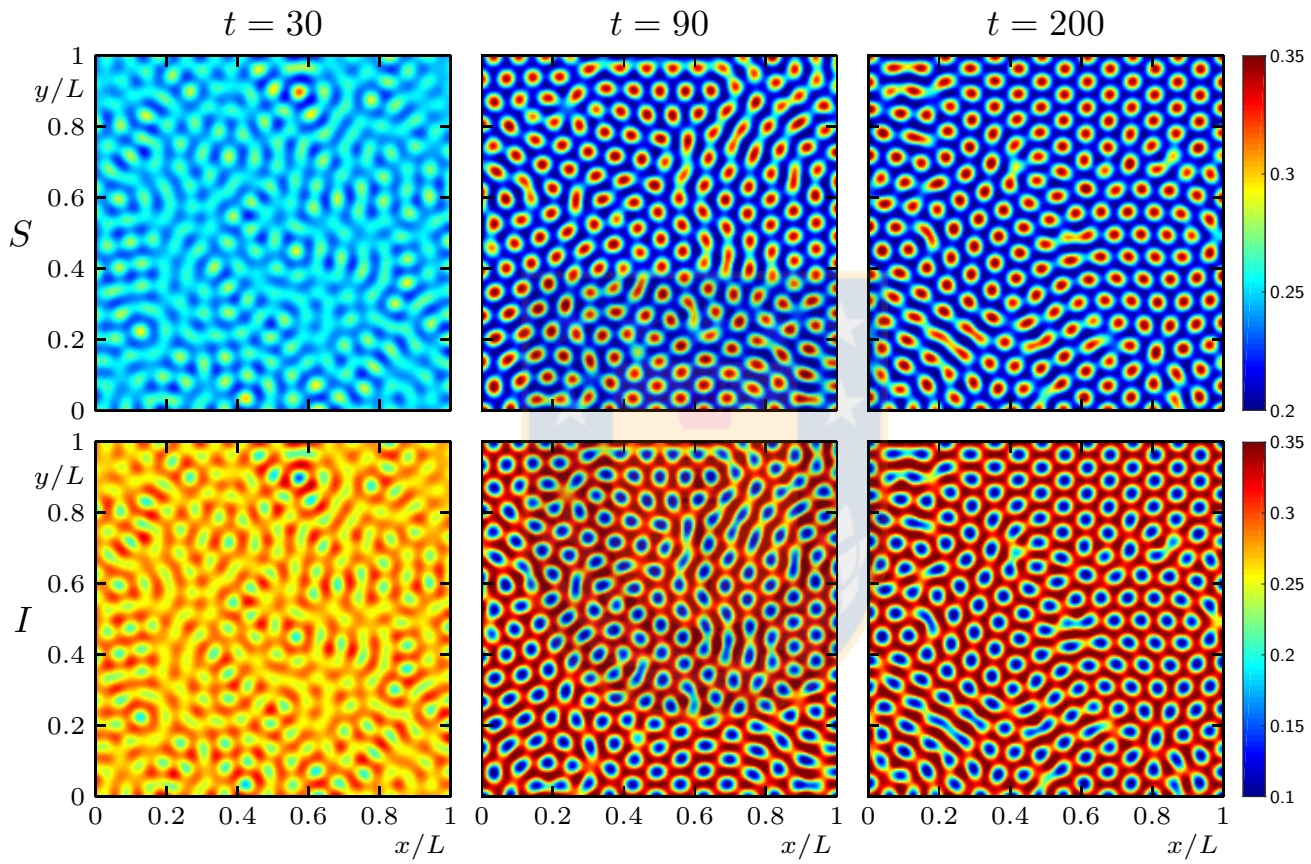

Figure 3.4: Example 1: numerical solution of (3.5) in absence of predators with parameters (3.4) and (3.12) at three different times. The initial datum is given in Figure 3.3 (a) (figure produced by author).

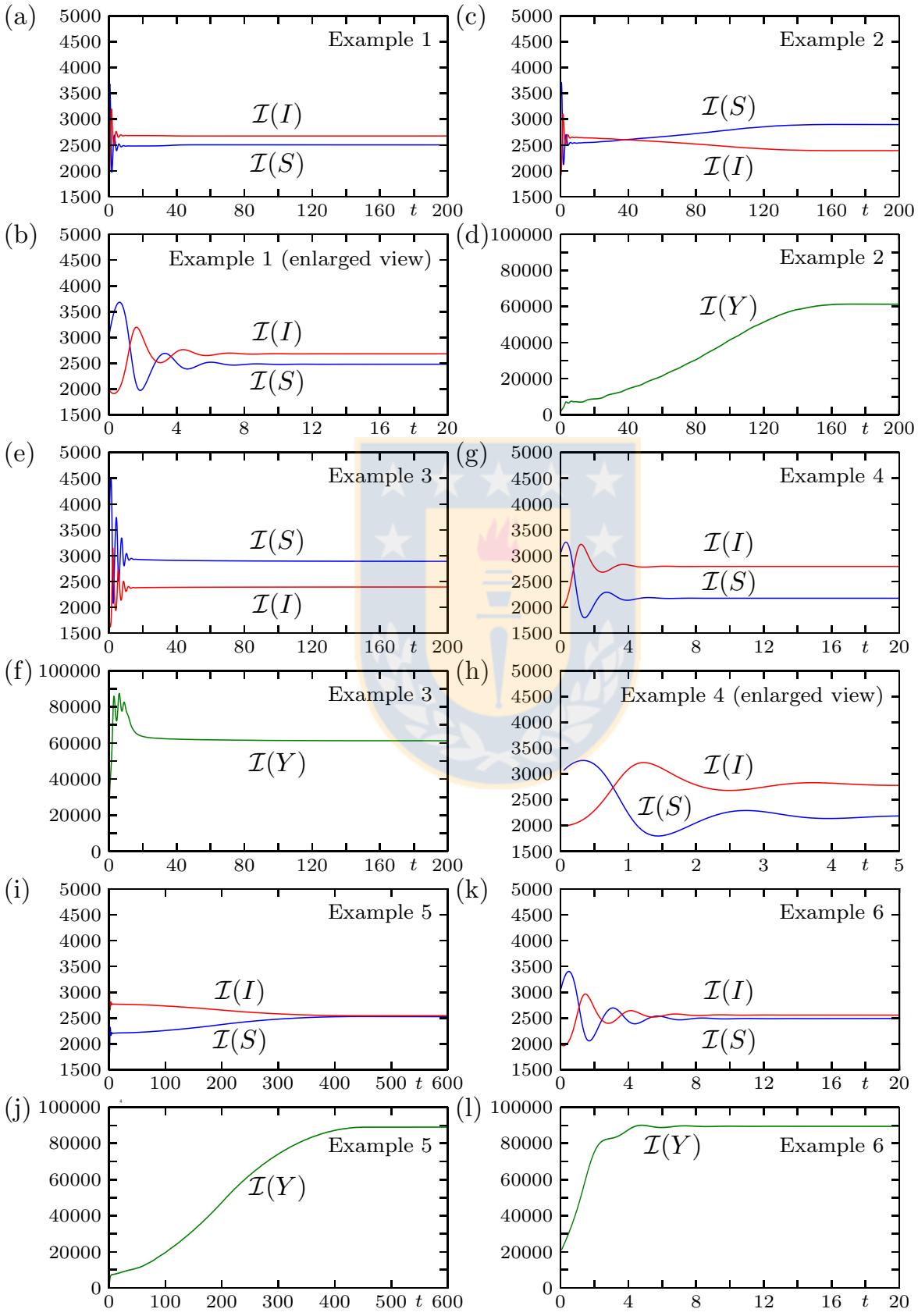

Figure 3.5: Examples 1 to 6: integral quantities (3.14) (figure produced by author).

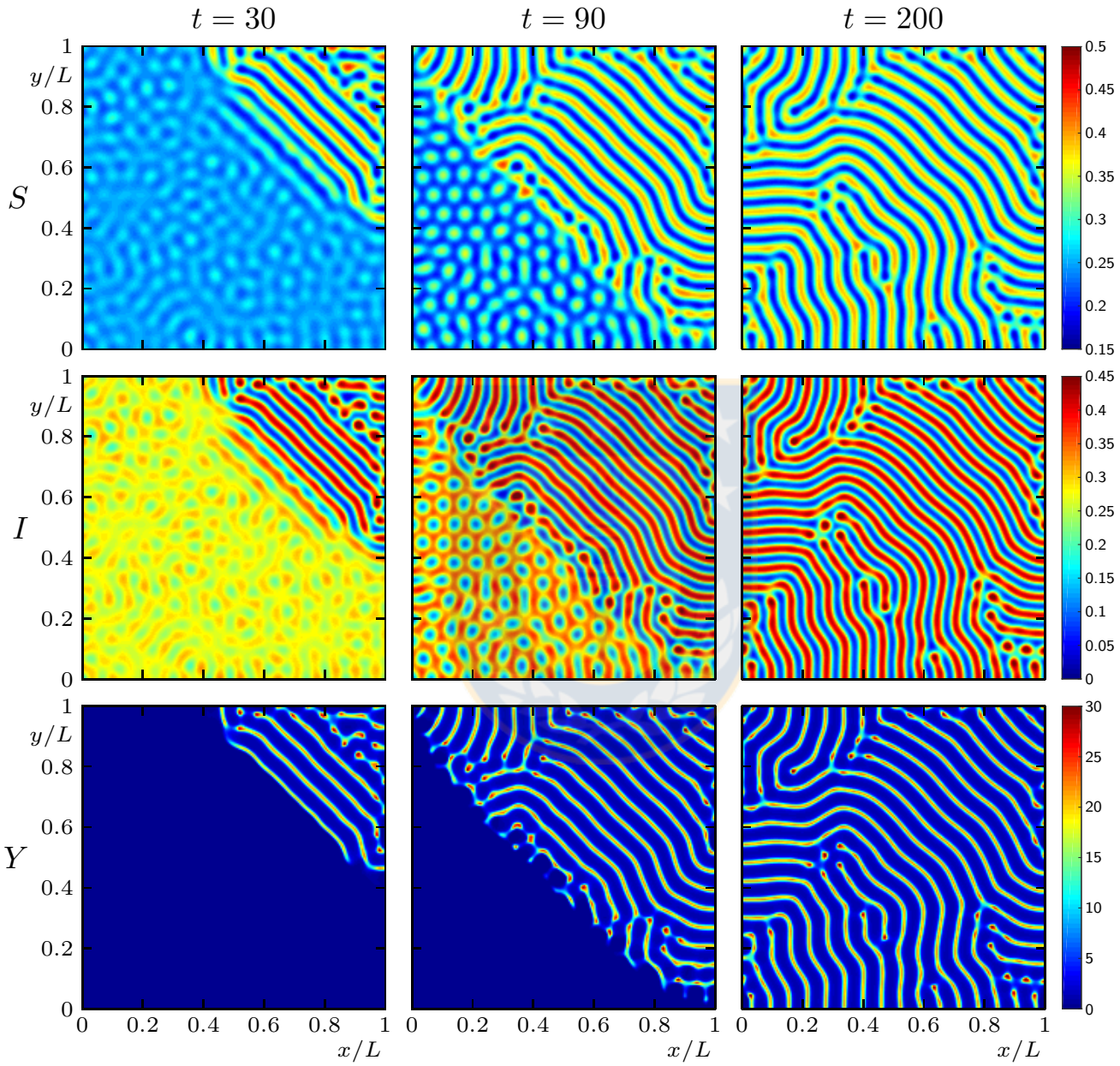

Figure 3.6: Example 2: numerical solution of (3.5) with parameters (3.4) and (3.12) at three different times. The initial datum is given in Figure 3.3 (b) (figure produced by author).

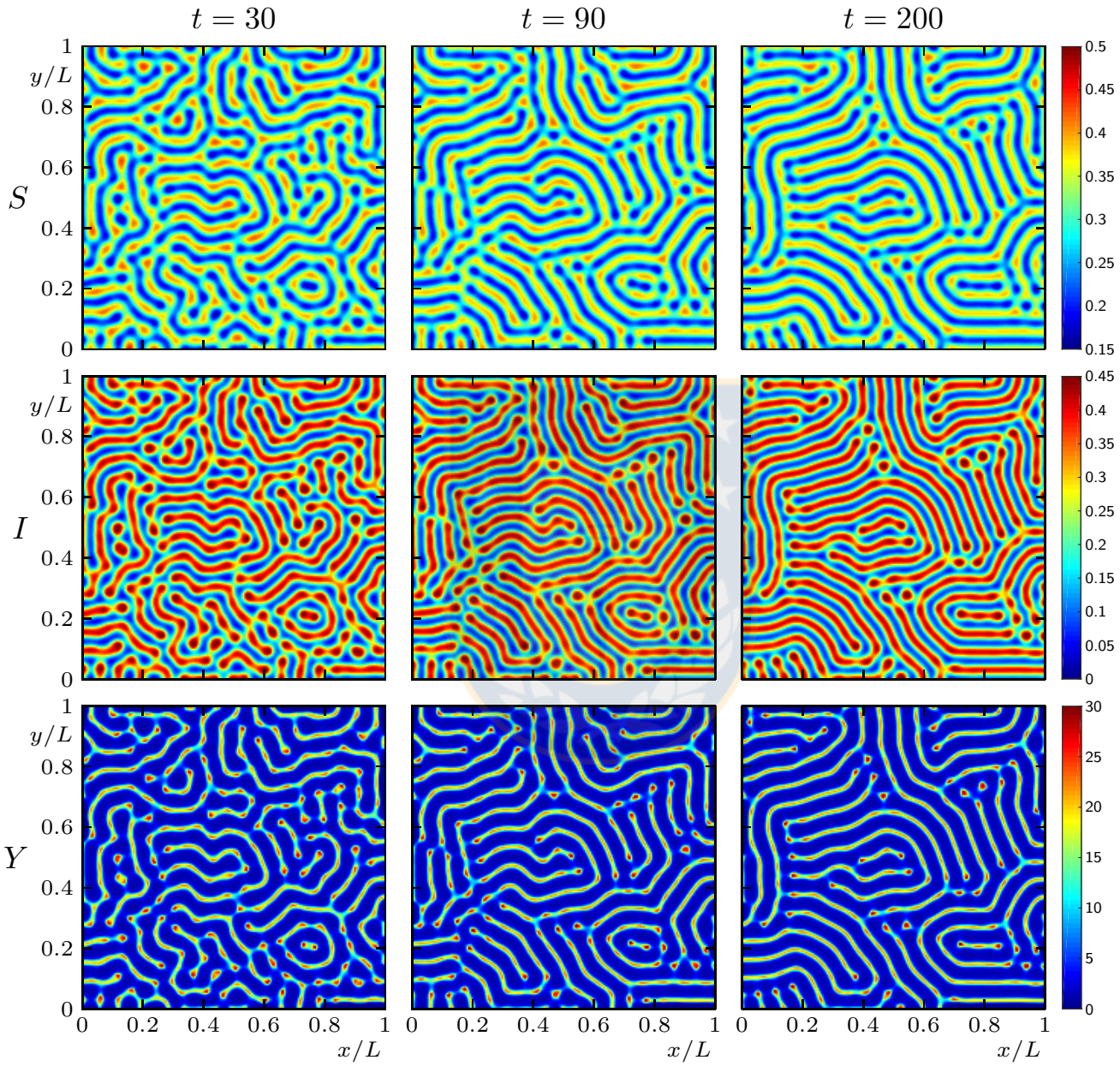

Figure 3.7: Example 3: numerical solution of (3.5) with parameters (3.4) and (3.12) at three different times. The initial datum is given in Figure 3.3 (c) (figure produced by author).

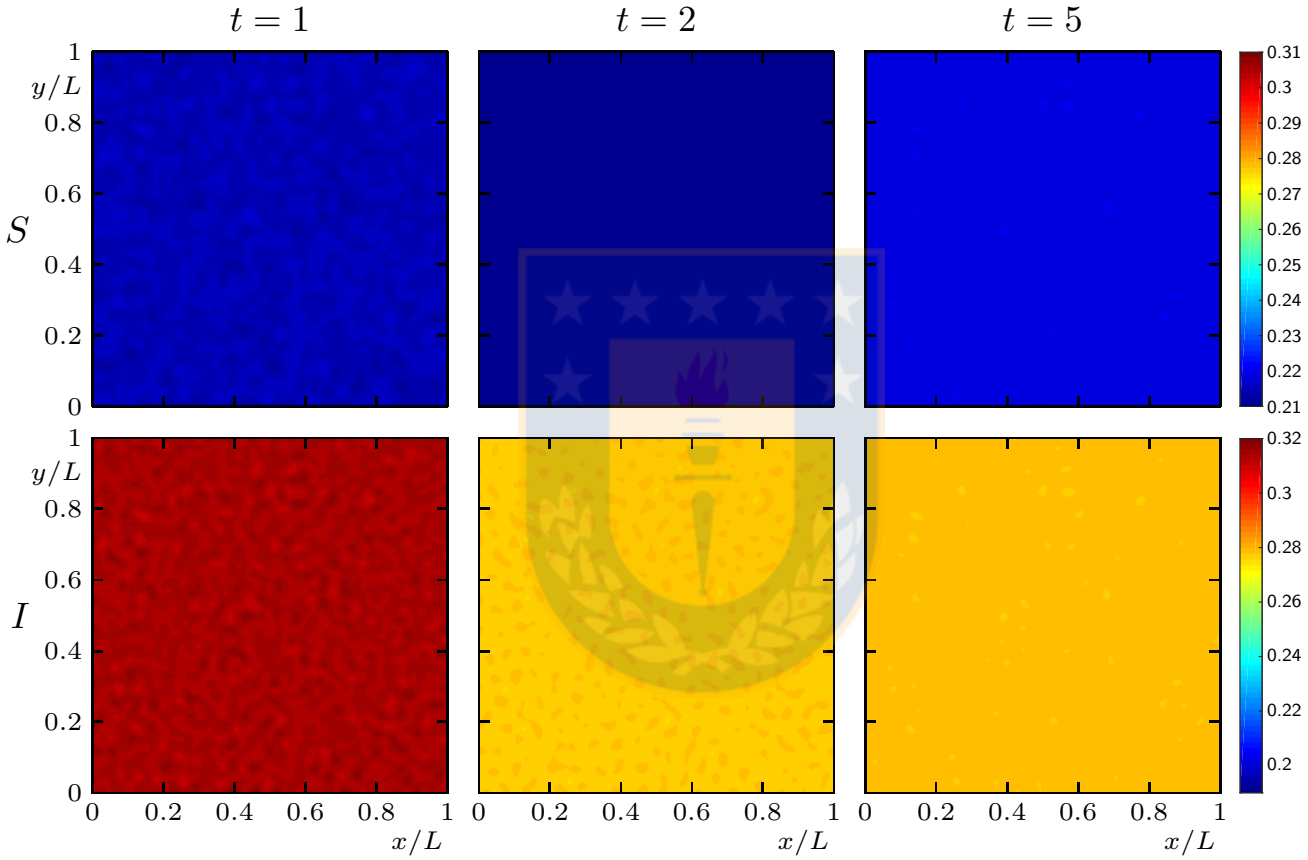

Figure 3.8: Example 4: numerical solution of (3.5) with parameters (3.4) and (3.15) at three different times. The initial datum is given in Figure 3.3 (a) (figure produced by author).

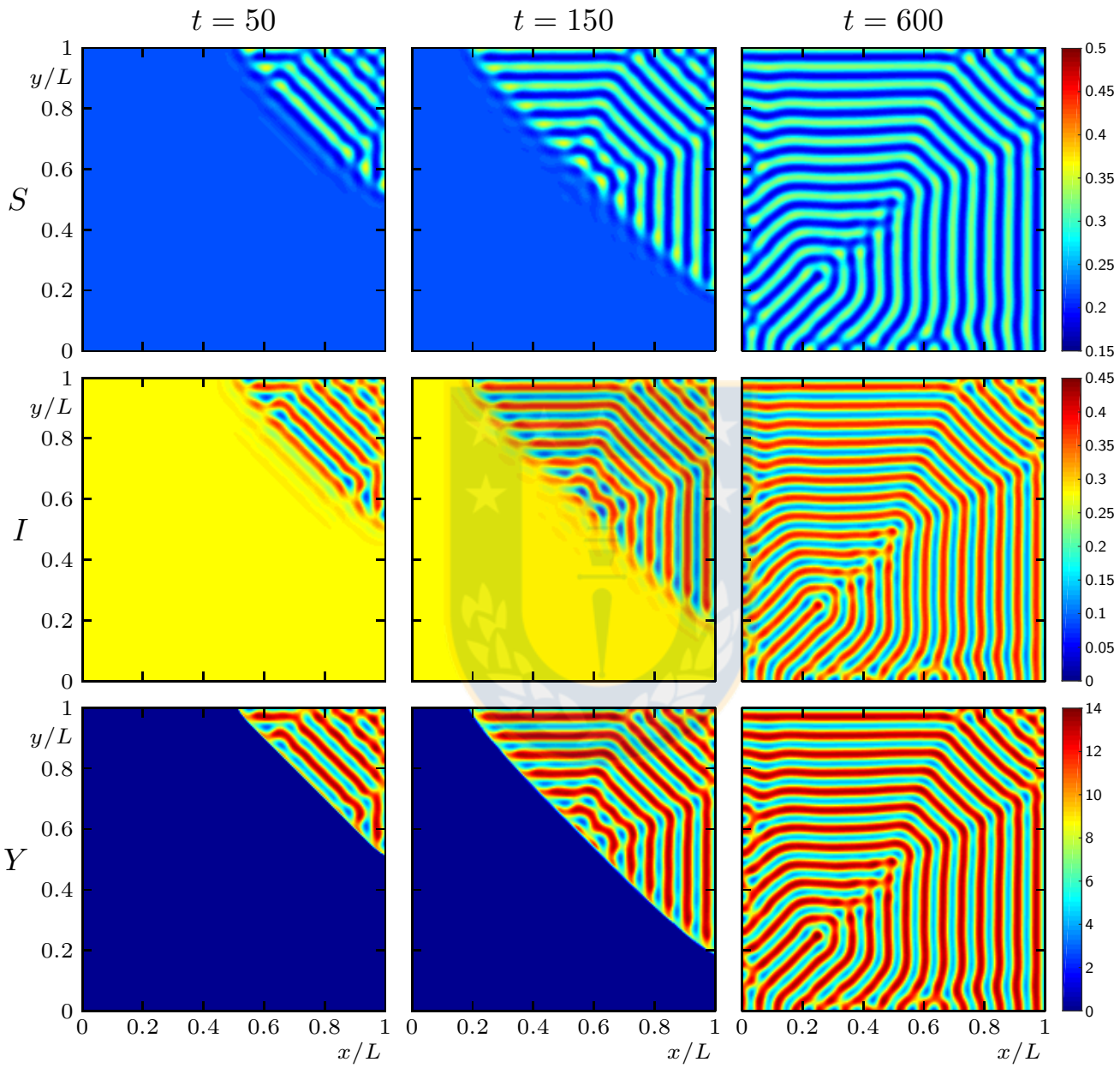

Figure 3.9: Example 5: numerical solution of (3.5) with parameters (3.4) and (3.15) at three different times. The initial datum is given in Figure 3.3 (b) (figure produced by author).

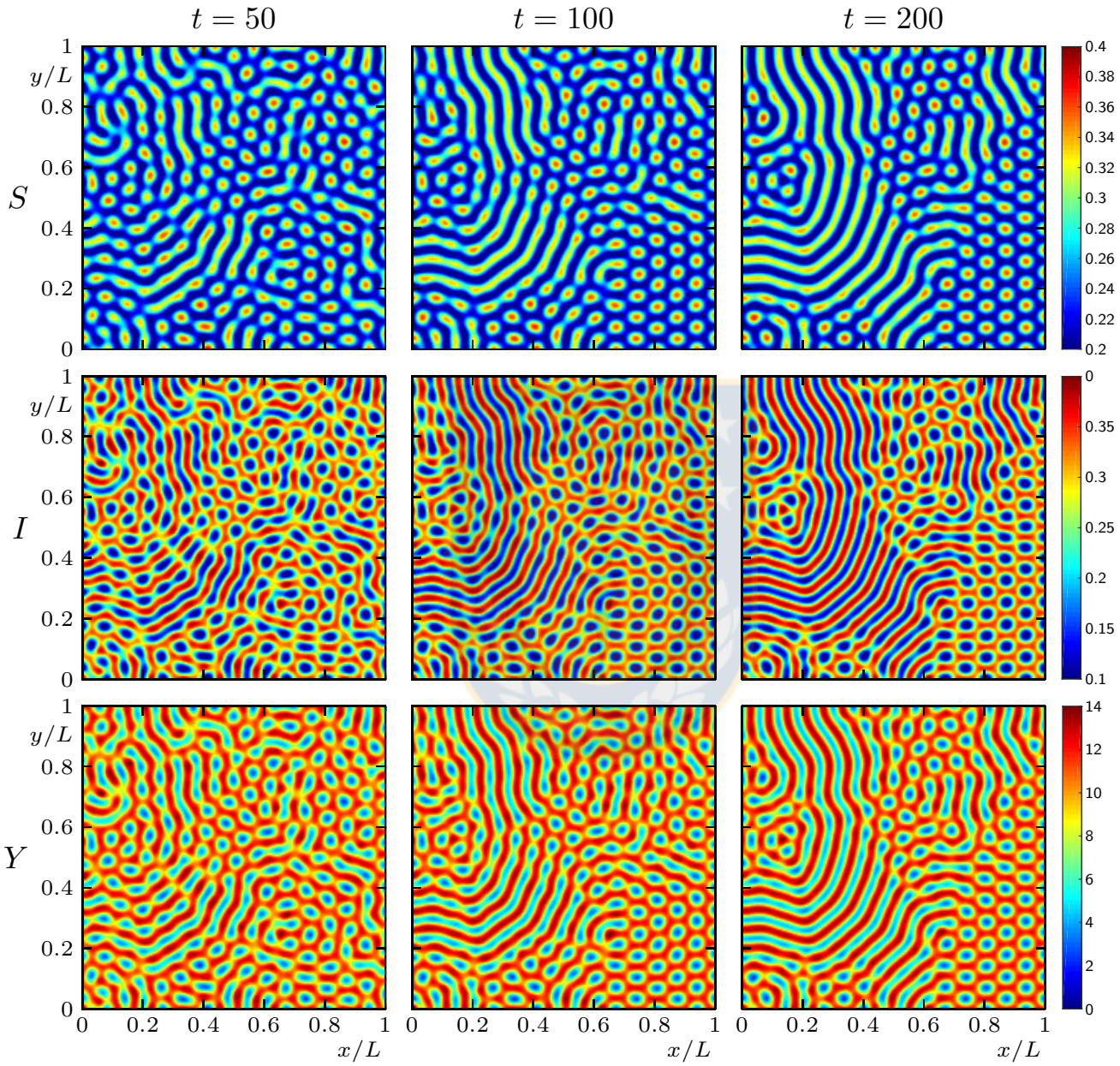

Figure 3.10: Example 6: numerical solution of (3.5) with parameters (3.4) and (3.15) at three different times. The initial datum is given in Figure 3.3 (c) (figure produced by author).

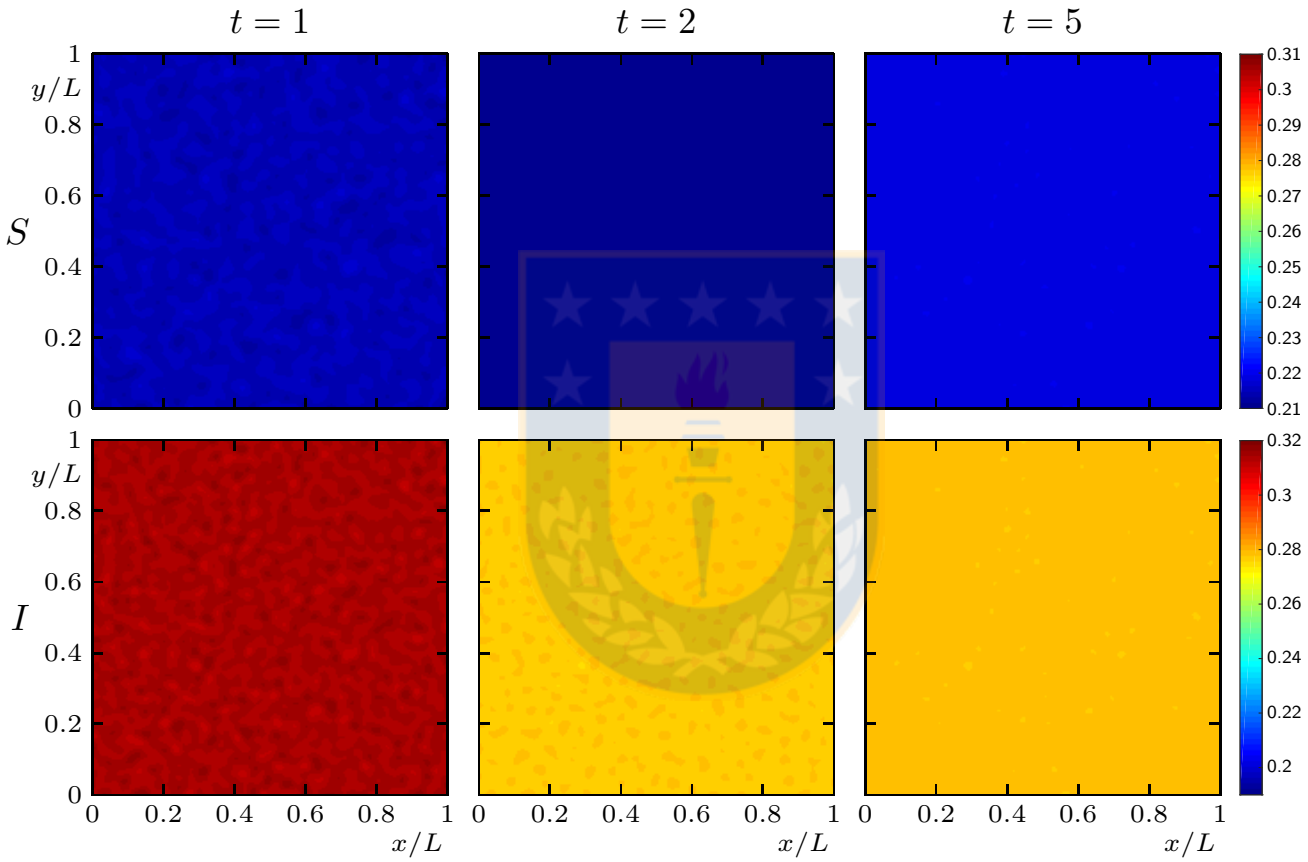

Figure 3.11: Example 7: numerical solution of (3.5) with parameters (3.4) and (3.18) at three different times. The initial datum is given in Figure 3.3 (a) (figure produced by author).

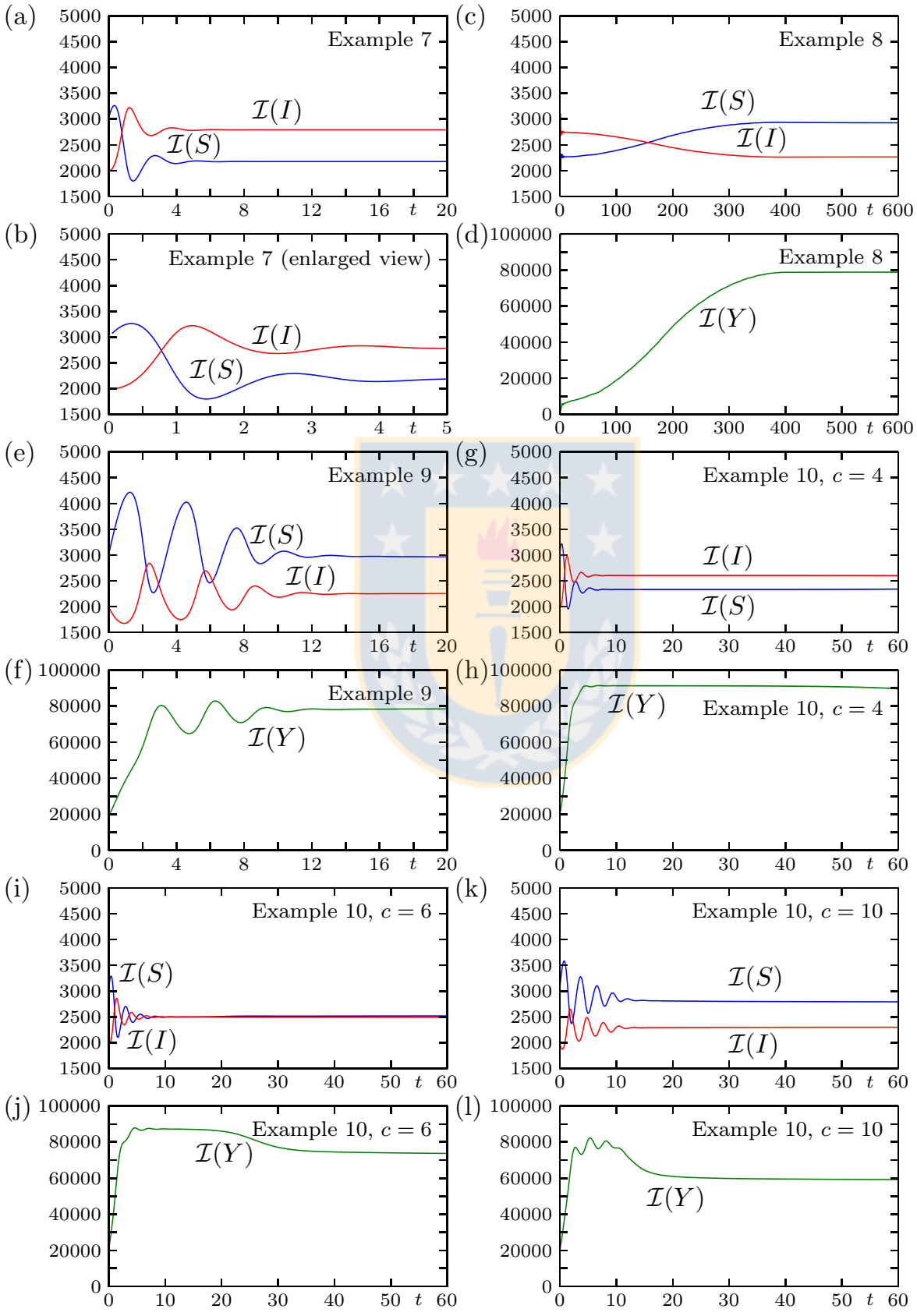

Figure 3.12: Examples 7 to 10: integral quantities (3.14) (figure produced by author).

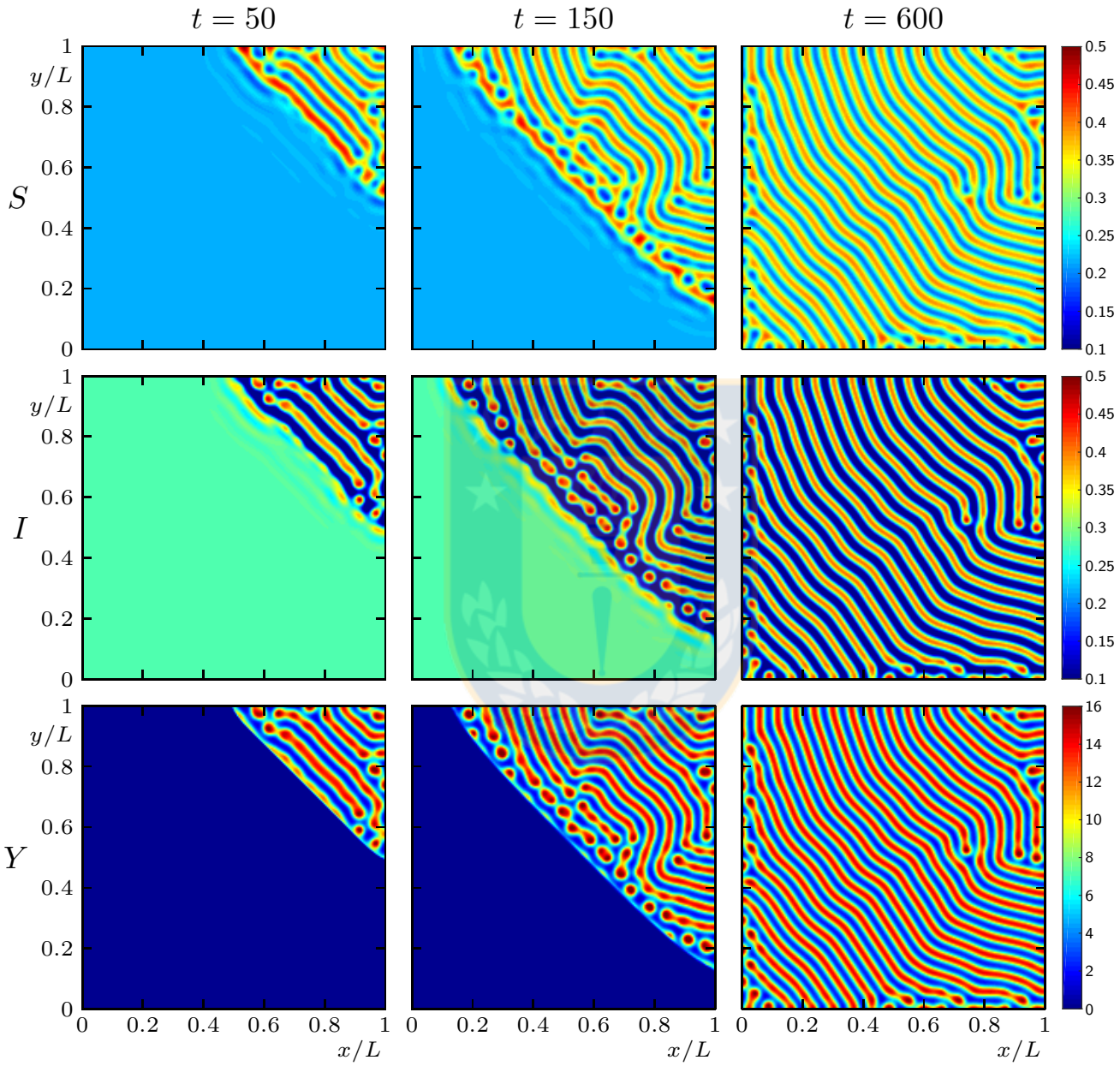

Figure 3.13: Example 8: numerical solution of (3.5) with parameters (3.4) and (3.18) at three different times. The initial datum is given in Figure 3.3 (b) (figure produced by author).

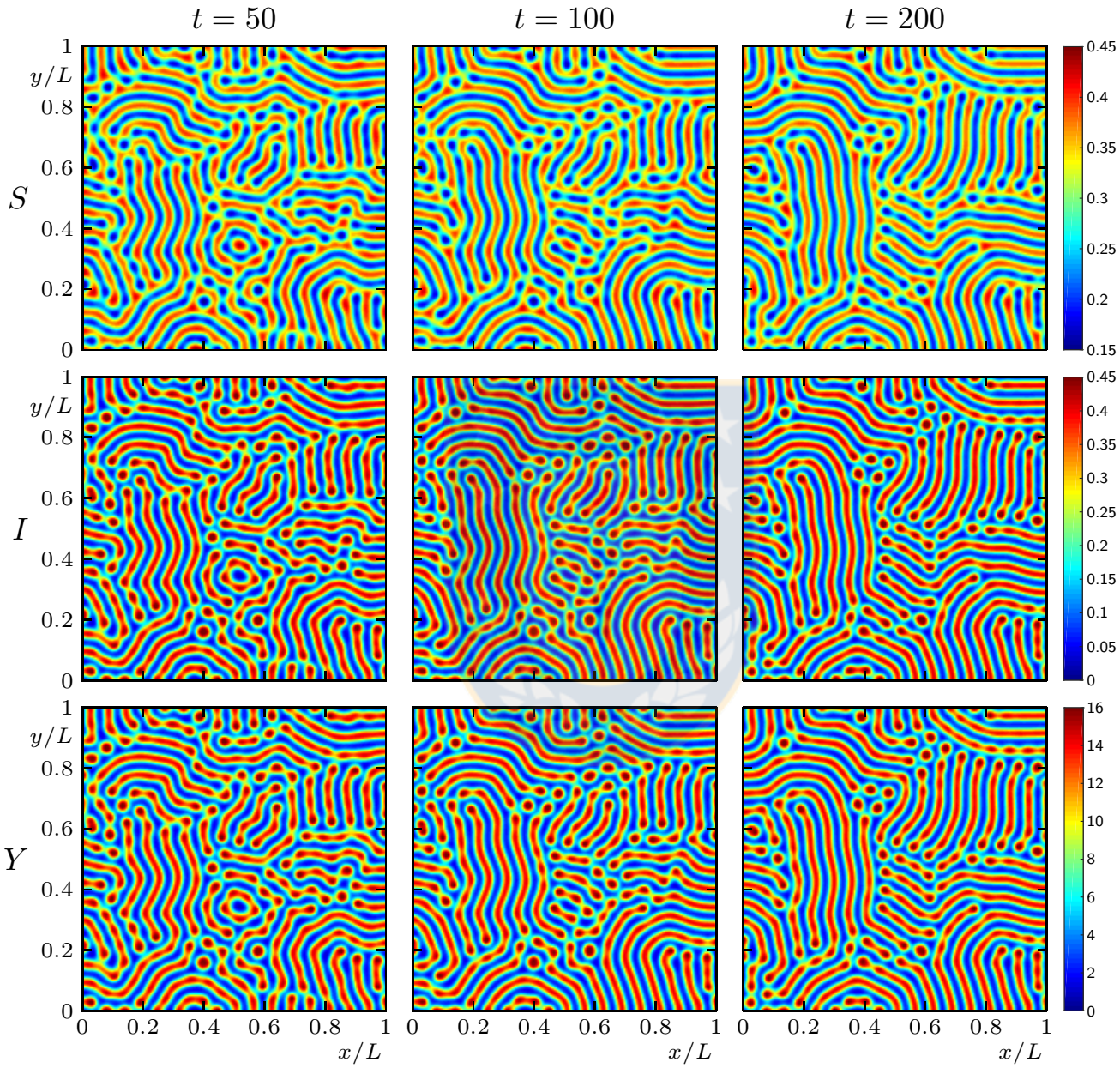

Figure 3.14: Example 9: numerical solution of (3.5) with parameters (3.4) and (3.18) at three different times. The initial datum is given in Figure 3.3 (c) (figure produced by author).

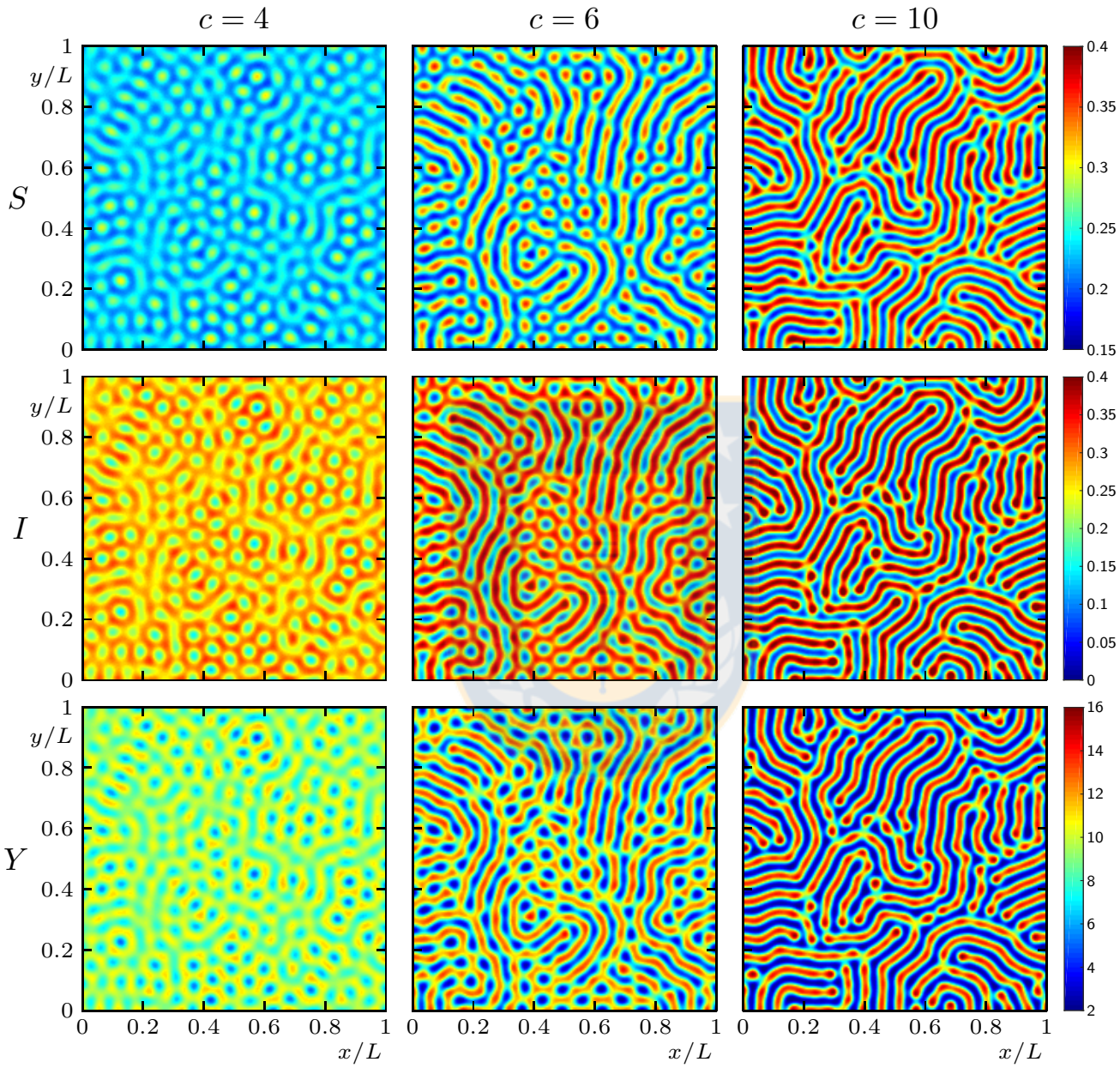

Figure 3.15: Example 10: variation of the parameter c for $\beta = 48$, showing the numerical solution atr $t = 50$ for (left) $c = 4$, (middle) $c = 6$ and (right) $c = 10$. All the remaining parameters are as in (3.4). The initial datum is as shown in Figure 3.3 (c) (figure produced by author).

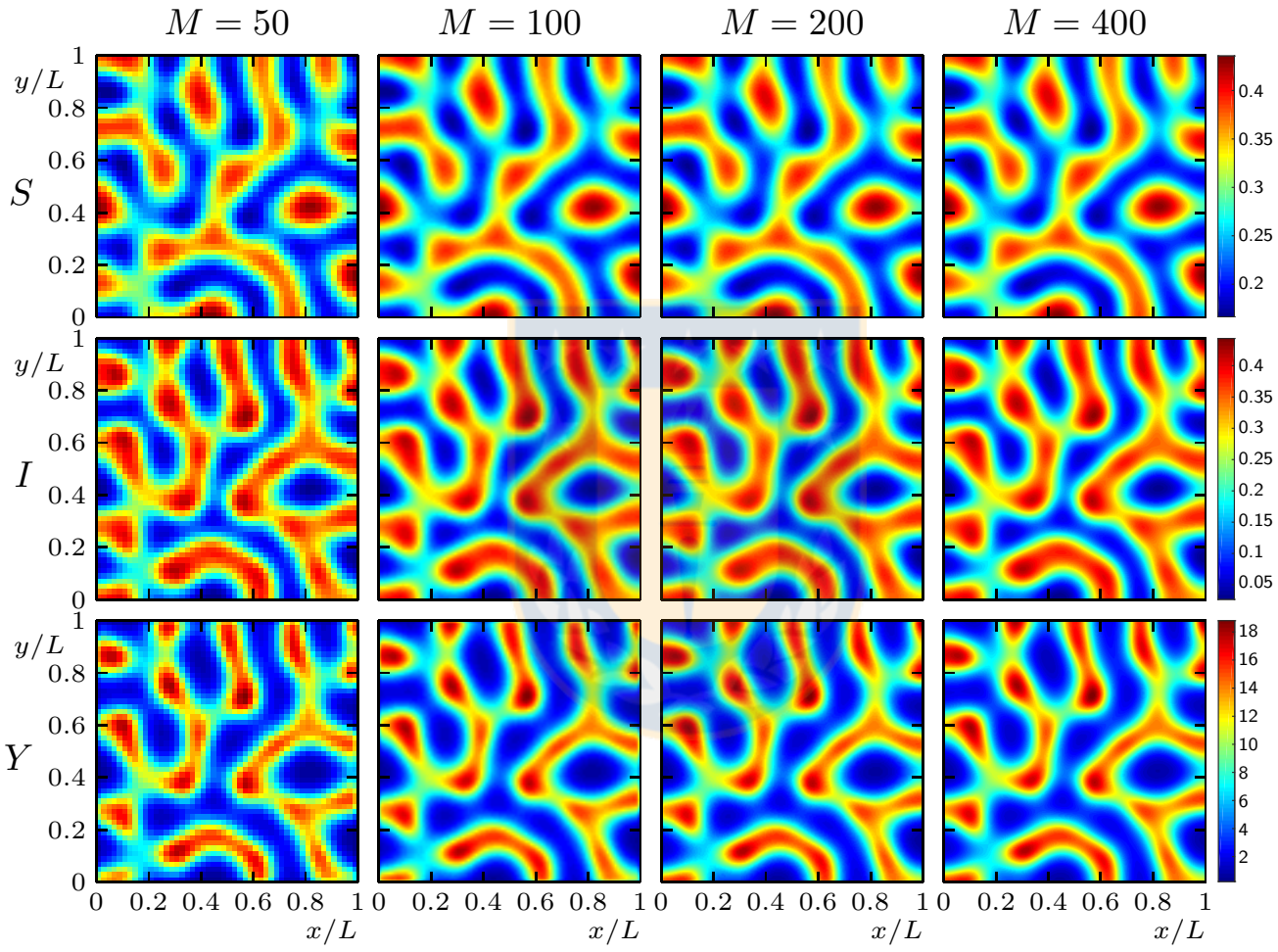

Figure 3.16: Example 11: variation of the spatial discretization $\Delta x = L/M$ of the numerical solution at $t = 15$ on a domain of side length $L = 25$ (figure produced by author).

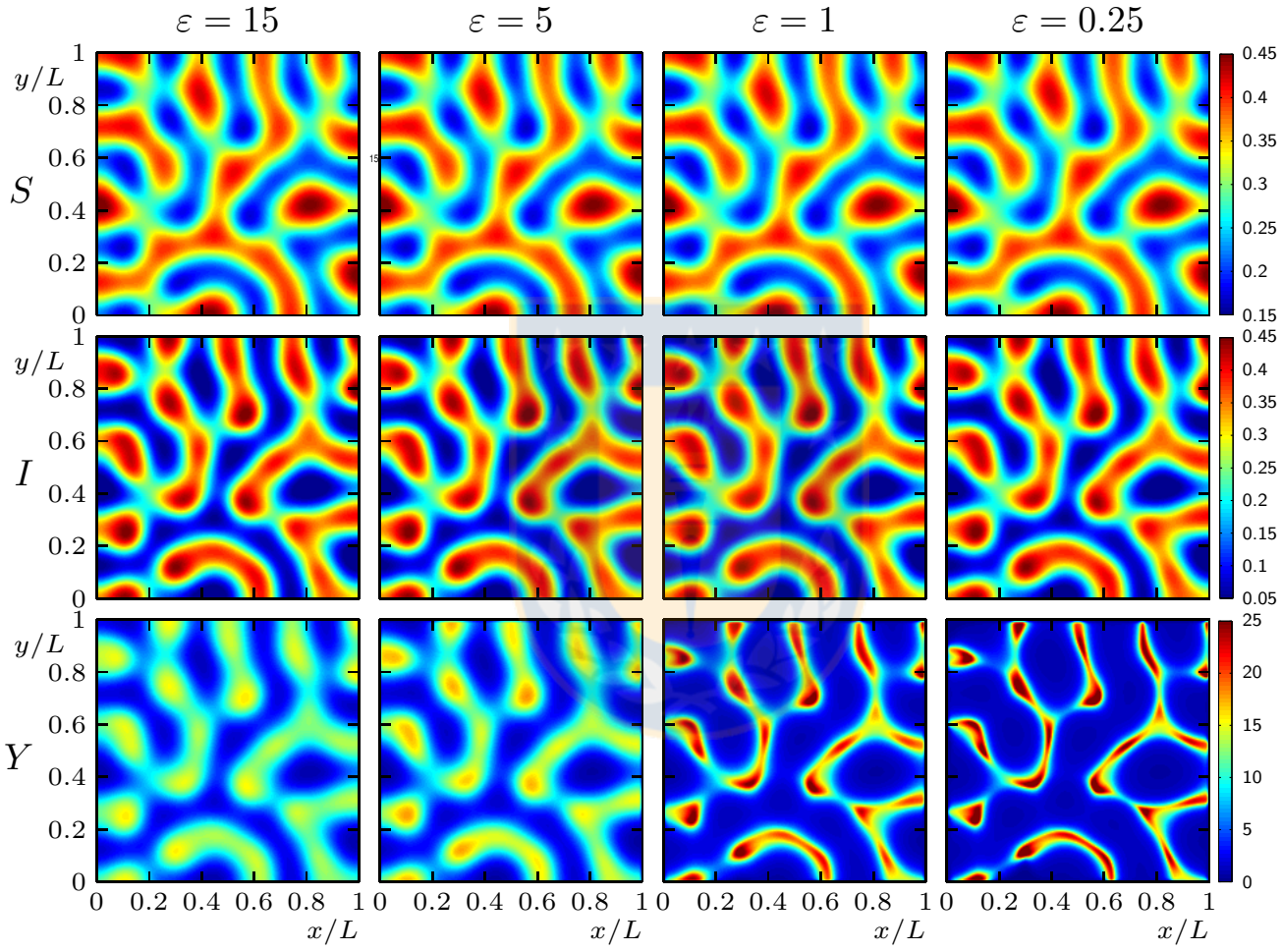

Figure 3.17: Example 12: effect of the variation of convolution radius ε on the numerical solution at $t = 15$ on a domain of side length $L = 25$ (figure produced by author).

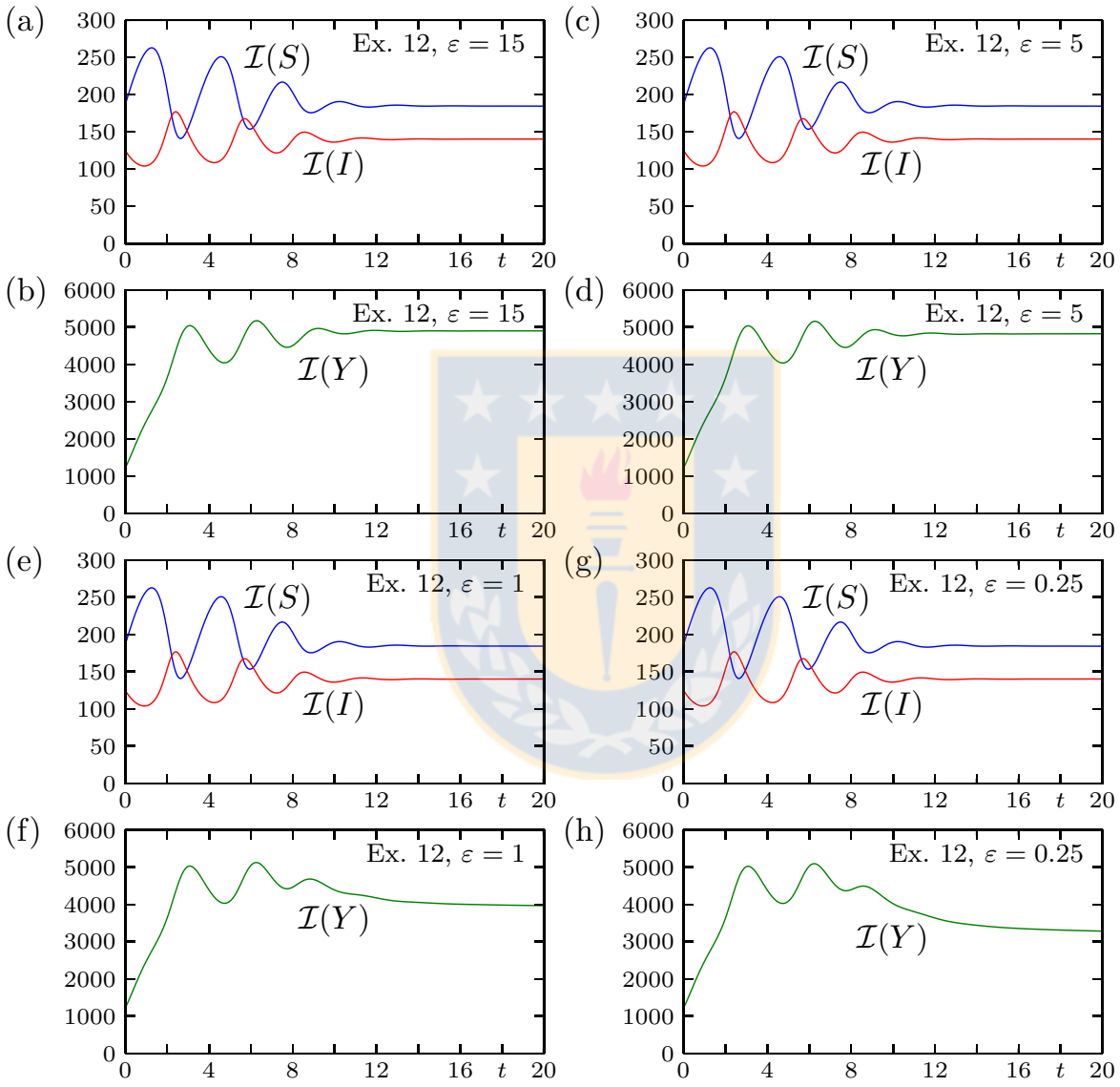

Figure 3.18: Example 12: integral quantities (3.14) (figure produced by author).

Chapter 4

Concluding remarks and future work

4.1 Concluding remarks

In this thesis we have studied convection-diffusion-reaction equations that are related to epidemic models. In the literature, such models are usually formulated as epidemic systems (systems of ordinary differential equations), where the only quantity of interest is the total number of individuals in each epidemiological compartment over time. In contrast, the approach pursed in this thesis also provides information on the spatial distribution of different states of the disease. A decisive tool to efficiently obtain this information is a combination of efficient finite difference WENO schemes, IMEX-RK methods, and discrete convolutions to numerically solve the system of partial differential equations. This method has been applied first to a SEIR model of Hantavirus in rodents, which are classified by gender and subsequently to an eco-epidemiological where initially there is pattern formation in the prey and then a predator invades the habitat.

In Chapter 2 we show that a relatively simple spatial-temporal model (2.1) structured by gender of Hantavirus transmission between rodents with a non-local velocity term (2.6), which arises in each of the models 1, 2 and 3 defined by (2.2), (2.3) and (2.5), respectively, can produce complex spatio-temporal profiles of the prevalence of the disease (Figures 2.2 to 2.8). However, in fact, several additional factors can affect the transmission dynamics of Hantavirus infections among rodents. Specifically, Hantavirus transmission has been associated with patterns of land use [17], elevation, vegetation types [9], as well as moisture and rain [77]. The growth of rodent populations may also be associated with the local temperature, since for example, temperature may affect the pregnancy rate, litter size, birth rate and the survival rate of rodent populations [75]. In addition, rodents tend to live in highly covered and less disturbed habitats, which are commonly found in agricultural areas and grassland areas [50, 76] to improve their reproductive capacity and survival [50].

The accuracy of the numerical method proposed in Chapter 2 deserves to be studied in later works, especially to establish that its order of convergence corresponds to its design order.

More scenarios (initial configuration, calibration of parameters) should be explored with these numerical tools in order to obtain and study more spatio-temporal patterns in the simulations. In this sense, among our proposed models, we consider Model 1 to be the most promising because it gives rise to spatio-temporal patterns and it is worthwhile to be analyzed as in [21, 49].

In Chapter 3 we have shown that a relatively simple three-species model can produce complex spatio-temporal patterns of predators and prey. The treatment combines the spatio-temporal epidemic model of [67], the non-spatial three-species predator-prey model analyzed in [32], the non-local velocity function introduced in [22] and the numerical method developed in [19]. The numerical method is not fully analyzed herein, and certainly leaves potential for further improvements. For instance, its accuracy deserves further investigation (particularly to establish that its order of convergence corresponds to its design order), and we use a second-order spatial discretization of the Laplacian and a second-order time-stepping, which limit the high-order accuracy of the fifth-order WENO spatial semidiscretization. Nevertheless, on the basis of our (limited) evidence of robustness of the scheme (provided by Examples 11 and 12 along with the fact that numerical solutions of Examples 1, 4 and 7 are consistent with those of [67], where, however, the domain Ω has slightly different dimensions), the numerical results allow us to draw some conclusions and conjectures about solutions of (3.5).

Let us first point out that long-time stable patterned configurations obtained in our numerical experiments are formed by stripes. This contrasts with the results in [22] obtained for a predator-prey model with one single prey species only, where the system tends to an asymptotic state with regular arrangements of spots of high predator concentrations, in agreement with the radial structure introduced by the nonlocal velocity function and where the diffusion caused by the Laplacian in the prey equation counterbalances the first order nonlocal differential operator in the predator equation [22]. A similar tendency was observed in some scenarios of the eight-compartment epidemiological model studied in [19], where male individuals are supposed to move non-locally in response to the sampled density of their female counterparts. Furthermore, it is calling to attention that in our Example 12, the dominant mechanism of pattern formation seems to be the interaction between susceptible and infected prey, since the solution (see Figure 3.17) for the prey compartments S and Y is practically independent of ε. That the effect of predator location on the formation of the prey pattern should be weak, at least for the parameters (3.4) and (3.15), can probably be explained by the relative smallness of the predation term on the right-hand side of (3.5b). Finally, it would be interesting to investigate whether the invasion of predators into a domain initially occupied by prey solely, as in Examples 2, 5 and 8, can possibly be modeled by simpler, spatially one-dimensional version of (3.5). Clearly, a more in-depth mathematical analysis to describe the mechanisms that compel these and other phenomena is necessary.

With respect to further extensions, we mention that the spatio-temporal approach could also be applied to the model by Greenhalgh et al. [31] that generalizes (3.1) and [32] in the sense that the assumption that the predator eats infected prey only is replaced by the assumption that the susceptible and infected populations are both exposed to the predator but to varying degrees. Concerning the numerical scheme, further analysis could compare results with higher-order discretizations of the diffusion operator and time-stepping scheme.

4.2 Future work

In general terms we can indicate that, more research is interesting about the qualitative analysis of the proposed or similar models using techniques analogous to those used in [22], extend the conclusions that can be deduced from Moran index I applied to numerical solutions of local or non-local PDEs (something that we believe is not done in the literature) and that although we use here a spatial discretization of the Laplacian second order and a step in the second order time, which limit the precision of high order of the fifth order WENO spatial semidiscretization, it is of interest to make comparisons with higher order discretizations of the diffusion operator and the time-stepping scheme. Other probable scenarios that are of interest in future research in the context of the numerical analysis of partial differential equations associated with Biomathematics problems are:

1. Analyze epidemic models where there is a connection between humans and animals.
2. Consider reaction-difussion models taking into account the effect of degenerated diffusion.
3. Study dynamics of predator-prey models by adding a third equation corresponding to a super-predator.

4.3 Conclusiones

En esta tesis hemos estudiado ecuaciones de reacción-difusión-convección que están relacionadas con modelos epidémicos. En la literatura, tales modelos generalmente se formulan como sistemas epidémicos (sistemas de ecuaciones diferenciales ordinarias), donde la única cantidad de interés es el total número de individuos en cada compartimiento epidemiológico. En contraste con esto, el enfoque seguido en esta tesis, es también proporcionar información sobre la distribución espacial de los diferentes estados de la enfermedad. Una herramienta decisiva para obtener de manera eficiente esta información es una combinación de esquemas de diferencias finitas WENO eficientes, métodos IMEX-RK y convoluciones discretas para resolver numéricamente el sistema de ecuaciones diferenciales parciales. Este método se aplicó primero a un modelo SEIR de Hantavirus en roedores, los cuales clasificaron por género y posteriormente a uno ecoepidemiológico donde inicialmente hay formación de patrones en la presa y luego un depredador invade el hábitat.

En el Capítulo 2 se exhibe un modelo espacio-temporal (2.1) relativamente simple estructurado por género de la transmisión de Hantavirus entre roedores con un término de velocidad no local (2.6), que surge en cada uno de los modelos 1, 2 y 3 definidos por (2.2), (2.3) and (2.5), respectivamente, puede producir perfiles espaciales-temporales complejos de la prevalencia de la enfermedad (Figures 2.2 a 2.8). Sin embargo, en realidad, varios factores adicionales pueden afectar la dinámica de transmisión de las infecciones por Hantavirus entre roedores. Específicamente, la transmisión de Hantavirus se ha asociado con patrones de uso de la tierra [17], elevación, tipos de vegetación [9], así como humedad y lluvia [77]. El crecimiento de las poblaciones de roedores también puede estar asociado con la temperatura local, ya que por ejemplo, la temperatura puede

afectar la tasa de preñez, el tamaño de la camada, la tasa de natalidad y la tasa de supervivencia de las poblaciones de roedores [75]. Además, los roedores tienden a vivir en hábitats altamente cubiertos y menos perturbados, que se encuentran comúnmente en zonas agrícolas y zonas de pastizales [50, 76] para mejorar su capacidad de reproducción y supervivencia [50].

La precisión del método numérico propuesto en este trabajo merece ser estudiada en trabajos posteriores, especialmente para establecer que su orden de convergencia corresponde a su orden de diseño. Más escenarios (configuración inicial, calibración de parámetros) deben explorarse con estas herramientas numéricas con el fin de obtener y estudiar más patrones espacio-temporales en las simulaciones. En este sentido, entre nuestros modelos propuestos, consideramos el Modelo 1 como es el más prometedor pues da lugar a patrones espacio-temporales y vale la pena ser analizado como en [21, 49].

En el Capítulo 3, hemos mostrado que un modelo relativamente simple de tres especies puede producir complejos patrones espacio-temporales de depredadores y presas. El tratamiento combina el modelo epidémico espacio-temporal de [67], el modelo de depredador-presa no espacial de tres especies analizado en [32], la función de velocidad no local introducida en [22] y el método numérico desarrollado en [19]. El método numérico no se analiza completamente en este documento, y ciertamente deja potencial para nuevas mejoras. Por ejemplo, su precisión merece una mayor investigación (particularmente para establecer que su orden de convergencia correspondiente a su diseño) y usamos discretización espacial de segundo orden del Laplaciano y una de segundo orden para el paso de tiempo, lo cual limita la precisión de la semi-discretización espacial WENO de quinto orden. Sin embargo, sobre la base de nuestra (limitada) evidencia de robustez del esquema (proporcionada por los Ejemplos 11 y 12 junto con el hecho de que las soluciones numéricas de los Ejemplos 1, 4 y 7 son consistentes con los de [67], donde, sin embargo, el dominio Ω tiene dimensiones ligeramente diferentes), los resultados numéricos nos permiten sacar algunas conclusiones y conjeturas sobre las soluciones de (3.5).

Primero señalemos que las configuraciones de patrones estables de larga duración en tiempo en nuestros experimentos numéricos están formadas por rayas. Esto contrasta con los resultados en [22] obtenidos para un modelo depredador-presa con una sola especie de presa solamente, donde el sistema tiende a un estado asintótico con arreglos regulares de manchas de altas concentraciones de depredadores, de acuerdo con la estructura radial introducida por la función de velocidad no local y donde la difusión causada por el Laplaciano en la presa la ecuación compensa el operador diferencial no local de primer orden en el depredador ecuación [22]. Se observó una tendencia similar en algunos escenarios del octavo compartimiento del modelo epidemiológico estudiado en [19], donde se supone que los roedores machos se trasladan no localmente en respuesta a la densidad muestreada de sus contrapartes hembras. Además, llama la atención en nuestro Ejemplo 12, el mecanismo dominante de formación de patrones parece ser la interacción entre presas susceptibles e infectadas, ya que la solución (ver Figura 3.17) para los compartimentos de presas S e Y es prácticamente independiente de ε. Que el efecto de la ubicación de los depredadores en la formación del patrón de presa debe ser débil, al menos para los parámetros (3.4) y (3.15), probablemente pueda explicarse por la relativa pequeñez del término de depredación en el lado derecho de (3.5b). Finalmente, sería interesante investigar si la invasión de depredadores en un dominio inicialmente ocupado únicamente por presas, como en los Ejemplos 2, 5 y 8, posible-

mente puede ser modelada por una versión más simple, espacialmente unidimensional de (**??**). Claramente, un análisis matemático más profundo para describir los mecanismos que obligan estos y otros fenómenos, es necesario.

Con respecto a extensiones adicionales, mencionamos que el enfoque espacio-temporal también podría ser aplicado al modelo por Greenhalgh et al. [31] que generaliza (3.1) y [32] en el sentido que la suposición que el depredador ataca presas infectadas solo se reemplaza por la suposición de que las poblaciones susceptibles e infectadas están ambas expuestas al depredador, pero en grados variables. En lo que respecta al esquema numérico, un análisis más detallado podría comparar los resultados discretizaciones de orden superior para el operador de difusión y el esquema de paso de tiempo.

4.4 Trabajo futuro

En líneas generales podemos indicar que, son de interés más investigaciones sobre el análisis cualitativo de los modelos propuestos o similares empleando técnicas análogas a las utilizadas en [22], ampliar las conclusiones que se pueden deducir del índice de Moran I aplicado a soluciones numéricas de PDEs locales o no locales (algo que a nuestro entender no se hace en la literatura) y que aunque aquí utilizamos una discretización espacial de segundo orden del Laplaciano y un paso en el tiempo de segundo orden, que limitan la precisión de alto orden de la semidiscretización espacial WENO de quinto orden, es de interés realizar comparaciones con discretizaciones de orden superior del operador de difusión y el esquema de paso del tiempo. Otros probables escenarios que son de interés en investigaciones futuras en el contexto del análisis numéricos de ecuaciones diferenciales parciales asociadas a problemas de Biomatemática, son:

1. Analizar modelos epidémicos en donde haya conexión entre humanos y animales.

2. Considerar modelos reacción difusión teniendo en cuenta el efecto de la difusión degenerada.

3. Estudiar dinámicas de modelos predador-presa agregando una tercera ecuación correspondiente a un super-depredador.

Bibliography

[1] G. Abramson and V.M. Kenkre, Spatiotemporal patterns in the Hantavirus infection, *Phys. Rev. E*, **66** (2002), paper 011912 (5pp).

[2] M.A. Aguirre, G. Abramson, A.R. Bishop and V.M. Kenkre, Simulations in the mathematical modeling of the spread of the Hantavirus, *Phys. Rev. E*, **66** (2002), paper 041908 (5pp).

[3] L.J.S. Allen, B.M. Bolker, Y. Lou and A.L. Nevai, Asymptotic of the steady states for an SIS epidemic patch model, *SIAM J. Appl. Math.*, **67** (2007), 1283–1309.

[4] L.J.S. Allen, R.K. McCormack and C.B. Jonsson, Mathematical models for hantavirus infection in rodents, *Bull. Math. Biol.* **68** (2006), 511–524.

[5] R.M. Anderson and R.M. May, Infectious Diseases of Humans: Dynamics and Control, Oxford Science Publications, 1991.

[6] J. Arino, Diseases in metapopulations. In Z. Ma, Y. Zhou and J. Wu (Eds.), Modeling and Dynamics of Infectious Diseases, Higher Education Press, Beijing, 2009, 64–122.

[7] J. Arino, J.R. Davis, D. Hartley, R. Jordan, J.M. Miller and P. van den Driessche, A multi-species epidemic model with spatial dynamics, *Mathematical Medicine and Biology*, **22** (2) (2005), 129–142.

[8] U. Ascher, S. Ruuth and J. Spiteri, Implicit-explicit Runge-Kutta methods for time dependent partial differential equations, *Appl. Numer. Math.*, **25** (1997), 151–167.

[9] P. Bi, X. Wu, F. Zhang, K.A. Parton and S. Tong, Seasonal rainfall variability, the incidence of hemorrhagic fever with renal syndrome, and prediction of the disease in low-lying areas of China, *Amer. J. Epidemiol.*, **148** (1998), 276–281.

[10] S. Boscarino, R. Bürger, P. Mulet, G. Russo and L.M. Villada, Linearly implicit IMEX Runge-Kutta methods for a class of degenerate convection-diffusion problems, *SIAM J. Sci. Comput.*, **37** (2015), B305–B331.

[11] S. Boscarino, F. Filbet and G. Russo, High order semi-implicit schemes for time dependent partial differential equations, *J. Sci. Comput.* **68** (2016), 975–1001.

[12] S. Boscarino, P.G. LeFloch and G. Russo, High-order asymptotic-preserving methods for fully nonlinear relaxation problems, *SIAM J. Sci. Comput.*, **36** (2014), A377–A395.

[13] S. Boscarino and G. Russo, On a class of uniformly accurate IMEX Runge-Kutta schemes and applications to hyperbolic systems with relaxation, *SIAM J. Sci. Comput.*, **31** (2009), 1926–1945.

[14] S. Boscarino and G. Russo, Flux-explicit IMEX Runge-Kutta schemes for hyperbolic to parabolic relaxation problems, *SIAM J. Numer. Anal.*, **51** (2013), 163–190.

[15] F. Brauer and C. Castillo-Chavez, Mathematical Models in Population Biology and Epidemiology, Second Ed., Springer, New York, 2012.

[16] F. Brauer and C. Kribs, Dynamical Systems for Biological Modeling: An Introduction, CRC Press, Boca Raton, FL, USA, 2016.

[17] M. Brummer-Korvenkontio, A. Vaheri, T. Hovi, C.H. von Bonsdorff, J. Vuorimies, T. Manni, K. Penttinen, N. Oker-Blom and J. Lähdevirta, Nephropathia epidemica: detection of antigen in bank voles and serologic diagnosis of human infection. *J. Infect. Dis.*, **141** (1980), 131–134.

[18] J. Buceta, C. Escudero, F.J. de la Rubia and K. Lindenberg, Outbreaks of Hantavirus induced by seasonality, *Phys. Rev. E*, **69** (2004), paper 021906 (8pp).

[19] R. Bürger, G. Chowell, E. Gavilán, P. Mulet, and L.M. Villada, Numerical solution of a spatio-temporal gender-structured model for hantavirus infection in rodents, *Math. Biosci. Eng.*, **15** (2018), 95–123.

[20] R. Bürger, G. Chowell, P. Mulet and L.M. Villada, Modelling the spatial-temporal progression of the 2009 A/H1N1 influenza pandemic in Chile, *Math. Biosci. Eng.*, **13** (2016), 43–65.

[21] R. Bürger, R. Ruiz-Baier, C. Tian, Stability analysis and finite volume element discretization for delay-driven spatio-temporal patterns in a predator-prey model, *Math. Comput. Simulation*, **132** (2017), 28–52.

[22] R.M. Colombo and E. Rossi, Hyperbolic predators versus parabolic preys, *Commun. Math. Sci.*, **13** (2015), 369–400.

[23] M. Crouzeix, Une méthode multipas implicite-explicite pour l'approximation des équations d'évolution paraboliques, *Numer. Math.*, **35** (1980), 257–276.

[24] O. Diekmann, H. Heesterbeek and T. Britton, Mathematical Tools for Understanding Infectious Disease Dynamics, Princeton Series in Theoretical and Computational Biology, Princeton University Press, 2012.

[25] R. Donat and I. Higueras, On stability issues for IMEX schemes applied to 1D scalar hyperbolic equations with stiff reaction terms, *Math. Comp.*, **80** (2011), 2097–2126.

[26] L. Edelstein-Keshet, Mathematical Models in Biology, reprint, SIAM, 2005.

[27] C. Escudero, J. Buceta, F.J. de la Rubia and K. Lindenberg, Effects of internal fluctuations on the spreading of Hantavirus, *Phys. Rev. E*, **70** (2004), paper 061907 (7pp).

[28] S. de Franciscis and A. d'Onofrio, Spatiotemporal bounded noises and transitions induced by them in solutions of the real Ginzburg-Landau model, *Phys. Rev. E*, **86** (2012), paper 021118 (9pp); Erratum, *Phys. Rev. E*, **94** (2016), paper 0599005(E) (1p).

[29] I.M. Foppa, A Historical Introduction to Mathematical Modeling of Infectious Diseases, Academic Press, London, UK, 2016.

[30] M. Garavello and B. Piccoli, Traffic Flow on Networks. Conservation Laws Models, Amer. Inst. Math. Sci., Springfield, MO, USA, 2006.

[31] D. Greenhalgh, Q.J.A. Khan, and J.S. Pettigrew, An eco-epidemiological predator-prey modelmwhere predators distinguish between susceptible and infected prey, *Math. Meth. Appl. Sci.*, **40** (2017), 146–166.

[32] D. Greenhalgh and M. Haque, A predator-prey model with disease in the prey species only, *Math. Meth. Appl. Sci.*, **30** (2007), 911–929.

[33] K.P. Hadeler and H.I. Freedman, Predator-prey populations with parasitic infection, *J. Math. Biol.*, **27** (1989), 609–631.

[34] G.S. Jiang and C.-W. Shu, Efficient implementation of weighted ENO schemes, *J. Comput. Phys.*, **126** (1996), 202–228.

[35] P. Kachroo, S.J. Al-Nasur, S.A. Wadoo and A. Shende, Pedestrian Dynamics, Springer-Verlag, Berlin, 2008.

[36] A. Källén, Thresholds and travelling waves in an epidemic model for rabies, *Nonlin. Anal. Theor. Meth. Appl.*, **8** (1984), 851–856.

[37] A. Källén, P. Arcuri and J.D. Murray, A simple model for the spatial spread and control of rabies, *J. Theor. Biol.*, **116** (1985), 377–393.

[38] Y. Katznelson, An Introduction to Harmonic Analysis, Third Ed., Cambridge University Press, Cambridge, UK, 2004.

[39] C.A. Kennedy and M.H. Carpenter, Additive Runge-Kutta schemes for convection-diffusion-reaction equations, *Appl. Numer. Math.*, **44** (2003), 139–181.

[40] W.O. Kermack and A.G. McKendrick, A contribution to the mathematical theory of epidemics, *Proc. Roy. Soc. A*, **115** (1927), 700–721.

[41] Y. Kuang and E. Beretta, Global qualitative analysis of a ratio-dependent predator-prey system, *J. Math. Biol.*, **36** (1998), 389–406.

[42] N. Kumar, R.R. Parmenter, and V.M. Kenkre, Extinction of refugia of hantavirus infection in a spatially heterogeneous environment, *Phys. Rev. E*, **82** (2010), paper 011920 (8pp).

[43] T. Kuniya, Y. Muroya and Y. Enatsu, Threshold dynamics of an SIR epidemic model with hybrid and multigroup of patch structures, *Math. Biosci. Eng.*, **11** (2014), 1375–1393.

[44] H.N. Liu, L.D. Gao, G. Chowell, S.X. Hu, X.L. Lin, X.J. Li, G.H. Ma, R. Huang, H.S. Yang, H. Tian and H. Xiao, Time-specific ecologic niche models forecast the risk of hemorrhagic fever with renal syndrome in Dongting Lake district, China, 2005–2010, *PLoS One*, **9** (2014), paper e106839 (8pp).

[45] P.H. Leslie and J.C. Gower, The properties of a stochastic model for the predator-prey type of interaction between two species, *Biometrika*, **47** (1960), 219–234.

[46] W.-M. Liu, H.W. Hethcote, and S.A. Levin, Dynamical behavior of epidemiological models with nonlinear incidence rates, *J. Math. Biol.*, **25** (1987), 359–380.

[47] W.-M. Liu, S.A. Levin, and Y. Iwasa, Influence of nonlinear incidence rates upon the behavior of SIRS epidemiological models, *J. Math. Biol.*, **23** (1986), 187–204.

[48] X.-D. Liu, S. Osher and T. Chan, Weighted essentially non-oscillatory schemes, *J. Comput. Phys.*, **115** (1994), 200–212.

[49] H. Malchow, S.V. Petrovskii and E. Venturino, Spatial Patterns in Ecology and Epidemiology: Theory, Models, and Simulation. Chapman & Hall/CRC, Boca Raton, FL, USA, 2008.

[50] J.N. Mills, B.A. Ellis, K.T. McKee, J.I. Maiztegui and J.E. Childs, Habitat associations and relative densities of rodent populations in cultivated areas of central Argentina, *J. Mammal.*, **72** (1991), 470–479.

[51] P.A.P. Moran, Notes on continuous stochastic phenomena, *Biometrika* **37** (1950), 17–23.

[52] J.D. Murray, Mathematical Biology II: Spatial Models and Biomedical Applications. Third Edition. Springer, New York, 2003.

[53] J.D. Murray, E.A. Stanley and D.L. Brown, On the spatial spread of rabies among foxes, *Proc. Roy. Soc. London B*, **229** (1986), 111–150.

[54] A. Okubo and S.A. Levin, Diffusion and Ecological Problems: Modern Perspectives. Second Edition, Springer-Verlag, New York, 2001.

[55] O. Ovaskainen and E.E. Crone, Modeling animal movement with diffusion, in S. Cantrell, C. Cosner and S. Ruan (Eds.), Spatial Ecology, Chapman & Hall/CRC, Boca Raton, FL, USA, 2010, 63–83.

[56] L. Pareschi and G. Russo, Implicit-Explicit Runge-Kutta schemes and applications to hyperbolic systems with relaxation, *J. Sci. Comput.*, **25** (2005), 129–155.

[57] J.A. Reinoso and F.J. de la Rubia, Stage-dependent model for the Hantavirus infection: The effect of the initial infection-free period, *Phys. Rev. E*, **87** (2013), paper 042706 (6pp).

[58] J.A. Reinoso and F.J. de la Rubia, Spatial spread of the Hantavirus infection, *Phys. Rev. E*, **91** (2015), paper 032703 (5pp).

[59] R. Riquelme, M.L. Rioseco, L. Bastidas, D. Trincado, M. Riquelme, H. Loyola and F. Valdivieso, Hantavirus Pulmonary Syndrome, Southern Chile, 1995–2012, *Emerg. Infect. Dis.*, **21** (2015), 562–568.

[60] C. Robertson, C. Mazzetta and A. d'Onofrio, Regional variation and spatial correlation. Chapter 5 in P. Boyle and M. Smans (Eds.), Atlas of Cancer Mortality in the European Union and the European Economic Area 1993–1997, IARC Scientific Publication No. 159, WHO Press, Geneva, Switzerland, 2008, 91–113.

[61] E. Rossi and V. Schleper, Convergence of a numerical scheme for a mixed hyperbolic-parabolic system in two space dimensions, *ESAIM Math. Modelling Numer. Anal.*, **50** (2016), 475–497.

[62] S. Ruan and J. Wu, Modeling spatial spread of communicable diseases involving animal hosts, in S. Cantrell, C. Cosner and S. Ruan (Eds.), Spatial Ecology, Chapman & Hall/CRC, Boca Raton, FL, USA, 2010, 293–316.

[63] L. Sattenspiel, The Geographic Spread of Infectious Diseases: Models and Applications, Princeton Series in Theoretical and Computational Biology, Princeton University Press, 2009.

[64] C.-W. Shu and S. Osher, Efficient implementation of essentially non-oscillatory shock-capturing schemes, II, *J. Comput. Phys.*, **83** (1988), 32–78.

[65] S.W. Smith, Digital Signal Processing: A Practical Guide for Engineers and Scientists. Demystifying technology series: by engineers, for engineers. Newnes, 2003.

[66] S.H. Strogatz, Nonlinear Dynamics and Chaos: with Applications to Physics, Biology, Chemistry, and Engineering, Second Edition, CRC Press, Boca Raton, FL, 2015.

[67] G. Q. Sun, Pattern formation of an epidemic model with diffusion, *Nonlinear Dynamics*, **69** (2012), 1097-1104.

[68] H.Y. Tian, P.B. Yu, A.D. Luis, P. Bi, B. Cazelles, M. Laine, S.Q. Huang, C.F. Ma, S. Zhou, J. Wei, S. Li, X.L. Lu, J.H. Qu, J.H. Dong, S.L. Tong, J.J. Wang, B. Grenfell and B. Xu, Changes in rodent abundance and weather conditions potentially drive hemorrhagic fever with renal syndrome outbreaks in Xi'an, China, 2005–2012, *PLoS Negl. Trop. Dis.*, **9** (2015), paper e0003530 (13pp).

[69] M. Treiber and A. Kesting, Traffic Flow Dynamics, Springer-Verlag, Berlin, 2013.

[70] P. van den Driessche, Deterministic compartmental models: extensions of basic models. In F. Brauer, P. van den Driessche and J. Wu (Eds.), Mathematical Epidemiology, Springer-Verlag, Berlin, 2008, 147–157.

[71] P. van den Driessche, Spatial structure: patch models. In F. Brauer, P. van den Driessche and J. Wu (Eds.), Mathematical Epidemiology, Springer-Verlag, Berlin, 2008, 179–189.

[72] P. van den Driessche and J. Watmough, Reproduction numbers and sub-threshold endemic equilibria for compartmental models of disease transmission, *Math. Biosci.*, **180** (2002), 29–48.

[73] E. Vynnycky and R.E. White, An Introduction to Infectious Disease Modelling, Oxford University Press, 2010.

[74] J. Wu, Spatial structure: partial differential equations models. In F. Brauer, P. van den Driessche and J. Wu (Eds.), Mathematical Epidemiology, Springer-Verlag, Berlin, 2008, 191–203.

[75] H. Xiao, X.L. Lin, L.D. Gao, X.Y. Dai, X.G. He and B.Y. Chen, Environmental factors contributing to the spread of hemorrhagic fever with renal syndrome and potential risk areas prediction in midstream and downstream of the Xiangjiang River [in Chinese], *Scientia Geographica Sinica*, **33** (2013), 123–128.

[76] C.J. Yahnke, P.L. Meserve, T.G. Ksiazek and J.N. Mills, Patterns of infection with Laguna Negra virus in wild populations of Calomys laucha in the central Paraguayan chaco, *Am. J. Trop. Med. Hyg.*, **65** (2001), 768–776.

[77] W.Y. Zhang, L.Q. Fang, J.F. Jiang, F.M. Hui, G.E. Glass, L. Yan, Y.F. Xu, W.J. Zhao, H. Yang and W. Liu, Predicting the risk of hantavirus infection in Beijing, People's Republic of China, *Am. J. Trop. Med. Hyg.*, **80** (2010), 678–683.

[78] W.Y. Zhang, W.D. Guo, L.Q. Fang, C.P. Li, P. Bi, G.E. Glass, J.F. Jiang, S.H. Sun, Q. Qian, W. Liu, L. Yan, H. Yang, S.L. Tong and W.C. Cao, Climate variability and hemorrhagic fever with renal syndrome transmission in Northeastern China, *Environ. Health Perspect.*, **118** (2010), 915–920.

[79] Y.-T. Zhang and C.-W Shu, ENO and WENO schemes. Chapter 5 in R. Abgrall and C.-W. Shu (eds.), Handbook of Numerical Methods for Hyperbolic Problems Basic and Fundamental Issues. Handbook of Numerical Analysis vol. 17, North Holland (2016), 103–122.

[80] X. Zhong, Additive semi-implicit Runge-Kutta methods for computing high-speed nonequilibrium reactive flows, *J. Comput. Phys.*, **128** (1996), 19–31.